Study of $\eta \to \pi^0\gamma\gamma$ and $\eta' \to \pi^0\gamma\gamma$ decays in processes of $J/\psi \to \gamma\eta$ and $J/\psi \to \gamma\eta'$

Jian-Ping Dai,* Hai-Bo Li,† Hai-Jun Yang,‡ and Bing-Song Zou§

Based on the 1.31×10^9 J/ψ data collected by the BESIII detector in 2009 and 2012, we study the rare electromagnetic decays: $\eta \to \pi^0\gamma\gamma$ and $\eta' \to \pi^0\gamma\gamma$ via the processes of $J/\psi \to \gamma\eta$ and $J/\psi \to \gamma\eta'$, respectively. For the $\eta' \to \pi^0\gamma\gamma$ channel, the branching fraction of inclusive process is measured to be: $\mathcal{BR}(\eta' \to \pi^0\gamma\gamma)_{Inc.}$ $= (3.20 \pm 0.07(\text{stat.}) \pm 0.22(\text{syst.})) \times 10^{-3}$. The first information on the dependence of the decay width, $\Gamma(\eta' \to \pi^0\gamma\gamma)$, on the two-photon invariant mass squared $(m^2_{\gamma\gamma})$ is provided. Assumption the $\eta' \to \pi^0\gamma\gamma$ decay is mainly from the coherent sum of $\rho-$ and $\omega-$exchange, and the other non-resonance contribution, a fit to the $\gamma\pi^0$ invariant mass spectrum is performed. The fit gives the branching fractions of $\omega-$exchange and non-resonance process as: $\mathcal{BR}(\eta' \to \gamma\omega \to \pi^0\gamma\gamma) = (2.38 \pm 0.07(\text{stat.}) \pm 0.21(\text{syst.})) \times 10^{-3}$ and $\mathcal{BR}(\eta' \to \pi^0\gamma\gamma)_{non-Res.} = (6.30 \pm 0.63(\text{stat.}) \pm 0.71(\text{syst.})) \times 10^{-4}$, respectively. For the $\eta \to \pi^0\gamma\gamma$ channel, no significant signal is observed, and an upper limit of branching ratio at 90% confidence level is determined to be 5.2×10^{-4}.

PACS numbers:

*Electronic address: daijianping@mail.ihep.ac.cn
†Electronic address: lihb@mail.ihep.ac.cn
‡Electronic address: haijun.yang@sjtu.edu.cn
§Electronic address: zoubs@mail.ihep.ac.cn

I. INTRODUCTION

Quantum chromodynamics (QCD), the accepted theory describing the strong interactions, it's unavailable at low energy where the perturbation expansion doesn't converge because of the large coupling constant of quark and gluon. At the low energy, Chiral Perturbation Theory (χPTh) has successfully interpreted the strong and electromagnetic interactions of pseudoscalar mesons [1].

For $\eta \to \pi^0\gamma\gamma$ decay mode, in the frame of χPTh, the tree level amplitudes, both at $O(p^2)$ and $O(p^4)$, are forbidden because there is no direct coupling of photons to the neutral π^0 and η. The second order ($O(p^4)$), is much suppressed due to the kaon masses from the loops involving kaons, or again suppressed due to the G-parity violating transitions from the pion loops. The first sizable contribution comes at $O(p^6)$ [2]. The coefficients involved at $O(p^6)$, which depend on the model used for the calculation, are not precisely determined, so there are some different models to be used to obtain the parameters [3–9]. Based on these models, the theoretical predictions for the decay rate of $\eta \to \pi^0\gamma\gamma$ in the framework of χPTh are summarized in Table I. Besides, the branching ratio of $\eta \to \pi^0\gamma\gamma$ has been also calculated with pure Vector Meson Dominance model (VMD) [10], the quark-box diagrams [10] and the coherent sum of the Linear σ Model and VMD contributions [11, 12], respectively. These predictions are also listed in Table I. Thus for $\eta \to \pi^0\gamma\gamma$ rare decay, it's the unique case to direct test the correctness of the calculations of the third order χPTh because of the first order being zero and the second being very small. In Ref. [11, 12], the total decay width of $\eta' \to \pi^0\gamma\gamma$ is also calculated, and the values are summarized in Table I.

From the experimental point of view, there were 13 experiments with contradictory and unconvincing results because of huge neutral backgrounds coming from $\eta \to 3\pi^0$ and other processes before 1980s [13]. In 1982, the first major high-energy detector used for η-decay studies, GAMS-2000, yielded $\mathcal{BR}(\eta \to \pi^0\gamma\gamma) = (9.5 \pm 2.3) \times 10^{-4}$ through the analysis of $\pi^- p \to \eta n$ reaction [14]. The data were later reanalyzed with a better program for the reconstruction of showers in GAMS, and a new result for the $\mathcal{BR}$ of $(7.1 \pm 1.4) \times 10^{-4}$ was reported in 1984 [15], based on a sample of 40 events. Later the branching ratio was also measured at the Crystal Ball detector at AGS using the same reaction, and obtained with $\mathcal{BR}(\eta \to \pi^0\gamma\gamma) = (3.5 \pm 0.7 \pm 0.6) \times 10^{-4}$ [16]. A new reanalysis of the data gives $\mathcal{BR}$=$(2.21 \pm 0.24 \pm 0.47) \times 10^{-4}$ through correcting the discrepancy in the shape between

TABLE I: Recent theoretical calculations and experimental measurements for the $\eta \to \pi^0\gamma\gamma$ and $\eta' \to \pi^0\gamma\gamma$ decay rates, respectively. ENJL: extended Nambu-Jona-Lasinio model.

Theory	$\mathcal{BR}(\eta \to \pi^0\gamma\gamma)$ ($\times 10^{-4}$)	Experiment	$\mathcal{BR}(\eta \to \pi^0\gamma\gamma)$ ($\times 10^{-4}$)
χPTh, $O(p^2)$ [2]	0	SND [13]	< 8.4 @90% C.L.
χPTh, ...+$O(p^4)$ [2]	0.031	GAMS-2000-82 [14]	9.5 ± 2.3
χPTh, ...+$O(p^6)$ [2]	3.23 ± 1.54	GAMS-2000-84 [15]	7.1 ± 1.4
χPTh, ...+$O(p^6)$ [4]	3.62	CB-AGS-05 [16]	$3.5 \pm 0.7 \pm 0.6$
χPTh, ENJL, ...+$O(p^6)$ [5]	4.46 ± 2.31	CB-AGS-08 [17]	$2.21 \pm 0.24 \pm 0.47$
χPTh, ENJL, ...+$O(p^6)$ [6]	$2.08^{+1.38}_{-0.54}$	CB-MAMI-B [18]	$2.25 \pm 0.46 \pm 0.17$
χPTh, ...+$O(p^6)$ [7]	3.38 ± 0.69	KLOE [19]	$0.84 \pm 0.27 \pm 0.14$
Unitarized χPTh [8, 9]	3.62 ± 0.77, 2.54 ± 0.62	CBTAPS-MAMI [20, 21]	2.54 ± 0.23
VMD [10]	2.31 ± 1.15	PDG14 [22]	2.7 ± 0.5
Quark Box diagram [10]	5.38		
VMD+LσM [11]	1.73		
VMD+LσM [12]	2.15		
Theory	$\mathcal{BR}(\eta' \to \pi^0\gamma\gamma)$ ($\times 10^{-4}$)	Experiment	$\mathcal{BR}(\eta' \to \pi^0\gamma\gamma)$ ($\times 10^{-4}$)
VMD+LσM [11][a]	57	GAMS-2000-87 [23]	< 8.0 @90% C.L.[b]
VMD+LσM [12][a]	65		

[a]Containing the contributions of $\rho-$ and $\omega-$exchange

[b]Deducting the contribution of ω-exchange

the real $\pi^- p \to \pi^0\pi^0 n$ background and its MC simulation [17]. A recent analysis with the Crystal Ball at MAMI provides the rate: $\mathcal{BR}$=$(2.25 \pm 0.46 \pm 0.17) \times 10^{-4}$ [18], based on the analysis of $\gamma p \to \eta p$ reaction. At the same time, the last two experiments have provided the invariant mass distribution for the two radiative photons, which is very useful to test the different theoretical interpretation. A more recent preliminary results from KLOE [19] are also available with values of $\mathcal{BR} = (0.84 \pm 0.27 \pm 0.14) \times 10^{-4}$ in view of the analysis of $\phi \to \gamma\eta$ process. In the last May, MAMI had published the new analysis results using the total data from 2007 and 2009. And a combined results of branching fraction is given out $\mathcal{BR} = (2.54 \pm 0.23) \times 10^{-4}$ [20, 21]. For $\eta' \to \pi^0\gamma\gamma$ decay, there is no experimental evidence after ω veto. Based on the analysis of $\pi^- p \to n4\gamma$ reaction at GAMS-2000 experiment,

only an upper limit of branching ratio of $\mathcal{BR} < 8 \times 10^{-4}$ at 90% C.L. is obtained for the non-resonant contribution [23]. All the above mentioned measurements are listed in Table I.

The highest statistics of J/ψ events in world, 1.31×10^9 [24, 25], has been accumulated at BESIII. Therefore using the η and η' events from $J/\psi \to \gamma\eta$ and $J/\psi \to \gamma\eta'$ decays respectively, we hope to test the predictions of the third order χPhT or other theoretical models in $\eta \to \pi^0\gamma\gamma$ decay, and measure the total decay width of inclusive decay $\eta' \to \pi^0\gamma\gamma$ and search for the possible contributions excluding the $\rho-$ and $\omega-$exchange. Here the inclusive decay is defined as the η' decay into $\gamma\gamma\pi^0$ final states which including the all possible intermediate contributions and the non-resonant contribution.

II. BESIII DETECTOR

The BESIII detector [26] is a large solid-angle magnetic spectrometer installed at the upgraded Beijing Electron Positron Collider (BEPCII) [27]. The BEPCII is a double ring e^+e^- collider with the designed peak luminosity of 10^{33} cm^{-2}s^{-1} at a beam current of 0.93 A. The BESIII detector consists of a Helium-gas based drift chamber (MDC), a Time-Of-Flight (TOF) system, a CsI (Tl) Electro-Magnetic Calorimeter (EMC), a superconducting solenoid magnet and a RPC-based muon chamber (MUC).

The nominal detector acceptance is 93% of 4π. In MDC, the single wire resolution is 135 μm, the dE/dX resolution is better than 6% and the momentum resolution in the 1 T magnetic field is better than 0.5% for charged track with a momentum of 1 GeV/c. In TOF, the intrinsic timing resolution is better than 90 ps. In EMC, the energy resolution is better than 2.5% and position resolution better than 6 mm for 1 GeV electron and γ. In MUC, the spatial resolution is better than 2 cm. The superconducting magnet can supply a central field of 1.0 Tesla. After upgrade BESIII have better scientific performance and more statistics data to study hadron spectroscopy and τ charm physics.

III. BESIII DATA SET AND MONTE CARLO SIMULATION

This analysis is based on the 1310.6×10^6 J/ψ events [24, 25]collected by BESIII detector. A GEANT4-based Monte Carlo package [28] is used in this analysis to optimize the selection criteria and estimate backgrounds. An inclusive MC sample of J/ψ decay to anything uses

KKMC [29] to generate J/ψ production, and BesEvtGen [30] to generate subsequent J/ψ decays. Under BesEvtGen framework, Lundcharm [30] model is used to generate about 50% J/ψ inclusive decays while the remain 50% J/ψ events decay according to the branching ratios in PDG14 [22]. Exclusive MC samples are also generated under KKMC + BesEvtGen framework.

This analysis is performed under BOSS 6.6.4 (BESIII Offline Software System). The signal MC of η channel is generated as: $J/\psi \to \gamma\eta, \eta \to \pi^0\gamma\gamma$ (VSP-PWAVE, PHSP); The signal MC of η' channel is generated as the incoherent sum of $J/\psi \to \gamma\eta', \eta' \to \gamma\omega \to \gamma\gamma\pi^0$ (VSP-PWAVE, SVP-HELAMP, VSP-PWAVE), $J/\psi \to \gamma\eta', \eta' \to \gamma\rho^0 \to \gamma\gamma\pi^0$ (VSP-PWAVE, SVP-HELAMP, VSP-PWAVE) and the $J/\psi \to \gamma\eta, \eta \to \pi^0\gamma\gamma$ (generated with vector-meson-dominant (VMD) model with $\rho(1450)$- and $\omega(1650)$-exchange). In the analysis, the $J/\psi \to \gamma\eta$ and $J/\psi \to \gamma\eta'$ decays are simulated by angular distribution (VSP-PWAVE) for all the signals MCs and backgrounds MCs.

IV. INITIAL EVENTS SELECTION

A. Good Charged Track Selection

- No good charged track ($R_{xy} < 1$ cm, $|z| < 10$ cm, $|cos\theta| < 0.93$) is reconstructed from MDC. Here we demonstrate why is the tight good track selection performed. After the final event selections, for $\eta \to \pi^0\gamma\gamma$ decay, the number of events with the requirement of no good charged track will be reduced from 21157 obtained without any requirement for charged track to 21143 for signal MC, but for Data, it will be reduced from 2323 to 2316. For $\eta' \to \pi^0\gamma\gamma$ decay, after the final event selections, the number of events with the requirement of no good charged track will be reduced from 98532 obtained without any requirement for charged track to 98477 for signal MC, but for Data, it will be reduced from 12798 to 12758. Therefore in view of the lost efficiencies of signal MCs and the values of $\frac{S}{\sqrt{S+B}}$, we require there is no good charged track in MDC;

B. Good Photon Selection

- For barrel ($|cos\theta|$ <0.8), the energy deposition is: $E > 25.0$ MeV;

- For end cap ($0.86 < |cos\theta| < 0.92$), the energy deposition is: $E > 50.0$ MeV;
- Number of good photon is: $N_\gamma = 5$;

Here we demonstrate the good photon distributions after final selections for signal MCs and dominant backgrounds respectively, see Fig. 1. From the Fig. 1, one can see that, for $\eta \to \pi^0\gamma\gamma$, if we select the events with $N_\gamma = 5$, then the efficiency of signal MC will only decrease 6.4%, but the efficiency of $J/\psi \to \gamma\eta \to \gamma 3\pi^0$ background MC will be reduced by 14.8%; for $\eta' \to \pi^0\gamma\gamma$, if we select the events with $N_\gamma = 5$, then the efficiency of signal MC will only decrease 6.0%, but the efficiency of $J/\psi \to \gamma\eta' \to \gamma\pi^0\pi^0\eta$ ($\eta \to \gamma\gamma$) background MC will be reduced by 25.4%. In addition, after the good photon selection with $N_\gamma = 5$, the value of $\frac{S}{\sqrt{S+B}}$ will increase from 435.7 estimated by the events with $N_\gamma = 5, 6$ to 439.3 for η decay and from 863.1 estimated by the events with $N_\gamma = 5, 6$ to 871.9 for η' decay, respectively. Therefore in the analysis, we only require $N_\gamma = 5$ for the good photon selection.

V. FINAL EVENTS SELECTION

A. $\eta \to \pi^0\gamma\gamma$

- A five constraint kinematic fit for energy-momentum conservation and π^0 mass is performed to the $\pi^0\gamma\gamma\gamma$ hypothesis, and $\chi^2_{\rm 5C} < 20$ is required. Here the $\chi^2_{\rm 5C}$ is optimized by the value of $\frac{S}{\sqrt{S+B}}$, as shown in Fig. 2 (a);
- Fig. 2 (b) shows the reconstructed photon energy distributions for radiative photon (E_{rad}), the maximum energy photon of the four photons of η decay chain ($E_{max}(\eta)$) and the maximum energy photon of the two photons of π^0 decay ($E_{max}(\pi^0)$) before the kinematic fit. In the 21143 signal MC events, using the method of truth match, the number of events with $E_{max}(\pi^0) > E_{rad}$ is only equal to 5. It indicates that about 99.98% radiatiave photons are the highest-energy ones in each event, thus the highest-energy photon hardly contaminate the photons of π^0 candidate. Therefore the π^0 is reconstructed by a pair of photons excluding the maximum-energy photon;
- In order to suppress the multi-π^0 backgrounds (mainly from $J/\psi \to \gamma\pi^0\pi^0$ backgrounds), we veto π^0 for the three photons except for the two photons used to reconstruct

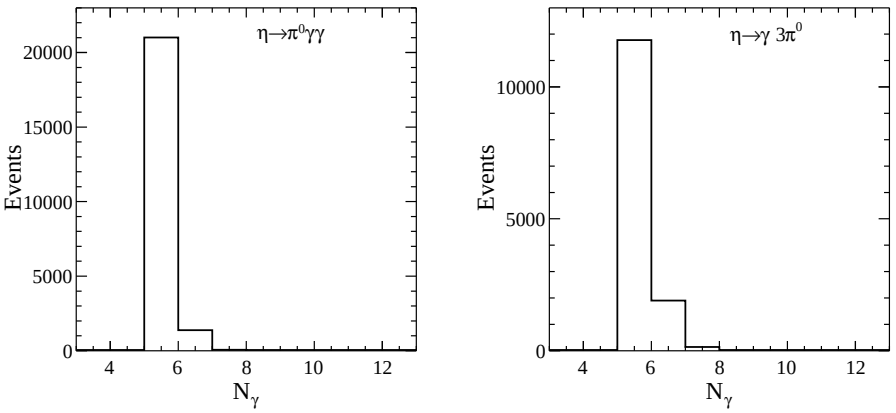

(a)Good photon distribution from signal MC: $J/\psi \to \gamma\eta$, $\eta \to \pi^0\gamma\gamma$.

(b)Good photon distribution from background MC: $J\psi \to \gamma\eta \to \gamma 3\pi^0$.

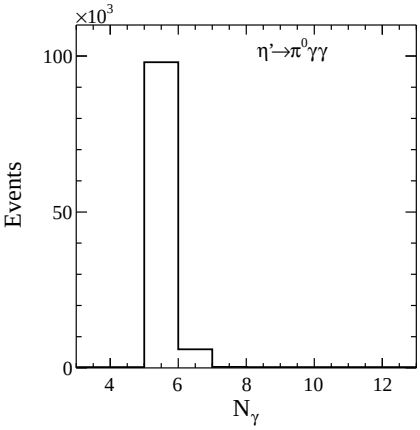

(c)Good photon distribution from signal MC: $J/\psi \to \gamma\eta'$, $\eta' \to \pi^0\gamma\gamma$.

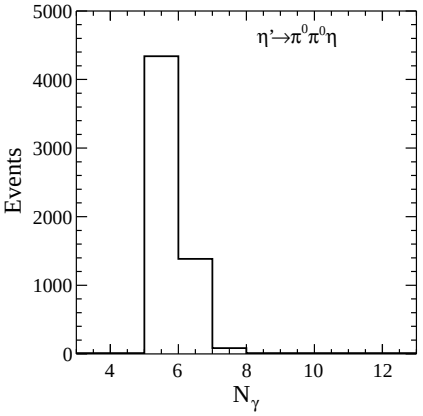

(d)Good photon distribution from background MC: $J/\psi \to \gamma\eta' \to \gamma\pi^0\pi^0\eta$ $(\eta \to \gamma\gamma)$.

FIG. 1: Good photon distributions of MC signals and dominant backgrounds for $\eta \to \pi^0\gamma\gamma$ and $\eta' \to \pi^0\gamma\gamma$, respectively.

π^0 candidate by $|M_{\gamma\gamma} - M_{\pi^0}| > 18$ MeV. The π^0 mass resolution is estimated about 6.3 MeV through fit to the $M_{\gamma\gamma}$ invariant mass before 5C fit. In addition, in order to suppress the multi-π^0 backgrounds and remove the miss-combination of π^0 candidate, the γ veto is performed by requiring $|M_{\gamma\gamma^{\pi^0}} - M_{\pi^0}| > 18$ MeV/c^2, namely each photon γ^{π^0} used to reconstruct signal π^0 candidate is not allowed to form additional π^0 with any other three photons;

- We select the best η candidate by requiring the minimum value of $|M_{\pi^0\gamma\gamma} - M_\eta|$. In

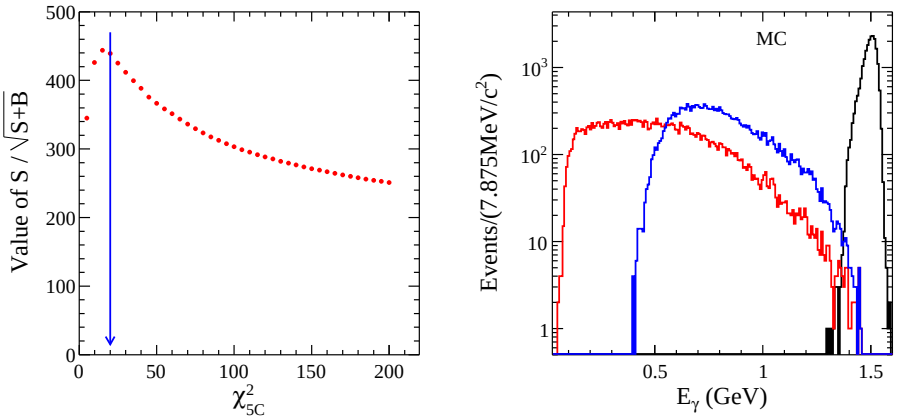

(a) $\frac{S}{\sqrt{S+B}}$ function as a χ^2_{5C} cut.

(b)Photon energy distributions from signal MC.

FIG. 2: Figure (a) shows the $\frac{S}{\sqrt{S+B}}$ distribution as a χ^2_{5C} cut; figure (b) shows the reconstructed photon energy distributions for radiative photon (Black line), the maximum energy photon of the four photons of η decay chain (Blue line) and the maximum energy photon of the two photons of π^0 decay (Red line) before kinematic fit.

the analysis, both in η and η' decays, the highest-energy photon isn't assigned as the radiative photon. If the maximum energy photon is selected as the radiative one, for η decay, the unmatched events is **5** in 21143 events. Whereas if the η candidate is selected by requiring the minimum value of $|M_{\pi^0\gamma\gamma} - M_\eta|$ and the remainder one photon is saw as the radiative photon (3 combinations), the unmatched events is only **4**. Therefore the most energetic photon is taken as the primary one from the J/ψ decay, and the rest two photons and π^0 are used to reconstruct the η' candidate

The comparisons of some distributions, such as χ^2_{5C}, $M_{\gamma\gamma}$ and $M_{\gamma\gamma\pi^0}$ between Data and signal MC are shown in Fig. 3 and Fig. 4, respectively.

B. $\eta' \to \pi^0\gamma\gamma$

- A five constraint kinematic fit for energy-momentum conservation and π^0 mass is performed to the $\pi^0\gamma\gamma\gamma$ hypothesis, and $\chi^2_{5C} < 30$ is required. Here the χ^2_{5C} is optimized by the value of $\frac{S}{\sqrt{S+B}}$, as shown in Fig. 5 (a);

- Fig. 5 (b) shows the reconstructed photon energy distributions for radiative photon

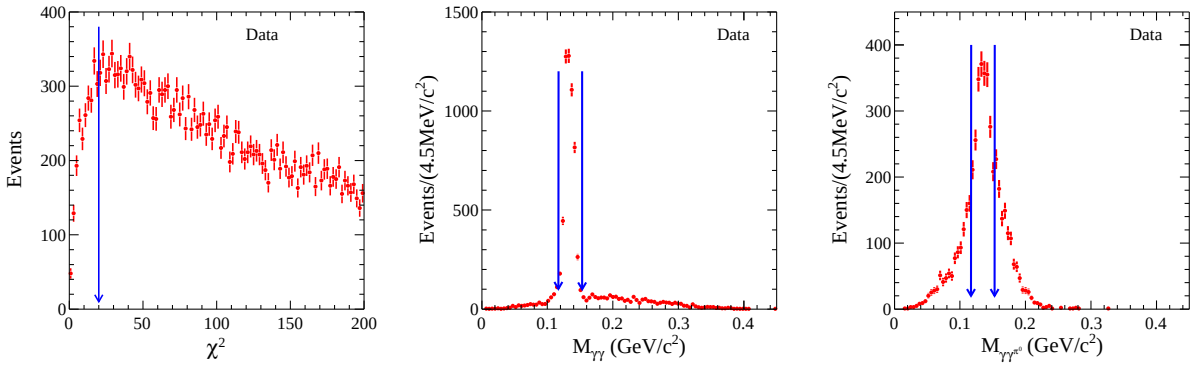

(a)χ^2_{5C} distribution. (b)$M_{\gamma\gamma}$ distribution for π^0 veto. (c)$M_{\gamma\gamma\pi^0}$ distribution for π^0 veto.

FIG. 3: χ^2_{5C}, $M_{\gamma\gamma}$ and $M_{\gamma\gamma\pi^0}$ distributions for Data.

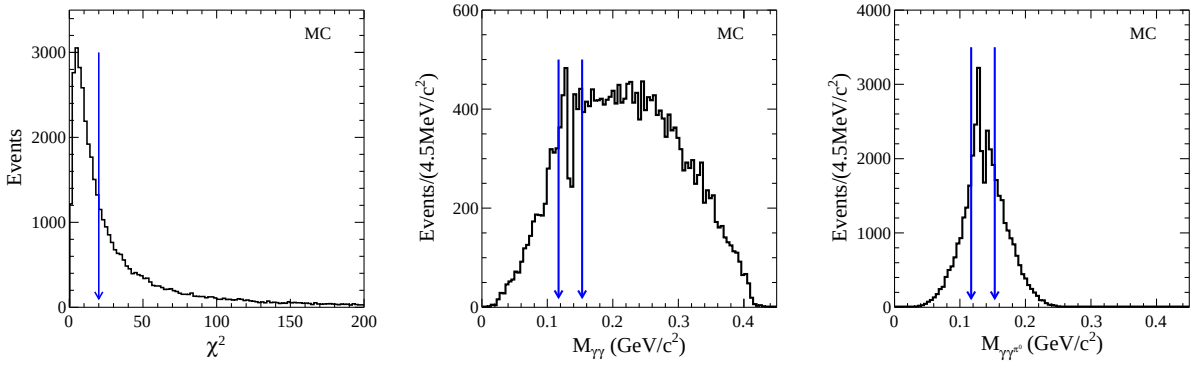

(a)χ^2_{5C} distribution. (b)$M_{\gamma\gamma}$ distribution for π^0 veto. (c)$M_{\gamma\gamma\pi^0}$ distribution for π^0 veto.

FIG. 4: χ^2_{5C}, $M_{\gamma\gamma}$ and $M_{\gamma\gamma\pi^0}$ distributions for Signal MC of $\eta \to \pi^0\gamma\gamma$ decay.

(E_{rad}), the maximum energy photon of the four photons of η' decay chain ($E_{max}(\eta')$) and the maximum energy photon of the two photons of π^0 decay ($E_{max}(\pi^0)$) before kinematic fit. In the 98477 signal MC events, the number of events with $E_{max}(\pi^0) > E_{rad}$ is only equal to 19. It indicates that about 99.98% radiatiave photons are the highest-energy ones in each event, thus the highest-energy photon hardly contaminate the photons of π^0 candidate. Therefore the π^0 is reconstructed by a pair of photons excluding the maximum-energy photon;

- In order to suppress the multi-π^0 backgrounds (mainly from $J/\psi \to \gamma\pi^0\pi^0$ backgrounds), we veto π^0 for the three photons except for the two photons used to reconstruct π^0 candidate by $|M_{\gamma\gamma} - M_{\pi^0}| > 18$ MeV. The π^0 mass resolution is estimated about 6.3 MeV through fit to the $M_{\gamma\gamma}$ invariant mass before 5C fit. In addition, in order to

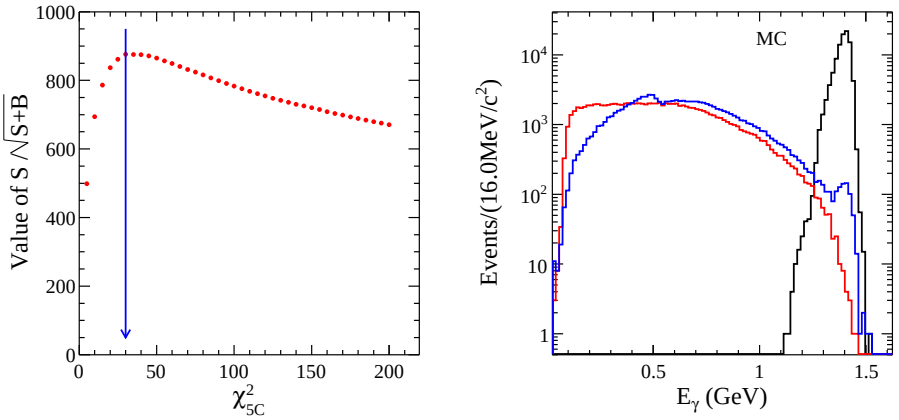

(a) $\frac{S}{\sqrt{S+B}}$ function as a χ^2_{5C} cut.

(b)Photon energy distributions from signal MC.

FIG. 5: Figure (a) shows the $\frac{S}{\sqrt{S+B}}$ distribution as a χ^2_{5C} cut; figure (b) shows the reconstructed photon energy distributions for radiative photon (Black line), the maximum energy photon of the four photons of η' decay chain (Blue line) and the maximum energy photon of the two photons of π^0 decay (Red line) before kinematic fit.

suppress the multi-π^0 backgrounds and remove the miss-combination of π^0 candidate, the γ veto is performed by requiring $|M_{\gamma\gamma^{\pi^0}} - M_{\pi^0}| > 18$ MeV/c^2, namely each photon γ^{π^0} used to reconstruct signal π^0 candidate is not allowed to form additional π^0 with any other three photons;

- We select the best η' candidate by requiring the minimum value of $|M_{\pi^0\gamma\gamma} - M_{\eta'}|$. In the analysis, the highest-energy photon isn't assigned as the radiative photon. If the maximum energy photon is selected as the radiative one, for η' decay, the unmatched events is **107** in 98477 events. Whereas if the η' candidate is selected by requiring the minimum value of $|M_{\pi^0\gamma\gamma} - M_{\eta'}|$ and the remainder one photon is saw as the radiative photon (3 combinations), the unmatched events is **51** for η' decay. Therefore in consideration of 0.5% difference, the most energetic photon is taken as the primary one from the J/ψ decay, and the rest two photons and π^0 are used to reconstruct the η' candidate.;

The comparisons of some distributions, such as χ^2_{5C}, $M_{\gamma\gamma}$ and $M_{\gamma\gamma^{\pi^0}}$ between Data and signal MC are shown in Fig. 6 and Fig. 7, respectively. Here it needs to explain why there are two peaks for $M_{\gamma\gamma^{\pi^0}}$ in Fig. 4 (c) and Fig. 7 (c). There are two reasons. One is because

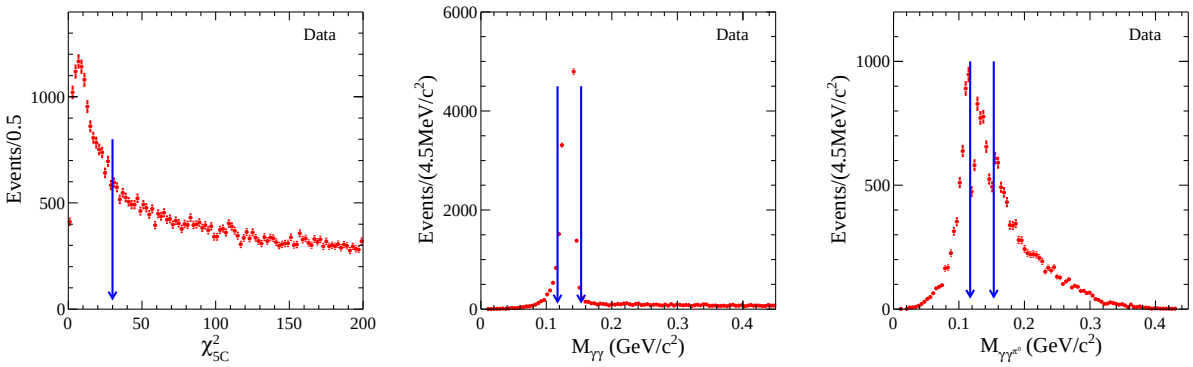

(a)χ^2_{5C} distribution. (b)$M_{\gamma\gamma}$ distribution for π^0 veto. (c)$M_{\gamma\gamma\pi^0}$ distribution for γ veto.

FIG. 6: χ^2_{5C}, $M_{\gamma\gamma}$ and $M_{\gamma\gamma\pi^0}$ distributions for Data.

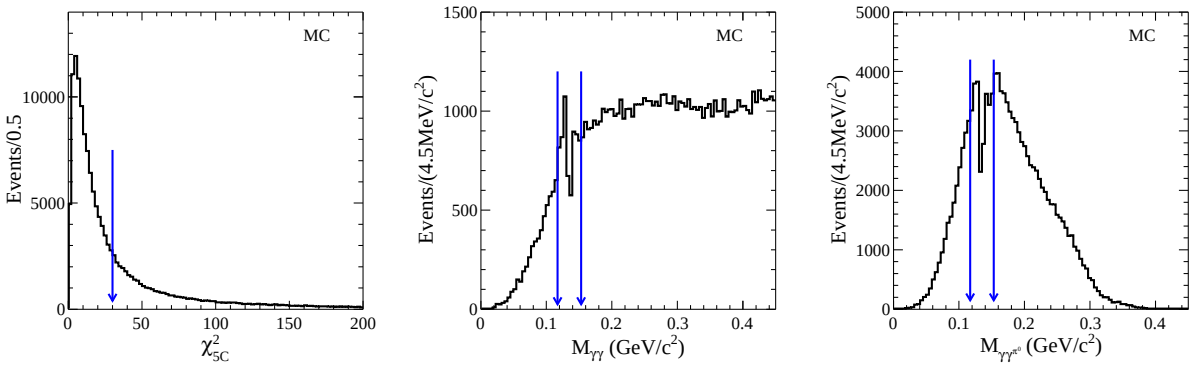

(a)χ^2_{5C} distribution. (b)$M_{\gamma\gamma}$ distribution for π^0 veto. (c)$M_{\gamma\gamma\pi^0}$ distribution for γ veto.

FIG. 7: χ^2_{5C}, $M_{\gamma\gamma}$ and $M_{\gamma\gamma\pi^0}$ distribution for Signal MC of $\eta' \to \pi^0\gamma\gamma$ decay.

the $M_{\gamma\gamma\pi^0}$ invariant mass spectrum has excluded the $M_{\gamma\pi^0\gamma\pi^0}$ of π^0 candidate. It will give rise to a dip. Another is because the spectrum is obtained by requiring the minimum value of $M_{\gamma\gamma\pi^0} - M_{\pi^0}|$. The requirement will lead to the more events moving to π^0 mass region. But since there is dip, the moved events will result in two peaks in the two sides of π^0 mass.

VI. BACKGROUND STUDY OF $\eta \to \pi^0\gamma\gamma$ DECAY

A. Study of Inclusive Sample

In this analysis, the final states are five photons. If a J/ψ decay channel contains similar final states, it's maybe the background of this analysis. The 225 M inclusive sample of $J/\psi \to anything$ which generated by Lund Charm Generator (We only use the MC to look over the possible dominant backgrounds) is used to estimate the possible background. With the studies of Inclusive MC, we find that the backgrounds are main from $J/\psi \to \gamma\pi^0\pi^0$, $\gamma\eta \to \gamma 3\pi^0$, $\gamma\eta \to 3\gamma$, $\gamma\eta' \to \gamma\pi^0\pi^0\eta$ ($\eta \to \gamma\gamma$), $\omega\pi^0 \to \gamma\pi^0\pi^0$, $J/\psi \to \gamma\pi^0$ decays and so on.

B. Study of Exclusive Sample

We generate the exclusive MC samples for the above backgrounds to estimate the expected shapes and normalized events. These backgrounds are generated as follow: $J/\psi \to \gamma\eta$, $\eta \to 3\pi^0$ (VSP-PWAVE, Dalitz) (Here the Dalitz amplitude of $\eta \to 3\pi^0$ decay is parameterized as: $|M|^2 \propto (1 + 2\alpha z)$. The value of α is taken from PDG12 [22].); $J/\psi \to \gamma\eta'$, $\eta' \to \pi^0\pi^0\eta$ (VSP-PWAVE, Dalitz) (Here the Dalitz amplitude of $\eta' \to \pi^0\pi^0\eta$ decay is parameterized as: $|M|^2 \propto (1+aY+bY^2+cX+dX^2)$. The values of a, b, c and d are taken from the measurements [31].); $J/\psi \to \omega\pi^0$, $\omega \to \gamma\pi^0$ (VVS-PWAVE, VSP-PWAVE); $J/\psi \to \gamma\pi^0$ (VSP-PWAVE). The $J/\psi \to \gamma\pi^0\pi^0$ background is generated without interferences between different resonances based on the results of partial wave analysis from Guang-Ming Xu [32]. For the generator, it needs to point out, in order to mainly check the shape of background in the η and η' signal regions, so we doesn't consider the interferences between different resonances. The Table II shows the efficiency flows of event selections and the normalized numbers of events for each background modes, respectively. According to the results in Table II, the $J/\psi \to \gamma\eta \to \gamma 3\pi^0$ decay is the most dominant background.

The $\pi^0\gamma\gamma$ invariant mass distributions for the above mentioned backgrounds are shown in Fig. 8. From the these plots, one can see that except for $J/\psi \to \gamma\eta \to \gamma 3\pi^0$ background, there is no peaking backgrounds under η signal. This background will be considered when fit to Data.

TABLE II: Efficiency flow of event selection for $\eta \to \pi^0\gamma\gamma$ analysis. Here the efficiency is estimated by sum of the events with invariant mass of $\pi^0\gamma\gamma$ between 0.4 GeV/c^2 $\sim$ 0.7 GeV/c^2. These backgrounds events are normalized to the total 1310.6×10^6 J/ψ Data.

Decay mode ($J/\psi \to$)	$\gamma\eta$ $\eta \to \pi^0\gamma\gamma$	$\gamma\eta \to \gamma 3\pi^0$	$\gamma\pi^0\pi^0$	$\gamma\eta \to 3\gamma$	$\gamma\eta' \to \gamma\pi^0\pi^0\eta$ $\eta \to \gamma\gamma$	$\omega\pi^0 \to \gamma\pi^0\pi^0$	$\gamma\pi^0$
Total events	262540	3281750	2625400	5250800	1969050	656350	525080
$N_{trk} = 0$	248045	3061368	2472879	5034346	1839241	619086	503603
$N_\gamma = 5$	83820	784725	1086952	39975	463807	269089	5163
$\chi^2_{5C} < 20$	44073	26932	636043	1837	3345	158928	961
π^0 veto	39096	24594	28658	1576	3269	6780	855
γ veto	21143	12117	1155	778	85	462	288
Efficiency	8.05%	0.37%	0.044%	0.015%	0.0043%	0.041%	0.055%
Normalized events		1680.2±53.1		84.4±2.6	24.2±1.1	33.6±3.9	24.8±2.3

VII. BACKGROUND STUDY OF $\eta' \to \pi^0\gamma\gamma$

A. Study of Inclusive Sample

Same as the $\eta \to \pi^0\gamma\gamma$ analysis, the 225 M inclusive sample of $J/\psi \to$ *anything* is used to estimate the background. With the studies of Inclusive MC, we find that the possible backgrounds are from $J/\psi \to \gamma\pi^0\pi^0$, $\gamma\eta' \to \gamma\pi^0\pi^0\eta$ ($\eta \to \gamma\gamma$), $\omega\eta$ ($\omega \to \gamma\pi^0$, $\eta \to \gamma\gamma$), $\omega\pi^0\pi^0 \to \gamma 3\pi^0$, $\gamma\pi^0\eta$, $\omega\pi^0 \to \gamma\pi^0\pi^0$, $b_1^0\pi^0 \to \omega\pi^0\pi^0 \to \gamma 3\pi^0$, $\gamma\eta' \to \gamma 3\pi^0$, $\gamma\eta' \to 3\gamma$, $J/\psi \to \gamma\eta \to 3\gamma$ decays and so on.

B. Study of Exclusive Sample

We generate the exclusive MC samples of the background channels to estimate the expected shapes and normalized events. These backgrounds are generated as follow: $J/\psi \to \omega\eta$ ($\eta \to \gamma\gamma$), $\omega \to \gamma\pi^0$ (VVS-PWAVE, VSP-PWAVE); $J/\psi \to \gamma\eta'$, $\eta' \to 3\pi^0$ (VSP-PWAVE, Dalitz) (Here the Dalitz amplitude of $\eta' \to 3\pi^0$ decay is parameterized as: $|M|^2 \propto (1+2\alpha z)$. The value of α is taken from the measurement [33].). The Table III shows the efficiency flows

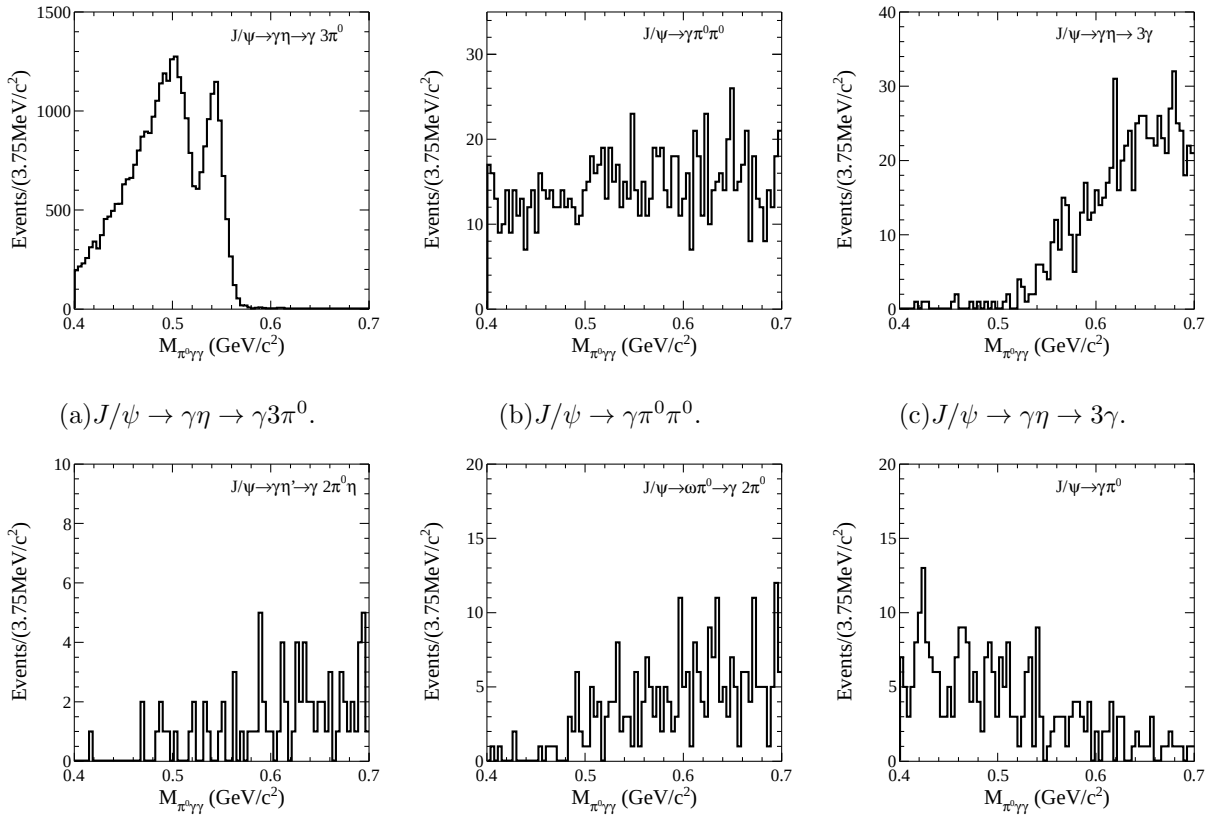

(a)$J/\psi \to \gamma\eta \to \gamma 3\pi^0$. (b)$J/\psi \to \gamma\pi^0\pi^0$. (c)$J/\psi \to \gamma\eta \to 3\gamma$.

(d)$J/\psi \to \gamma\eta' \to \gamma\pi^0\pi^0\eta$. (e)$J/\psi \to \omega\pi^0 \to \gamma\pi^0\pi^0$. (f)$J/\psi \to \gamma\pi^0$.

FIG. 8: $\pi^0\gamma\gamma$ invariant mass distributions of the main backgrounds.

of event selections and the normalized numbers of events for background modes, respectively. According to the results in Table III, the $J/\psi \to \gamma\eta' \to \gamma\pi^0\pi^0\eta$ ($\eta \to \gamma\gamma$), $\omega\eta \to \gamma\gamma\gamma\pi^0$ and $\gamma\pi^0\eta$ decays are the remarkable backgrounds, and $J/\psi \to \omega\pi^0\pi^0 \to \gamma 3\pi^0$, $\omega\pi^0 \to \gamma\pi^0\pi^0$, $b_1^0\pi^0 \to \omega\pi^0\pi^0 \to \gamma 3\pi^0$, $\gamma\eta' \to \gamma 3\pi^0$, $\gamma\eta' \to 3\gamma$, $\gamma\eta \to 3\gamma$ decays are the visible backgrounds in the analysis.

The $\pi^0\gamma\gamma$ invariant mass distributions for the above eleven main backgrounds are shown in Fig. 9. From these plots, one can see that there is no peaking backgrounds under the η' signal. When fit to data, these non-peaking backgrounds from η' decay, namely $J/\psi \to \gamma\eta' \to \gamma\pi^0\pi^0\eta$, $\gamma\eta' \to 3\pi^0$ and $\gamma\eta' \to 3\gamma$, will be particularly considered.

TABLE III: Efficiency flow of event selection for $\eta' \to \pi^0\gamma\gamma$ analysis. The efficiency is estimated by sum of the events with invariant mass of $\pi^0\gamma\gamma$ between 0.7 GeV/c^2 $\sim$ 1.1 GeV/c^2. Here except for the branching fraction of $\eta' \to 3\pi^0$ estimated by the BESIII measurements [34], the branching fraction of $J/\psi \to \gamma\pi^0\eta$ estimated by the Shuo-Pin Wen's measurement [35], all the other branching ratios are taken from PDG14 [22]. These backgrounds events are normalized to the total 1310.6×10^6 J/ψ Data.

Decay mode $(J/\psi \to)$	$\gamma\eta' \to \gamma\gamma\omega$ $\omega \to \gamma\pi^0$	$\gamma\eta' \to \gamma\gamma\rho^0$ $\rho^0 \to \gamma\pi^0$	$\gamma\eta'$ $\eta' \to \pi^0\gamma\gamma$ (VMD)	$\gamma\eta' \to \gamma\pi^0\pi^0\eta$ $\eta \to \gamma\gamma$	$\gamma\pi^0\pi^0$	$\omega\eta \to \gamma\pi^0\eta$ $\eta \to \gamma\gamma$
Total events	525080	131270	131270	5907150	2625400	525080
$N_{trk} = 0$	494696	123775	123778	5520504	2472879	494639
$N_\gamma = 5$	183815	45289	46733	1394967	1086952	208627
$\chi^2_{5C} < 30$	113144	27973	28570	18477	756221	117349
π^0 veto	106595	26307	27172	18043	40119	114918
γ veto	83286	20582	22544	13576	27116	105063
Efficiency	15.86%	15.68%	17.17%	0.220%	0.135%	3.65%
Normalized events	2410.9±222.4	182.7±25.3		1269.0±60.7		2676.4 ± 321.0

$\omega\pi^0\pi^0$ $\omega \to \gamma\pi^0$	$\gamma\pi^0\eta$ $\eta \to \gamma\gamma$	$\omega\pi^0 \to \gamma\pi^0\pi^0$	$b_1^0\pi^0 \to \omega\pi^0\pi^0$ $\omega \to \gamma\pi^0$	$\gamma\eta' \to \gamma 3\pi^0$	$\gamma\eta' \to 3\gamma$	$\gamma\eta \to 3\gamma$
1312700	525080	656350	1969050	262540	3938100	5250800
1216955	493546	619086	1827315	245020	3771310	5034346
241915	218807	269089	343492	55212	29350	39975
5802	114337	189270	7297	1755	2827	3473
5538	112114	9417	6796	1678	2496	3038
5009	100303	6794	6024	1302	1990	2370
0.0353%	2.39%	0.434%	0.0379%	0.487%	0.0449%	0.0161%
125.9 ± 29.9	259.0 ± 37.7	207.2±24.1	91.3±24.0	113.0±13.2	66.8±3.2	91.5±2.9

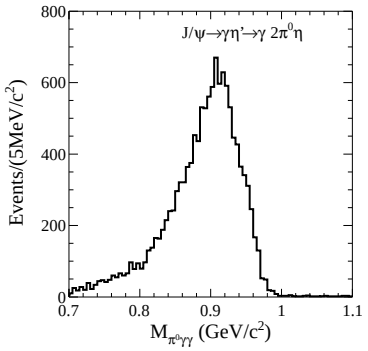

(a)$J/\psi \to \gamma\eta' \to \gamma\pi^0\pi^0\eta$.

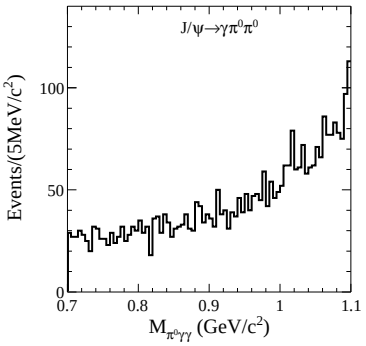

(b)$J/\psi \to \gamma\pi^0\pi^0$.

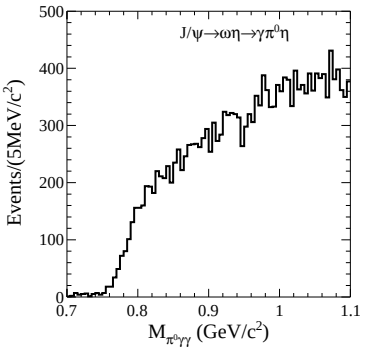

(c)$J/\psi \to \omega\eta \to \gamma\gamma\gamma\pi^0$.

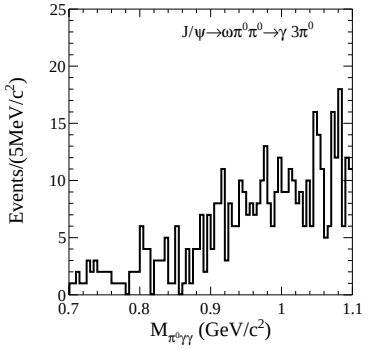

(d)$J/\psi \to \omega\pi^0\pi^0 \to \gamma 3\pi^0$.

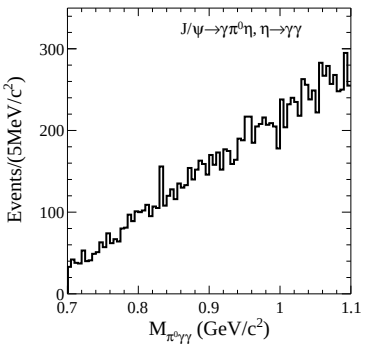

(e)$J/\psi \to \gamma\pi^0\eta,\ \eta \to \gamma\gamma$.

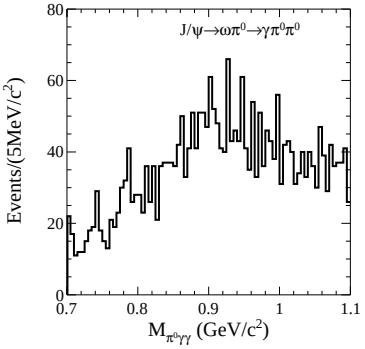

(f)$J/\psi \to \omega\pi^0 \to \gamma\pi^0\pi^0$.

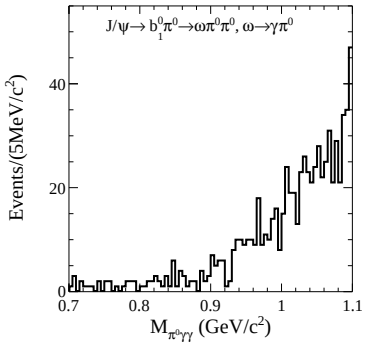

(g)$J/\psi \to b_1^0\pi^0 \to \pi^0\pi^0\omega \to \gamma 3\pi^0$.

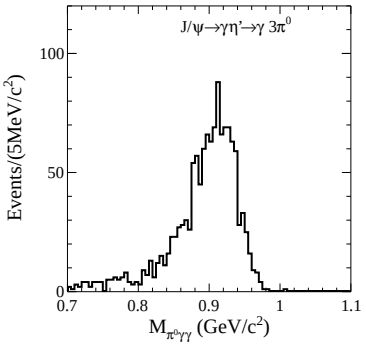

(h)$J/\psi \to \gamma\eta' \to \gamma 3\pi^0$.

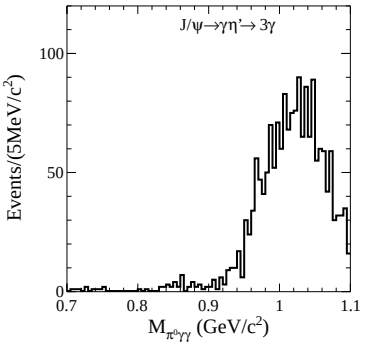

(i)$J/\psi \to \gamma\eta' \to\ 3\gamma$.

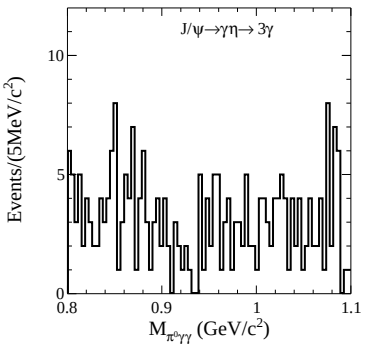

(j)$J/\psi \to \gamma\eta \to\ 3\gamma$.

FIG. 9: $\pi^0\gamma\gamma$ invariant mass distributions of main backgrounds.

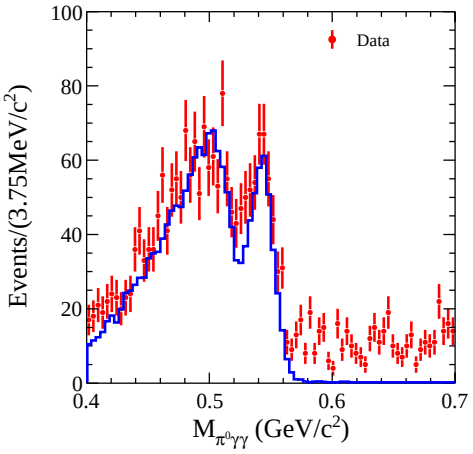

FIG. 10: $\pi^0\gamma\gamma$ invariant mass spectra of Data and normalized backgrounds. Here the Blue histogram is from $J/\psi \to \gamma\eta \to \gamma\ 3\pi^0$ background.

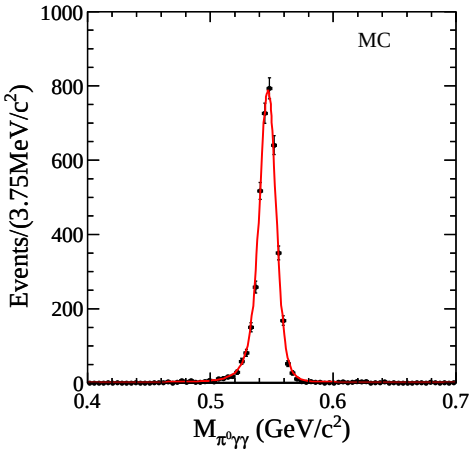

FIG. 11: $\pi^0\gamma\gamma$ invariant mass spectrum of MC.

VIII. BRANCHING RATIO MEASUREMENTS

A. Branching ratio of $\eta \to \pi^0\gamma\gamma$

The $\pi^0\gamma\gamma$ invariant mass spectra of Data and normalized backgrounds are shown in Fig. 10. Here the Blue histogram is from $J/\psi \to \gamma\eta \to \gamma\ 3\pi^0$ background.

An unbinned maximum likelihood (ML) fit is used for η or η' signal to determine the event yield. The signal probability density function (PDF) of η is extracted from MC simulation, see Fig. 11. The $J/\psi \to \gamma\eta \to \gamma 3\pi^0$ background is described with fixed shape taken from MC simulations but with free intensity. The shape for the remaining backgrounds is described by a second order Chebychev Polynomial, and the background yield and its PDF parameters are floated in the fit. The fitting range for η is $0.4 - 0.7$ GeV/c^2. Fig. 12 shows the results of the fit to Data, and fit yields 20 ± 24 signal events. The χ^2 of fit is: $\chi^2/n.o.f = 16.8/25$. Using the Bayesian method, the upper limit for the number of η signal events is 54.6 at 90% confidence level (C.L.). Fig. 13 shows the likelihood distribution as a function of the signal yield with the 90% C.L. upper limit value indicated by an arrow.

The Figure 14 shows the comparison between the fitted Polynomial and Inclusive MC in the η (η') fit. Here from the Fig. 14(a), it indicates that the second order Polynomial can well describe the remaining backgrounds of Inclusive MC except for the $J/\psi \to \gamma\eta \to \gamma\ 3\pi^0$

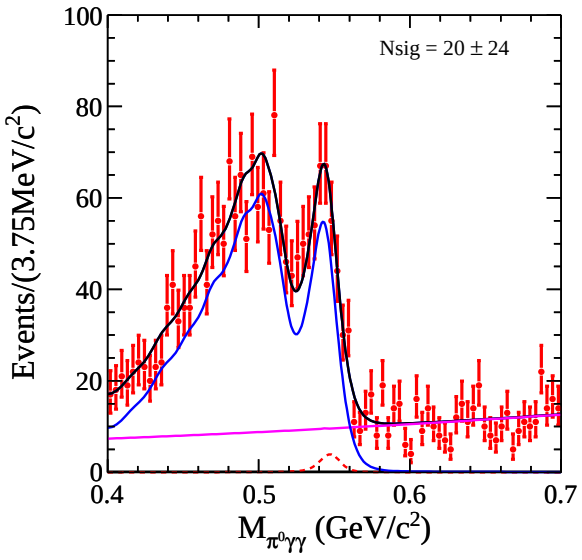

FIG. 12: The η fitting results. Here Red dots with error bars are Data; Blue line is from $J/\psi \to \gamma\eta \to \gamma\ 3\pi^0$ background; Pink line is the sum of other backgrounds. Here the shape of $J/\psi \to \gamma\eta \to \gamma\ 3\pi^0$ background is fixed to MC simulations, but the yield is free.

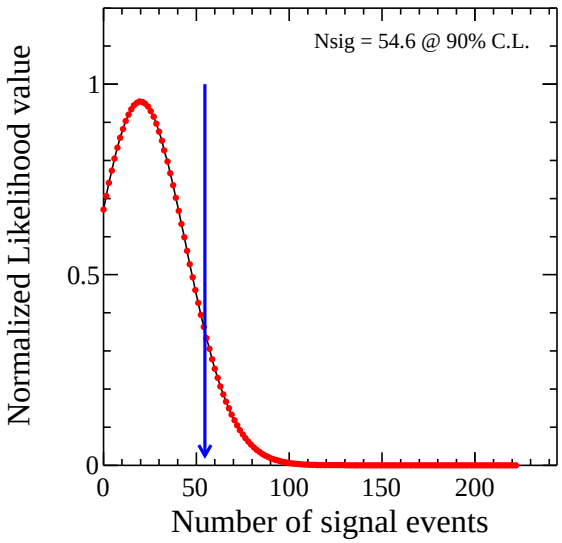

FIG. 13: Likelihood distribution as a function of the signal yield. The arrow is the position of the 90% C.L. upper limit on the signal yield.

background.

B. Branching ratio of $\eta' \to \pi^0\gamma\gamma$

The $\pi^0\gamma\gamma$ invariant mass spectra of Data and normalized backgrounds are shown in Fig. 15. Here the Green histogram is the sum of $J/\psi \to \gamma\eta' \to \gamma\pi^0\pi^0\eta$ ($\eta \to \gamma\gamma$), $\gamma\eta' \to \gamma 3\pi^0$, $\gamma\eta' \to 3\gamma$ backgrounds. From the Fig. 15, one can see that there is an prominent η' signal.

In the fit to η', the signal PDF is extracted from MC simulation with the incoherent sum of ρ, ω and non-resonant contributions. see Fig. 16. The possible contributions from the vector mesons ρ, ω and non-resonance are discussed below, and their fractions are measured to be $(5.4 \pm 1.4)\%$, $(70.9 \pm 6.6)\%$ and $(18.8 \pm 2.8)\%$, respectively. The $J/\psi \to \gamma\eta' \to \gamma\pi^0\pi^0\eta$ ($\eta \to \gamma\gamma$), $\gamma\eta' \to \gamma 3\pi^0$, $\gamma\eta' \to 3\gamma$ backgrounds are fixed to MC simulations at their expected

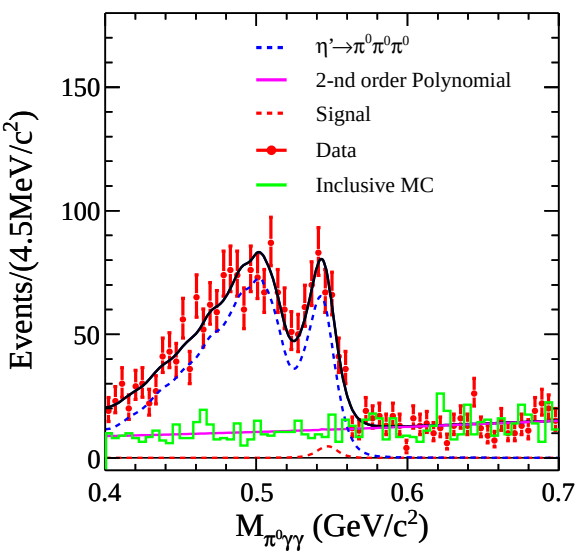

(a)Situation of η fit. Here Red dots with error bars are Data; Blue dashed-line is from $J/\psi \to \gamma\eta \to \gamma\ 3\pi^0$ background; Pink line is the fitted Polynomial; Green line is from the Inclusive MC.

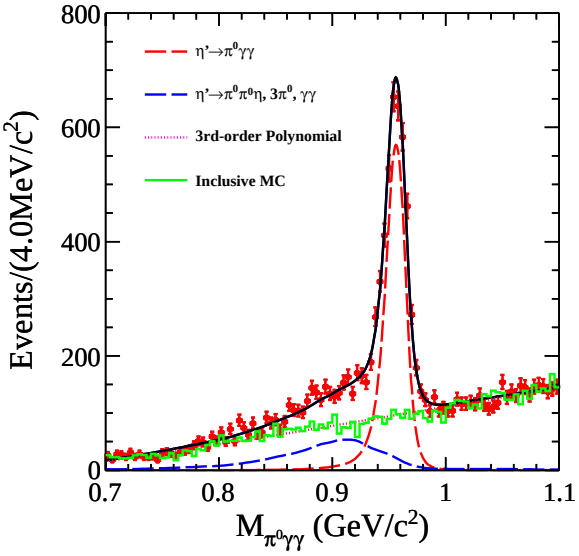

(b)Situation of η' fit. Here Blue dashed-line is the sum of $J/\psi \to \gamma\eta' \to \gamma\pi^0\pi^0\eta\ (\eta \to \gamma\gamma)$, $\gamma\eta' \to \gamma 3\pi^0$, $\gamma\eta' \to 3\gamma$ backgrounds; Pink line is the fitted Polynomial; Green line is from the Inclusive MC.

FIG. 14: Comparison between the fitted Polynomial and Inclusive MC for the η and η' fit.

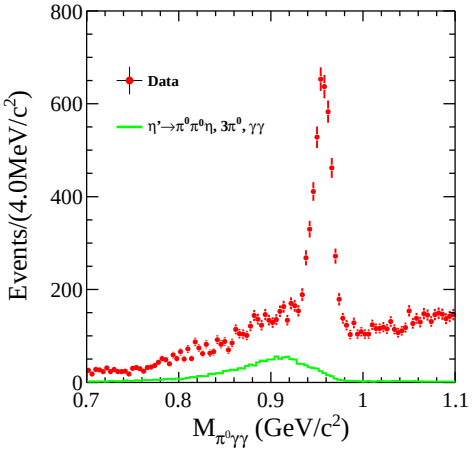

FIG. 15: $\pi^0\gamma\gamma$ invariant mass spectra of Data and normalized backgrounds. Here the Green histogram is the sum of $J/\psi \to \gamma\eta' \to \gamma\pi^0\pi^0\eta$ $(\eta \to \gamma\gamma)$, $\gamma\eta' \to \gamma 3\pi^0$, $\gamma\eta' \to 3\gamma$ backgrounds.

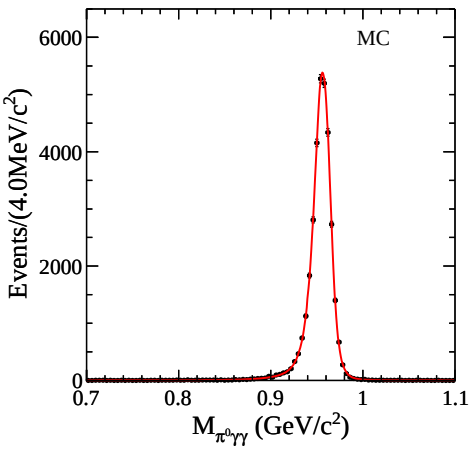

FIG. 16: $\pi^0\gamma\gamma$ invariant mass spectrum of MC.

intensities, respectively. The shape for the rest of background is described by a third order Chebychev Polynomial function, and the background yield and its PDF parameters are floated in the fit. The fitting range for η' is $0.7-1.1$ GeV/c^2. Figure 17 shows the results of the fit to Data, and fit yields 3435 ± 76 signal events. The χ^2 of fit is: $\chi^2/n.o.f = 108.0/95$.

The comparison between the fitted Polynomial and Inclusive MC is shown in Fig. 14(b). From the picture, one can see that the fitted second order Polynomials are consistent with the Inclusive MC except for the fixed backgrounds.

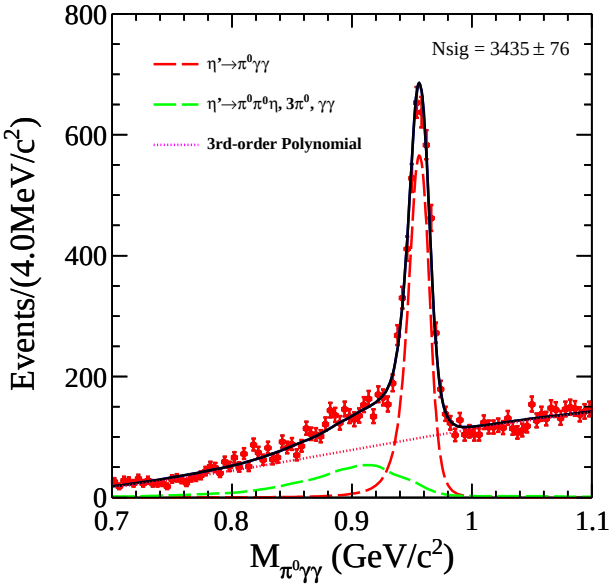

FIG. 17: The η' fitting results. Here Red Dots with error bars are data; Green line is the sum of $J/\psi\to\gamma\eta'\to\gamma\pi^0\pi^0\eta$ ($\eta\to\gamma\gamma$), $\gamma\eta'\to\gamma3\pi^0$, $\gamma\eta'\to3\gamma$ backgrounds; Pink line is the sum of other remainder backgrounds.

C. Measurement of $\mathbf{d}\Gamma(\eta'\to\pi^0\gamma\gamma)/\mathbf{d}m^2_{\gamma\gamma}$

We give out the information on the dependence of decay width, $\Gamma(\eta'\to\pi^0\gamma\gamma)$, on the two photon invariant mass squared ($m^2_{\gamma\gamma}$). Here the two photon invariant mass squared is divided into 13 intervals, see the Table IV. In consideration of the sample statistics, the fit range will be shrunk from $0.7-1.1$ GeV/c^2 to $0.8-1.1$ GeV/c^2. Same as the procedure of η' fit in the above section, for each $m^2_{\gamma\gamma}$ interval, the signal PDF is extracted from MC simulation; the $J/\psi\to\gamma\eta'\to\gamma\pi^0\pi^0\eta$ ($\eta\to\gamma\gamma$), $\gamma\eta'\to\gamma3\pi^0$, $\gamma\eta'\to3\gamma$ backgrounds

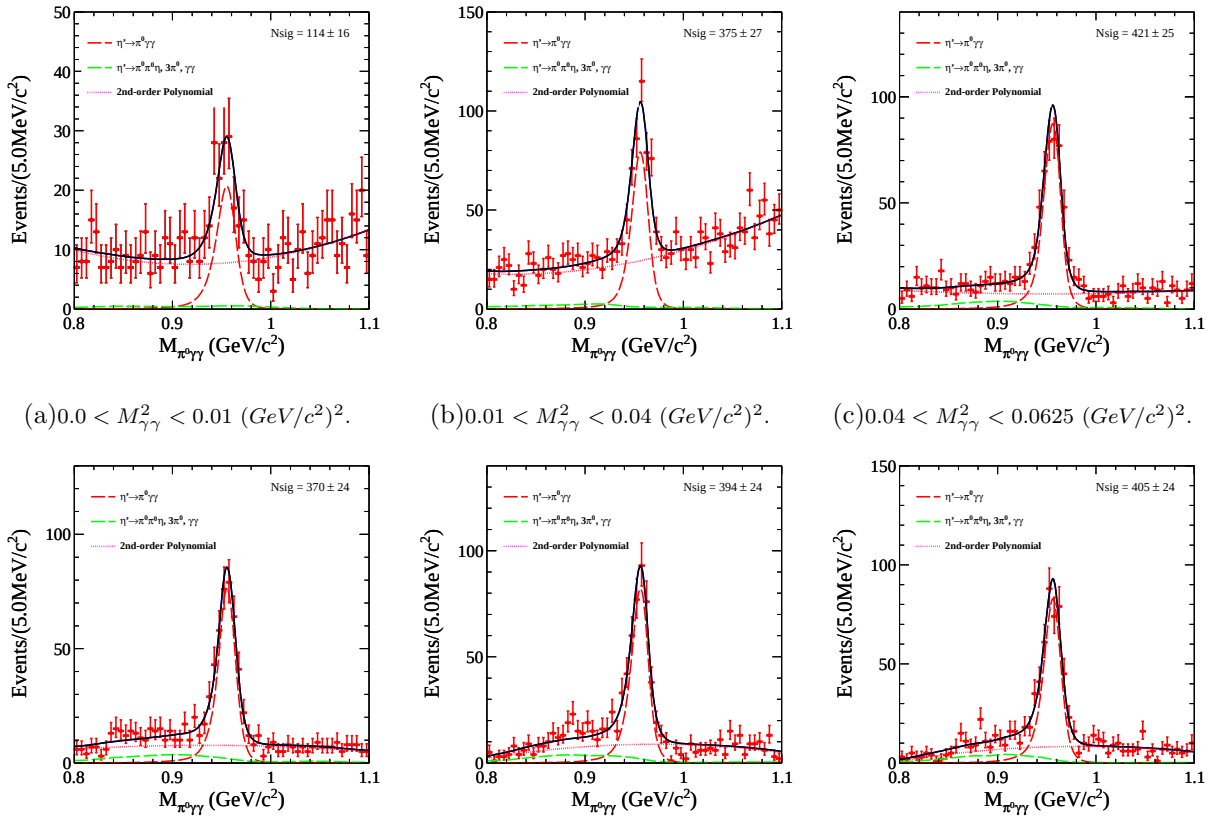

(a)$0.0 < M^2_{\gamma\gamma} < 0.01\ (GeV/c^2)^2$. (b)$0.01 < M^2_{\gamma\gamma} < 0.04\ (GeV/c^2)^2$. (c)$0.04 < M^2_{\gamma\gamma} < 0.0625\ (GeV/c^2)^2$.

(d)$0.0625 < M^2_{\gamma\gamma} < 0.09\ (GeV/c^2)^2$. (e)$0.09 < M^2_{\gamma\gamma} < 0.1225\ (GeV/c^2)^2$. (f)$0.1225 < M^2_{\gamma\gamma} < 0.16\ (GeV/c^2)^2$.

FIG. 18: η' fitting results for these bins ($(GeV/c^2)^2$): (a) $M^2_{\gamma\gamma} \subset (0.0, 0.01)$; (b) $M^2_{\gamma\gamma} \subset (0.01, 0.04)$; (c) $M^2_{\gamma\gamma} \subset (0.04, 0.0625)$; (d) $M^2_{\gamma\gamma} \subset (0.0625, 0.09)$; (e) $M^2_{\gamma\gamma} \subset (0.09, 0.1225)$; (f) $M^2_{\gamma\gamma} \subset (0.1225, 0.16)$.

are fixed to MC simulations at their expected intensities, respectively. The shape for the rest of background is described by a second order Chebychev Polynomial function, and the background yield and its PDF parameters are floated in the fit.

Figure 18 and 53 show the results of the fit to Data for each $m^2_{\gamma\gamma}$ interval. The corresponding normalized numbers of fixed backgrounds and fit yields of η' signal are tabulated in Table IV.

D. Branching ratio of non-resonance process in the decay of $\eta' \to \pi^0\gamma\gamma$

Assumption that the inclusive process of $\eta' \to \pi^0\gamma\gamma$ decay is mainly from the coherent sum of ρ- and ω-exchange, and other non-resonance contribution, we will fit to the $\gamma\pi^0$ invariant mass spectrum to extract the contribution of non-resonance process. Since the ρ

TABLE IV: The expected numbers (N_i^{BG}) of backgrounds of $J/\psi \to \gamma\eta' \to \gamma\pi^0\pi^0\eta$ ($\eta \to \gamma\gamma$), $\gamma\eta' \to \gamma 3\pi^0$, $\gamma\eta' \to 3\gamma$ decays from the MC simulations, and the fitted signal yields (N_i^{obs}) for each $m^2_{\gamma\gamma}$ interval.

$M^2_{\gamma\gamma}$ $((GeV/c^2)^2)$	$[0., 0.01]$	$[0.01, 0.04]$	$[0.04, 0.0625]$	$[0.0625, 0.09]$	$[0.09, 0.1225]$	$[0.1225, 0.16]$
N_i^{BG}	20.2	74.4	94.3	102.6	101.2	95.5
N_i^{obs}	114±16	375±27	421 ± 25	370±24	394±24	405±24
$[0.16, 0.2025]$	$[0.2025, 0.25]$	$[0.25, 0.2809]$	$[0.2809, 0.3136]$	$[0.3136, 0.36]$	$[0.36, 0.4225]$	$[0.4225, 0.64]$
85.4	56.1	26.3	70.4	103.8	162.2	352.9
464±25	477±25	207±17	101±19	76±12	37±10	67±15

and ω mesons have same spin-parity (1^-) and closed nominal mass, we need consider the interference between ρ-exchange and ω-exchange. In the fit, the $\gamma\pi^0$ invariant mass spectrum is only chosen in the η' signal region as $0.933 \sim 0.988$ GeV/c^2, marked by the red solid-line with arrow in Fig. 21. The distribution of $m_{\gamma\pi^0}$ for Data and backgrounds are shown in Fig. 22. Because the two isolated photons couldn't distinguish in experiments, two entries for each event are put into one histogram.

The PDF of fit is written as:

$$\begin{aligned} & f \cdot \sigma \otimes [\varepsilon(M_{\gamma\pi^0}) \times |BW(\omega) + \alpha e^{i\theta} BW(\rho)|^2 \times E^3(\gamma^{\eta'}) E^3(\gamma^V) B^2(q_{\gamma\eta'}) B^2(q_{\gamma^V})] \\ & + (1-f) \cdot PDF(CombinatorialBG) + N_3 \cdot PDF(non-Resonance) + \\ & N_4 \cdot PDF(FixedBG) + N_5 \cdot PDF(\eta' Sideband). \end{aligned} \tag{1}$$

Here σ is the mass resolution determined from the MC of $\eta' \to \gamma\omega$, $\omega \to \gamma\pi^0$ decay, which generated with $\Gamma(\omega) = 0$ MeV; $\varepsilon(M_{\gamma\pi^0})$ is the detection efficiency curve obtained from the MC of $\eta' \to \gamma\rho^0$, $\rho^0 \to \gamma\pi^0$ decay, shown in Fig. 20. $BW(\omega)$ ($BW(\rho)$) is the relativistic Breit-Wigner formula: $\frac{1}{s-M^2+iM\Gamma_{tot}}$. In the fit, the M_ω, M_ρ and Γ_ω are fixed at 782.65 MeV, 134.98 MeV and 8.49 MeV using the PDG14 value [22], respectively; but for the total width of ρ meson, an expression dependent on the $\gamma\pi^0$ invariant mass is taken: $\Gamma_\rho(m) = \Gamma_\rho(M)\frac{M_\rho^2 q_\gamma^3(m)}{m^2 q_\gamma^3(M)}$, where M_ρ and $\Gamma_\rho(M)$ are the nominal mass and total width, and $q_\gamma^3(M/m)$ is the photon momentum of η' decay in the rest system of η' meson with mass of M/m. The parameter of $\alpha e^{i\theta}$ is the complex coupling constant. $E(\gamma^{\eta'})$ ($E(\gamma^V)$) is the photon energy of η' (V-vector meson) decay in the rest system of η' (V-vector) meson. $B(q_{\gamma\eta'/V})$

is the Blatt-Weisskopf barrier factor $B = \sqrt{\frac{2}{Q_0^2+q^2_{\gamma\eta'/V}}}$, where $Q_0 = 0.197221/R$ GeV/c with $R = 0.75$ (fm). The combinatorial background is the combination between the π^0 and the photon decaying from the η' ($m_{\gamma^V\pi^0}$), and the f represents the ratio of events between the coherent sum of ρ-ω contributions and the combinatorial backgrounds. The fixed backgrounds is from the sum of $\eta' \to \pi^0\pi^0\eta$, $\eta' \to 3\pi^0$, $\eta' \to 2\gamma$ decays. The η' sidebands are selected in the two regions of $1.008 \sim 1.058$ GeV/c^2 and $0.738 \sim 0.788$ GeV/c^2, marked by the blue solid-line with arrow in Fig. 21.

In the fit, the PDF of non-resonance process is extracted from MC simulation, which generated using VMD model with $\rho(1450)$- and $\omega(1650)$-exchange. The $\eta' \to \pi^0\pi^0\eta$, $\eta' \to \gamma 3\pi^0$, $\eta' \to 2\gamma$ backgrounds are fixed to MC simulations at their expected intensities, respectively. The PDF of combinatorial backgrounds is extracted from MC simulations of $\eta' \to \gamma\omega/\rho \to \pi^0\gamma\gamma$ decays. But the fraction f representing the ratio of yields between the coherent contribution of ρ-ω signals and the combinatorial backgrounds is fixed to be (0.5094 ± 0.020) from the MC simulation. The fitting range is $0.2 - 0.92$ GeV/c^2. In consideration of the low statistics of ρ signal events in this analysis and the relative reliable $Br(\eta' \to \gamma\rho)$ and $Br(\rho \to \gamma\pi^0)$ which be measured at SND using 36513 events of $e^+e^- \to \gamma\pi^0$ process in the energy region of $\sqrt{s} = 0.60 \sim 0.97$ GeV [36], we fix the parameter of α in our fit. The α can be determined with the expression of $\sqrt{\frac{Br(\rho)}{Br(\omega)} \times \frac{\varepsilon_\rho Int_\omega}{\varepsilon_\omega Int_\rho}}$, where $Br(\omega)$ ($Br(\eta' \to \gamma\omega) \times Br(\omega \to \gamma\pi^0) = (2.28 \pm 0.21) \times 10^{-3}$) and $Br(\rho)$ ($Br(\eta' \to \gamma\rho) \times Br(\rho \to \gamma\pi^0) = (1.76 \pm 0.38) \times 10^{-4}$) are the branching fractions of $\eta' \to \gamma\omega \to \pi^0\gamma\gamma$ and $\eta' \to \gamma\rho \to \pi^0\gamma\gamma$ decays; ε_ω (14.77%) and ε_ρ (14.29%) are the detection efficiencies in the fit range. The value of $Int_{\rho/\omega}$ is the integrations of ρ/ω-exchange PDF ($\sigma \otimes [\varepsilon(M_{\gamma\pi^0}) \times |BW(\rho/\omega)|^2 \times E^3(\gamma^{\eta'})E^3(\gamma^V)B^2(q_{\gamma^{\eta'}})B^2(q_{\gamma^V})]$) on the phase space. Thus the α can be calculated to be 1.03 ± 0.12. Fig. 22 shows the results of the fit to Data. In Fig. 22, the black points with error bars are the data; the red long dashed-line is from the $\eta' \to \gamma\omega \to \pi^0\gamma\gamma$ decay; the green long dashed-line is from the $\eta' \to \gamma\rho \to \pi^0\gamma\gamma$ decay; the blue long dashed-line is from the ρ-ω interference; the dotted line is from the non-resonance; the green short dashed line is from the η' sidebands; the blue short dashed line is from the $\eta' \to \pi^0\pi^0\eta$, $\eta' \to \gamma 3\pi^0$, $\eta' \to 2\gamma$ backgrounds; the pink dot-dashed line is from the combinatorial backgrounds. Using the integrations of PDFs on the phase space

and the covariance matrix, we can calculated the each events yields for ω signal, ρ signal and their interference. The fit yields of ω, ρ signals and non-resonance process are listed in Table V. In view of the accurate measurements on the branching fractions of $\eta' \to \gamma\omega$ and $\omega \to \gamma\pi^0$, in order to test the validity of our fit, we will give the branching ratio of cascade decay of $\eta' \to \gamma\omega$, $\omega \to \pi^0\gamma\gamma$.

TABLE V: Fitted yields of fit to $\gamma\pi^0$ invariant mass spectrum. Here ε_ω, ε_ρ and $\varepsilon_{non-Res.}$ are the detection efficiencies of $\eta' \to \gamma\omega \to \pi^0\gamma\gamma$, $\eta' \to \gamma\rho \to \pi^0\gamma\gamma$ decays and non-resonance process; θ is the interference phase; N_ω, N_ρ, $N_{Inter.}$ and $N_{non-Res.}$ are the fitted yields of ω decay, ρ decay, ρ-ω interference and the non-resonance process.

ε_ω	ε_ρ	$\varepsilon_{non-Res.}$	α	θ	N_ω	N_ρ	$N_{Inter.}$	$N_{non-Res.}$
14.77%	14.29%	15.92%	1.03	0.93 ± 0.19	2350 ± 71	174±5	159±90	670±67

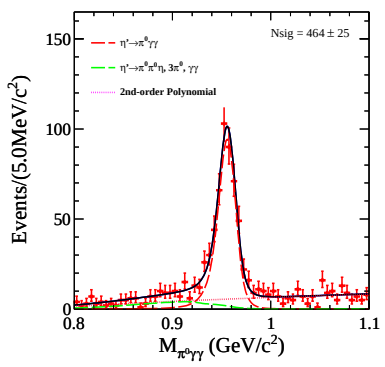

(a)$0.16 < M^2_{\gamma\gamma} < 0.2025\ (GeV/c^2)^2$.

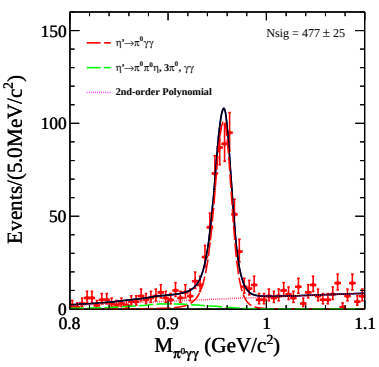

(b)$0.2025 < M^2_{\gamma\gamma} < 0.25\ (GeV/c^2)^2$.

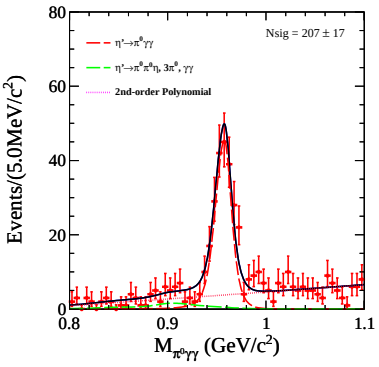

(c)$0.25 < M^2_{\gamma\gamma} < 0.2809\ (GeV/c^2)^2$.

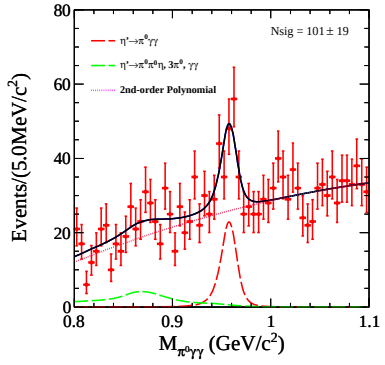

(d)$0.2809 < M^2_{\gamma\gamma} < 0.3136\ (GeV/c^2)^2$.

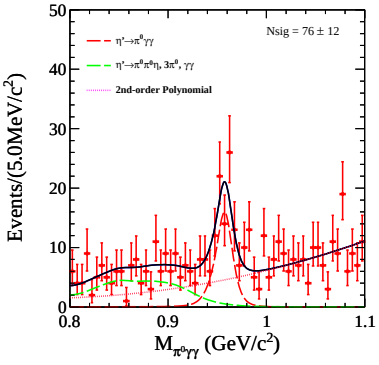

(e)$0.3136 < M^2_{\gamma\gamma} < 0.36\ (GeV/c^2)^2$.

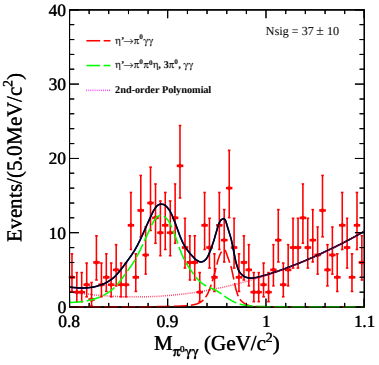

(f)$0.36 < M^2_{\gamma\gamma} < 0.4225\ (GeV/c^2)^2$.

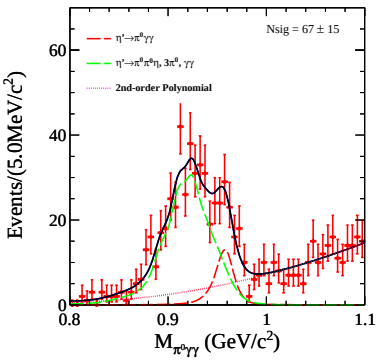

(g)$0.4225 < M^2_{\gamma\gamma} < 0.64\ (GeV/c^2)^2$.

FIG. 19: η' fitting results for these bins ($(GeV/c^2)^2$): (a) $M^2_{\gamma\gamma} \subset (0.0, 0.01)$; (b) $M^2_{\gamma\gamma} \subset (0.01, 0.04)$; (c) $M^2_{\gamma\gamma} \subset (0.04, 0.0625)$; (d) $M^2_{\gamma\gamma} \subset (0.0625, 0.09)$; (e) $M^2_{\gamma\gamma} \subset (0.09, 0.1225)$; (f) $M^2_{\gamma\gamma} \subset (0.1225, 0.16)$.

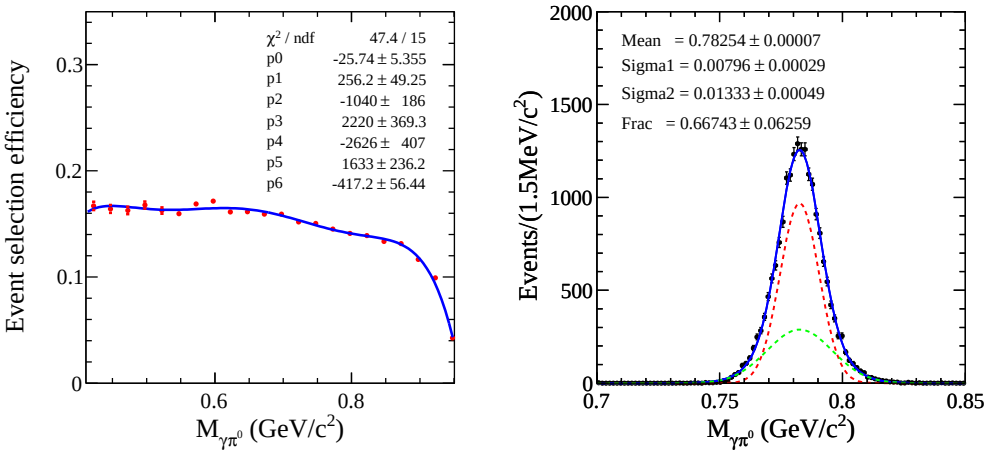

(a)Efficiency curve. (b)Mass resolution.

FIG. 20: Detection efficiency curve obtained from the MC of $J/\psi \to \gamma\eta'$, $\eta' \to \gamma\rho \to \pi^0\gamma\gamma$ and mass resolution determined from the MC of $J/\psi \to \gamma\eta'$, $\eta' \to \gamma\omega \to \pi^0\gamma\gamma$ generated with $\Gamma = 0$ MeV.

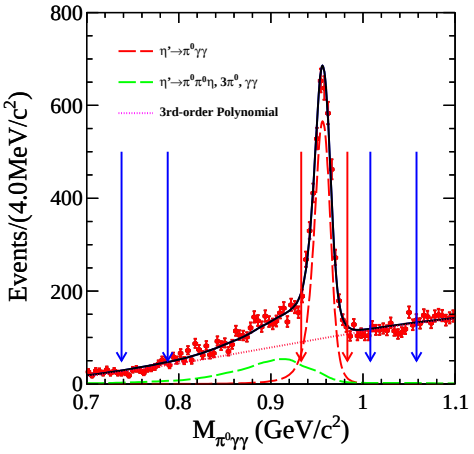

FIG. 21: η' signal region and sidebands. The signal region ($0.933 \sim 0.988$ GeV/c^2) is assigned with the red solid-lines with arrow; the η' sidebands ($1.008 \sim 1.058$ GeV/c^2 and $0.738 \sim 0.788$ GeV/c^2) are marked with blue solid-lines with arrow.

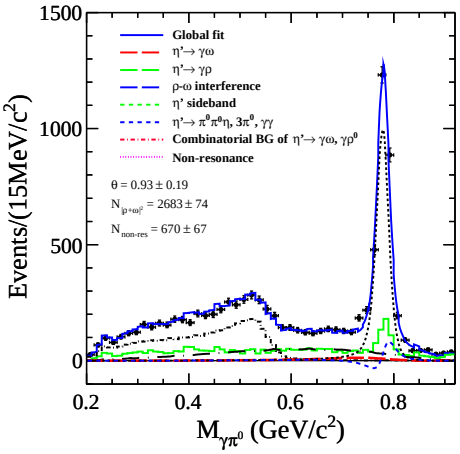

FIG. 22: Fitting results of $\pi^0\gamma$ invariant mass spectrum. Here $N_{|\rho+\omega|^2}$ means the total events of ω-exchange, ρ-exchange and their interference.

IX. SYSTEMATIC ERROR ANALYSIS

A. Photon Efficiency

The uncertainty due to photon reconstruction is about 1% per photon [37]. This is determined from studies of photon detection efficiencies in the process of $J/\psi \to \rho^0\pi^0$, $\rho^0 \to \pi^+\pi^-$, $\pi^0 \to \gamma\gamma$. Thus the total systematic error of five photons in this analysis is 5%.

B. $N_\gamma = 5$

We choose $J/\psi \to \gamma\eta' \to \gamma\gamma\omega$, $\omega \to \gamma\pi^0$ as control sample to estimate the systematic error of selection efficiency of good photons with $N_\gamma = 5$. The event selection is as follow:

- No good charged track is reconstructed from MDC ($R_{xy} < 1$ cm, $|z| < 10$ cm, $|cos\theta| < 0.93$);
- Good photon selection: for barrel, $|cos\theta|$ <0.8, $E > 25.0$ MeV; for end cap, $0.86 < |cos\theta| < 0.92$, $E > 50.0$ MeV; $5 \leq N_\gamma \leq 8$;
- Do five constants kinematic fit and require $\chi^2_{5\mathrm{C}} < 30$. Here π^0 is reconstructed by one pair of photons excluding the photon with maximum energy;
- In order to suppress the multi-π^0 backgrounds (mainly from $J/\psi \to \gamma\pi^0\pi^0$ backgrounds), we veto π^0 for the other photons (including the photon which don't pass the requirement of 5C kinematic fit) except for the two photons used to reconstruct π^0 candidate by $|M_{\gamma\gamma} - M_{\pi^0}| > 18$ MeV. In order to suppress the multi-π^0 backgrounds and remove the miss-combination of π^0 candidate, the γ veto is performed by requiring $|M_{\gamma\gamma^{\pi^0}} - M_{\pi^0}| > 18$ MeV/c^2, namely each photon γ^{π^0} used to reconstruct signal π^0 candidate is not allowed to form additional π^0 with any other photons (including the photon which don't pass the requirement of 5C kinematic fit);
- Select the best ω candidate by $|M_{\gamma\pi^0} - M_\omega| < 30$ MeV/c^2 and require $P_{\gamma\pi^0} > 0.7$ GeV;
- In order to remove $J/\psi \to \omega\eta$ background, select a best η candidate with the minimum value of $|M_{\gamma\gamma} - M_\eta|$ and require the recoiling mass of η doesn't fall in ω mass region ($|Recmass(\eta) - M_\omega| > 30$ MeV);

- Select the η' candidate by requiring the minimum value of $|M_{\gamma\omega} - M_{\eta'}|$;

The selection efficiency of good photons with $N_\gamma = 5$ is defined as:

$$\varepsilon = \frac{N^{'}}{N}, \tag{2}$$

where N is the number of total events; $N^{'}$ is only the number of events with $N_\gamma = 5$. The obtained N_γ distribution is shown in Fig. 23. From the plot, one can obtain that the systematic error from selection of good photons with $N_\gamma = 5$ is about 0.5%.

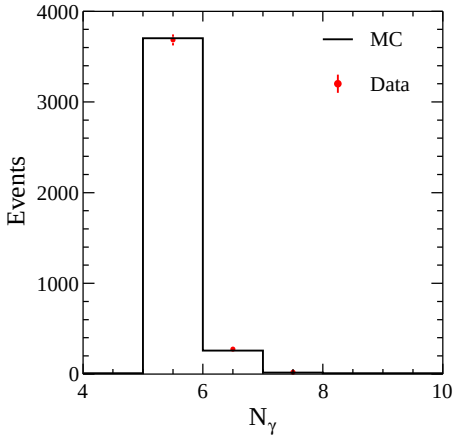

FIG. 23: Good photon distribution of $J/\psi \to \gamma\eta' \to \gamma\gamma\omega$, $\omega \to \gamma\pi^0$ control sample.

C. 5C Fit

We choose $J/\psi \to \gamma\eta' \to \gamma\gamma\omega$, $\omega \to \gamma\pi^0$ as control sample to estimate the systematic error of five constraints kinematic fit. The event selection is as follow:

- No good charged track is reconstructed from MDC ($R_{xy} < 1$ cm, $|z| < 10$ cm, $|cos\theta| < 0.93$);

- Good photon selection:

  for barrel, $|cos\theta|$ <0.8, $E > 25.0$ MeV;

  for end cap, $0.86 < |cos\theta|$ <0.92, $E > 50.0$ MeV;

  $N_\gamma = 5$;

- With the purpose of improving the resolution of η', we do five constraints kinematic fit and require $\chi^2_{5C} < 800$. After the requirement of $\chi^2_{5C} < 800$, about 0.1% signal events will be lost, which is negligible in the estimation of the systematic error. Here the π^0 is reconstructed by one pair of photons excluding the photon with maximum energy;

- In order to suppress the multi-π^0 backgrounds (mainly from $J/\psi \to \gamma\pi^0\pi^0$ backgrounds), we veto π^0 for the three photons except for the two photons used to reconstruct π^0 candidate by $|M_{\gamma\gamma} - M_{\pi^0}| > 18$ MeV. In order to suppress the multi-π^0 backgrounds and remove the miss-combination of π^0 candidate, the γ veto is performed by requiring $|M_{\gamma\gamma^{\pi^0}} - M_{\pi^0}| > 18$ MeV/c^2, namely each photon γ^{π^0} used to reconstruct signal π^0 candidate is not allowed to form additional π^0 with any other three photons;

- Select the best ω candidate by $|M_{\gamma\pi^0} - M_\omega| < 30$ MeV/c^2 and require $P_{\gamma\pi^0} > 0.7$ GeV;

- In order to remove $J/\psi \to \omega\eta$ background, select a best η candidate with the minimum value of $|M_{\gamma\gamma} - M_\eta|$ and require the recoiling mass of η doesn't fall in ω mass region ($|Recmass(\eta) - M_\omega| > 30$ MeV);

- Select the η' candidate by requiring the minimum value of $|M_{\gamma\omega} - M_{\eta'}|$;

The 5C fit efficiency is defined as:

$$\varepsilon = \frac{N_{X_i}}{N}, \tag{3}$$

where N is the number of total events; N_{X_i} is the number of events with $\chi^2_{5C} \leq X_i$. The obtained χ^2_{5C} distributions, fitted results for MC and Data are shown in Fig. 24 and Fig. 25, respectively. Therefore the efficiencies of kinematic fit is depicted in Fig. 26. From the plot, one can get that the systematic error from five constraints kinematic fit is determined about 3.8% (2.7%) for η fit (η' fit) through the calculation of the MC-Data difference of efficiencies. Here the errors of fit to Data have been considered.

D. Signal Shape

In the fit to η or η', since the signal PDF is extracted from the MC simulation, the possible discrepancy is described by a smearing Gaussian, where a non-zero σ represents the MC-data difference in the mass resolution. The differences of yields will provide the

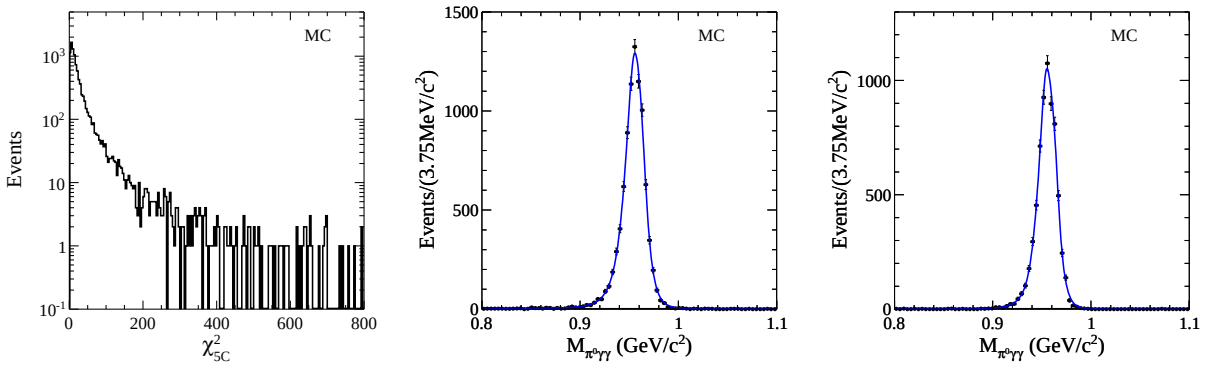

(a)χ^2_{5C} distribution of MC. (b)$\pi^0\gamma\gamma$ invariant spectrum of MC with $\chi^2_{5C} < 800$. (c)$\pi^0\gamma\gamma$ invariant spectrum of MC with $\chi^2_{5C} < 30$.

FIG. 24: χ^2_{5C} distribution and $\pi^0\gamma\gamma$ invariant spectra of MC for $J/\psi \to \gamma\eta' \to \gamma\gamma\omega$, $\omega \to \gamma\pi^0$ control sample.

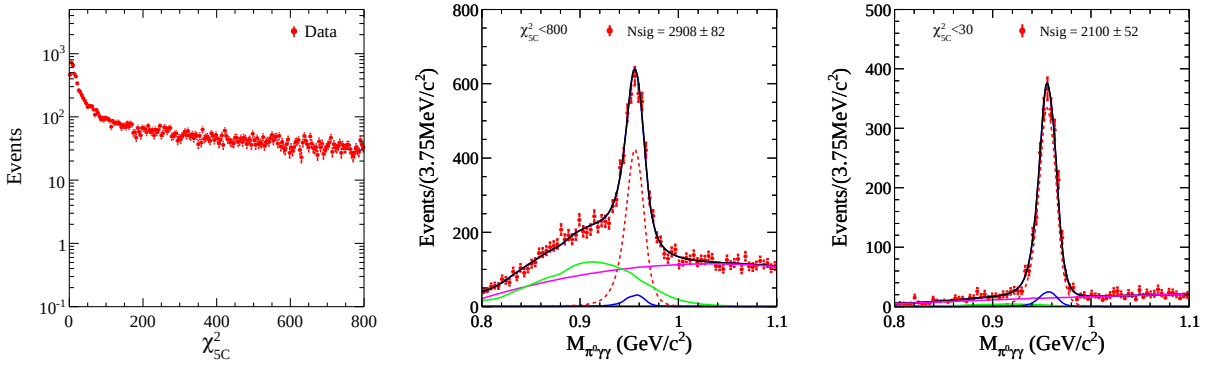

(a)χ^2_{5C} distribution of Data. (b)$\pi^0\gamma\gamma$ invariant spectrum of Data with $\chi^2_{5C} < 800$. (c)$\pi^0\gamma\gamma$ invariant spectrum of Data with $\chi^2_{5C} < 30$.

FIG. 25: χ^2_{5C} distribution and $\pi^0\gamma\gamma$ invariant spectra of Data. In (b) and (c), the Blue line is the sum of normalized peaking backgrounds of η' decay: $J/\psi \to \gamma\eta' \to \gamma\gamma\rho^0$ ($\rho^0 \to \gamma\pi^0$) and $J/\psi \to \gamma\eta'$, $\eta' \to \pi^0\gamma\gamma$; Green line is the sum of normalized non-peaking backgrounds of η' decays: $J/\psi \to \gamma\eta' \to \gamma\pi^0\pi^0\eta$ ($\eta \to \gamma\gamma$), $\gamma\eta' \to 3\gamma$ and $\gamma\eta' \to \gamma 3\pi^0$.

systematic errors due to signal shape. Here the σ is obtained from the $J/\psi \to \gamma\eta' \to \gamma\gamma\omega$, $\omega \to \gamma\pi^0$ control sample. The event selection is as follow:

- No good charged track is reconstructed from MDC ($R_{xy} < 1$ cm, $|z| < 10$ cm, $|cos\theta| < 0.93$);
- Good photon selection:

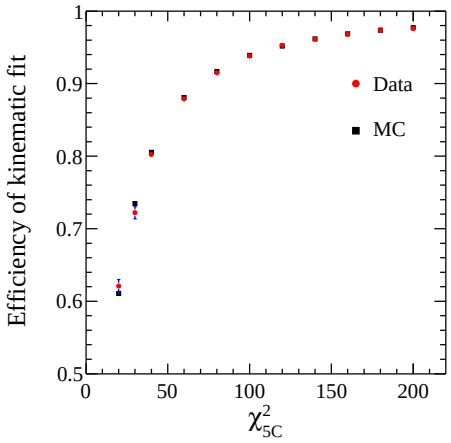

FIG. 26: Efficiencies of five constraints kinematic fit for $J/\psi \to \gamma\eta' \to \gamma\gamma\omega$, $\omega \to \gamma\pi^0$ control sample. Black rectangles are from MC, Red points are from Data.

for barrel, $|cos\theta|$ <0.8, $E > 25.0$ MeV;

for end cap, $0.86 < |cos\theta|$ <0.92, $E > 50.0$ MeV;

$N_\gamma = 5$;

- Do five constraints kinematic fit and require $\chi^2_{5C} < 30$. Here the π^0 is reconstructed by one pair of photons excluding the photon with maximum energy;

- In order to suppress the multi-π^0 backgrounds (mainly from $J/\psi \to \gamma\pi^0\pi^0$ backgrounds), we veto π^0 for the three photons except for the two photons used to reconstruct π^0 candidate by $|M_{\gamma\gamma} - M_{\pi^0}| > 18$ MeV. In order to suppress the multi-π^0 backgrounds and remove the miss-combination of π^0 candidate, the γ veto is performed by requiring $|M_{\gamma\gamma^{\pi^0}} - M_{\pi^0}| > 18$ MeV/c^2, namely each photon γ^{π^0} used to reconstruct signal π^0 candidate is not allowed to form additional π^0 with any other three photons;

- Select the best ω candidate by $|M_{\gamma\pi^0} - M_\omega| < 30$ MeV/c^2;

- In order to remove $J/\psi \to \omega\eta$, $\omega \to \gamma\pi^0$ background, select a best η candidate with the minimum value of $|M_{\gamma\gamma} - M_\eta|$ and require the recoiling mass of η doesn't fall in ω mass region ($|Recmass(\eta) - M_\omega| > 30$ MeV);

- Select the η' candidate by requiring the minimum value of $|M_{\gamma\omega} - M_{\eta'}|$;

After the above selection, the $\gamma\omega$ invariant mass distributions for MC and Data are shown in Fig. 27 (a) and Fig. 27 (b), respectively. Here the fit PDF is consisted of the signal MC shape convolution a Gaussian function with a fixed width of 1.5 MeV, where the width of Gaussian function represents the MC-data difference of mass resolution, the MC shape describing the peaking backgrounds of η' decay: $J/\psi \to \gamma\eta' \to \gamma\gamma\rho^0$ ($\rho^0 \to \gamma\pi^0$) and $J/\psi \to \gamma\eta'$, $\eta' \to \pi^0\gamma\gamma$ and a second-order Chebychev Polynomial depicting the other backgrounds. The fitting results are displayed in Fig. 27(b). From the picture, one can obtain that the value of σ is about 1.5 MeV. Thus the systematic error for η (η') fit will be obtained through refit to $\pi^0\gamma\gamma$ invariant mass with the signal PDF smearing a Gaussian function with the fixed width of 1.5 MeV. The refitting situations and systematic errors are shown in Fig. 27 (c)-(d) and Table XX, respectively.

For the measurement of $\mathrm{d}\Gamma(\eta' \to \pi^0\gamma\gamma)/\mathrm{d}m^2_{\gamma\gamma}$, the re-fitting results for each $m^2_{\gamma\gamma}$ interval are shown in APPENDIX A. And the corresponding systematic errors estimated from the changed fitted yields are listed in Table VI.

TABLE VI: Systematic errors due to the signal shape for the measurements of $\mathrm{d}\Gamma(\eta' \to \pi^0\gamma\gamma)/\mathrm{d}m^2_{\gamma\gamma}$. Here N_i^{obs} and σ_i are the fitted signal yields and the systematic error for each $m^2_{\gamma\gamma}$ interval, respectively.

$M^2_{\gamma\gamma}$ $((GeV/c^2)^2)$	$[0., 0.01]$	$[0.01, 0.04]$	$[0.04, 0.0625]$	$[0.0625, 0.09]$	$[0.09, 0.1225]$	$[0.1225, 0.16]$
N_i^{obs}	116±17	381±27	423 ± 25	371±24	395±25	409±25
σ_i	1.8%	1.6%	0.5%	0.3%	0.3%	1.0%
$[0.16, 0.2025]$	$[0.2025, 0.25]$	$[0.25, 0.2809]$	$[0.2809, 0.3136]$	$[0.3136, 0.36]$	$[0.36, 0.4225]$	$[0.4225, 0.64]$
466±25	479±25	209±17	102±19	78±13	38±10	66±15
0.2%	0.4%	1.0%	1.0%	2.0%	1.4%	0.8%

In the fit to $M_{\gamma\pi^0}$, the mass resolution is fixed from the MC simulations. In order to estimate the systematic error due to the discrepancy of Data-MC mass resolution, we do an alternative fit with fixed ratio between the two Gaussian functions but with free widths. Fig. 28 shows the fitting results, and the fit yields for ω signal events and non-resonance process are listed in Table VII. The varied yields of 0.1% (1.8%) for ω-contribution (non-resonant process) will be taken as the systematic uncertainty.

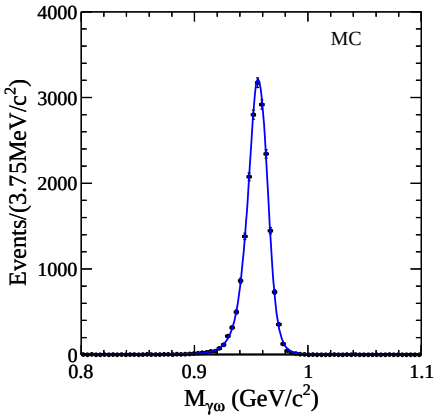

(a)$\gamma\omega$ invariant mass spectrum of MC.

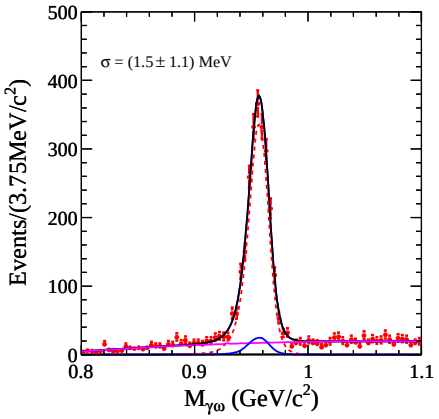

(b)$\gamma\omega$ invariant mass spectrum and fitting results of Data.

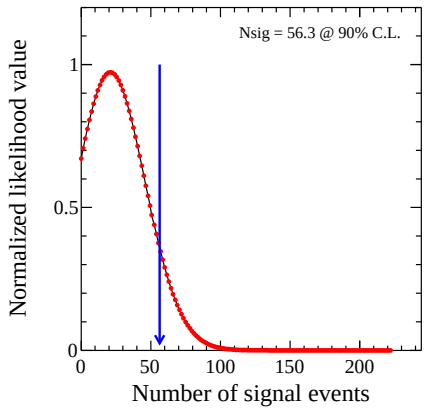

(c)Likelihood distribution as a function of the signal yield for η refit.

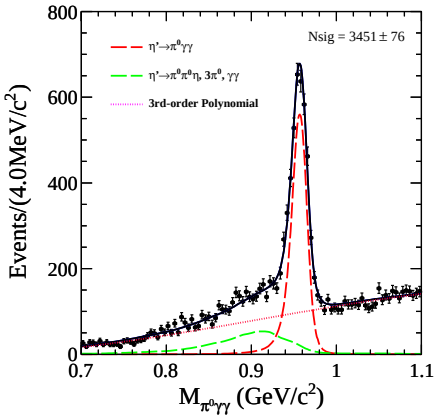

(d)η' refit results.

FIG. 27: (a)-(b): Discrepancy of mass resolution between MC and Data reckoned with $J/\psi \to \gamma\eta' \to \gamma\gamma\omega$, $\omega \to \gamma\pi^0$ control sample; (c)-(d): η and η' refit results in consideration of MC-Data difference for mass resolution. In (b), the Blue line is the sum of normalized peaking backgrounds of η' decay: $J/\psi \to \gamma\eta' \to \gamma\gamma\rho^0$ ($\rho^0 \to \gamma\pi^0$) and $J/\psi \to \gamma\eta'$, $\eta' \to \pi^0\gamma\gamma$.

TABLE VII: Fitted yields of fit to $M_{\gamma\pi^0}$ with float widths of detection mass resolution. Here θ is the interference phase; N_ω and $N_{non-res}$ are the fitted yields of ω signal events and non-resonance process.

θ	N_ω	$N_{non-res}$
0.95 ± 0.19	2350 ± 71	682 ± 68

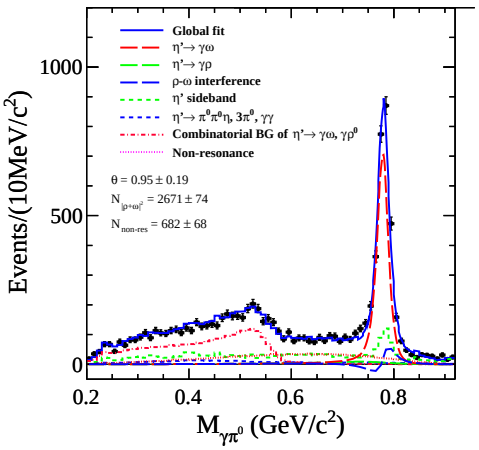

FIG. 28: Fitting results of $\pi^0\gamma$ invariant mass spectrum with float widths of detect--ion mass resolution.

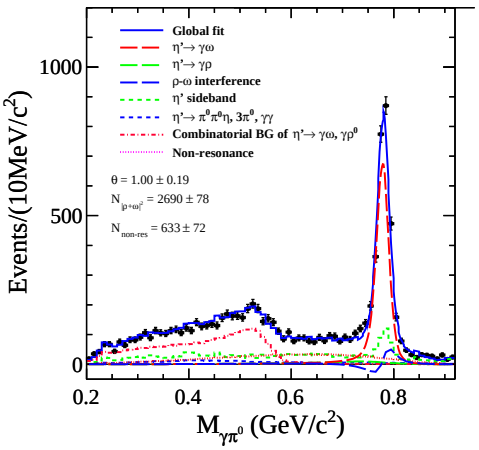

FIG. 29: Fitting results of $\pi^0\gamma$ invariant mass spectrum with $R = 0.35$ (fm).

For the normal fit to $\gamma\pi^0$ invariant mass spectrum, the parameter of R for Blatt-Weisskopf barrier factor is taken at 0.75 (fm). An alternative fit is to change the parameter of R from 0.75 (fm) to 0.35 (fm). The difference of yields (1.5% for ω and 1.0% for non-resonance) will be considered as the systematic error arising from the signa model, see Table XX. The fitting results is shown in Fig. 29. The Table VIII listed the fit yields for ω signal events and non-resonance process.

TABLE VIII: Fitted yields of fit to $M_{\gamma\pi^0}$ with $R = 0.35$ (fm). Here θ is the interference phase; N_ω and $N_{non-res}$ are the fitted yields of ω signal events and the non-resonance process.

θ	N_ω	$N_{non-res}$
1.00 ± 0.19	2385 ± 73	663 ± 72

E. Signal model

For $\eta \to \pi^0\gamma\gamma$ mode, the detection efficiency is determined with MC simulation by assuming an angular distribution with phase space. Just as statement in the introduction, the decay of $\eta \to \pi^0\gamma\gamma$ has been studied in the framework of different theoretical models, especially for χPTh and VMD model. Here it needs to point out that, in χPTh calculation,

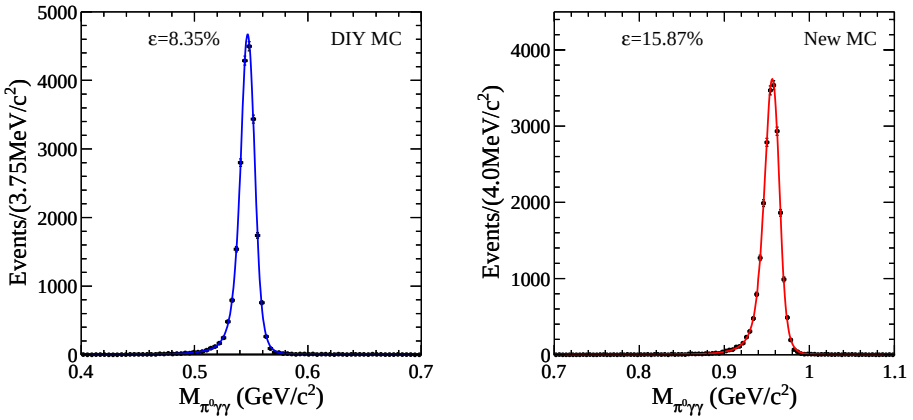

(a)$\pi^0\gamma\gamma$ invariant mass spectrum of new MC for η signal.

(b)$\pi^0\gamma\gamma$ invariant mass spectrum of new MC for η' signal.

FIG. 30: $\pi^0\gamma\gamma$ invariant mass spectra of new MCs generated with VMD model for η mode and with the coherent sum of ρ- and ω-exchange for η' mode.

the contribution from vector meson exchange is dominant. Therefore we regenerated the decay process based on the amplitude formulism of VMD model [12]. Here only these vector mesons above the η mass threshold are considered, namely ρ^0- and ω-exchange. The difference of efficiency between the new MC and phase space MC is taken as the systematic error from MC model. The $\pi^0\gamma\gamma$ invariant mass spectra from the new MC after correcting the angular distribution are shown in Fig. 30(a).

For $\eta' \to \pi^0\gamma\gamma$ mode, the detection efficiency is determined with MC simulation by assuming an incoherent sum of ρ-, ω-exchange and the off-shell vector meson exchange ($\rho(1450)$ and $\omega(1650)$). Whereas actually, there exist a negligible contribution between the ρ- and ω-exchange. Thus we generate the signal MC again with considering the interference of ρ- and ω-exchange and varying the ratio of $\rho(1450)$- and $\omega(1650)$-exchange within a reasonable error. The efficiency difference of 1.3% between the new MC and the MC without the interference of ρ- and ω-exchange is taken as the systematic error from MC model. The $\pi^0\gamma\gamma$ invariant mass spectra is shown in Fig. 30(b). In addition, the VMD is replaced with an uniform angular distribution to generated the non-resonance process. The efficiency difference of 1.1% is as well taken as the systematic error from the signal model. The systematic errors arising from the MC model for η and η' mode are listed in Table XX.

We simulate the non-resonance process using a uniform angular distribution, and use the

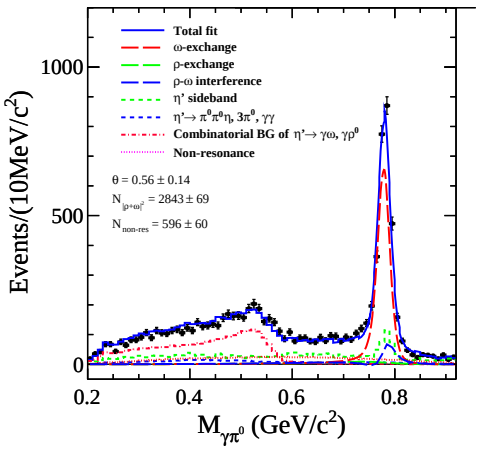

FIG. 31: Fitting results of $\pi^0\gamma$ invariant mass spectrum with the non-resonance process described from the PHSP MC.

new MC sample to describe the PDF of non-resonance process. Fig. 31 shows the fitting results, and the ω signal events, event selection efficiency and fitted signal yield for non-resonance process are listed in Table IX. The difference of 1.2% (4.2%) for the measured branching fractions of ω-contribution (non-resonant process) will be as well taken as the systematic uncertainty due to the signal shape, see Table XX.

TABLE IX: Fitted yields of fit to $M_{\gamma\pi^0}$ with the PDF of non-resonant process described from a PHSP MC samples. Here $\varepsilon_{non-res}$ is the detection efficiencies determined by the PHSP MC; N_ω and $N_{non-res}$ are the fitted yields of ω signal events and the non-resonance process.

$\varepsilon_{non-res}$	θ	N_ω	$N_{non-res}$
14.79%	0.56 ± 0.14	2321 ± 57	596±60

F. Fit Range

The systematic uncertainties due to the fitting range are evaluated by changing the fitting ranges from $0.4-0.7$ GeV/c^2 to $0.43-0.67$ GeV/c^2 (η), and from $0.7-1.1$ GeV/c^2 to $0.8-1.1$ GeV/c^2 (η'), respectively. The changes in yields for these variations give systematic uncertainties due to the chooses of fitting range. The re-fitting results are shown in Fig. 32. So the systematic errors due to the fitting range are listed in Table XX.

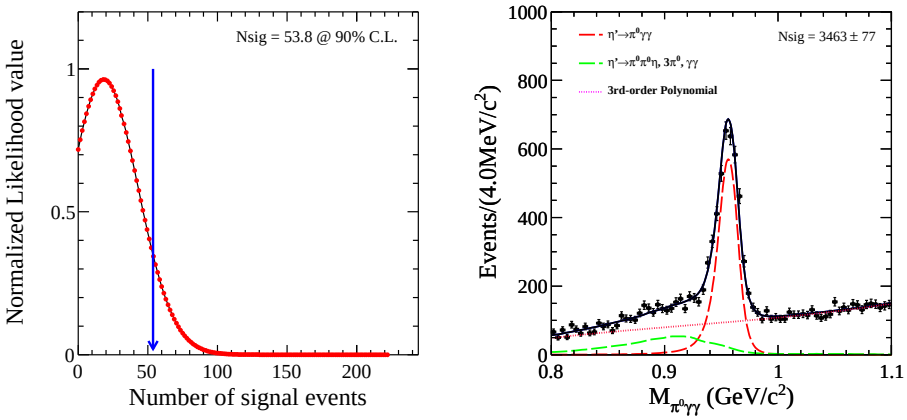

(a)Likelihood distribution as a function of the signal yield for η refit.

(b)η' refitting results.

FIG. 32: η and η' refit results with the varied fit ranges.

For the measurement of $\mathrm{d}\Gamma(\eta' \to \pi^0\gamma\gamma)/\mathrm{d}m^2_{\gamma\gamma}$, the re-fitting results with changing the fit range from $0.8 - 1.1$ GeV/c^2 to $0.83 - 1.1$ GeV/c^2 are shown in APPENDIX B. And the corresponding systematic errors calculated from the varied fitted yields are tabulated in Table X.

TABLE X: Systematic errors due to the fitting range for the measurements of $\mathrm{d}\Gamma(\eta' \to \pi^0\gamma\gamma)/\mathrm{d}m^2_{\gamma\gamma}$.

$M^2_{\gamma\gamma}$ $((GeV/c^2)^2)$	$[0., 0.01]$	$[0.01, 0.04]$	$[0.04, 0.0625]$	$[0.0625, 0.09]$	$[0.09, 0.1225]$	$[0.1225, 0.16]$
N_i^{obs}	115±17	379±28	423 ± 25	376±24	399±25	400±25
σ_i	0.9%	1.1%	0.5%	1.6%	1.3%	1.3%
$[0.16, 0.2025]$	$[0.2025, 0.25]$	$[0.25, 0.2809]$	$[0.2809, 0.3136]$	$[0.3136, 0.36]$	$[0.36, 0.4225]$	$[0.4225, 0.64]$
457±25	475±25	203±17	98±20	72±12	35±10	70±16
1.5%	0.4%	1.9%	2.5%	4.6%	4.1%	3.7%

For the fit to $\gamma\pi^0$ invariant mass spectrum, the systematic uncertainty due to the fit range is estimated by changing the range from $0.20 \sim 0.92$ GeV/c^2 to $0.30 \sim 0.92$ GeV/c^2. It need to point out that since the event selection efficiencies are lightly varied, the parameter of α will be determined to be 1.04 ± 0.12 again. And the parameter f related with the ratio of yields between the coherent contribution of ρ-ω signals and the combinatorial backgrounds is fixed to be (0.5364 ± 0.0268). The fitting situation, fit yields of ω signal events and non-

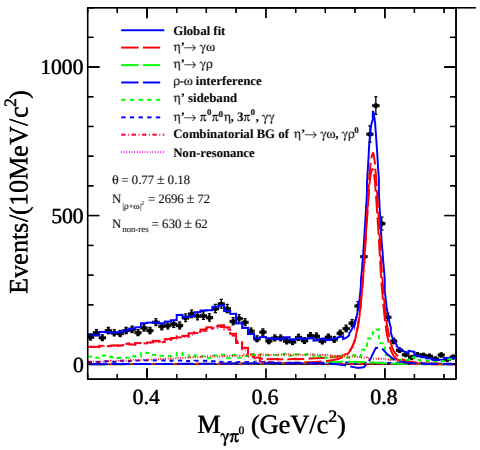

FIG. 33: Fitting results of $\pi^0\gamma$ invariant mass spectrum with fitting range of $0.30 \sim 0.92$ GeV/c^2.

resonance process are shown in Fig. 33 and Table XI. The varied yields will be considered as the systematic error (2.6% for ω and 2.9% for non-resonance) coming from the fit range, see Table XX.

TABLE XI: Fitted yields of fit to $M_{\gamma\pi^0}$ with fitting range of $0.30 \sim 0.92$ GeV/c^2. Here ε_ω, ε_ρ and $\varepsilon_{non-res}$ are the detection efficiencies of $\eta' \to \gamma\omega \to \pi^0\gamma\gamma$, $\eta' \to \gamma\rho \to \pi^0\gamma\gamma$ decays and non-resonance process; θ is the interference phase; N_ω and $N_{non-res}$ are the fitted yields of ω signal events and the non-resonance process.

ε_ω	ε_ρ	$\varepsilon_{non-res}$	α	θ	N_ω	$N_{non-res}$
14.74%	14.26%	15.42%	1.04	0.77 ± 0.18	2284 ± 64	630±62

G. α

In the fit to $M_{\gamma\pi^0}$, the parameter of α is fixed in middle mean. We will vary it from 0.91 to 1.15 to estimate the systematic error due to the parameter of α. The fitting situation is shown in Fig. 34. The fit yields of ω signal events and non-resonance process are summarized in Table XII. The maximum difference of yields between the two fits and the normal fit will be considered as the systematic error (1.8% for ω and 6.7% for non-resonance) arising from the parameter of α, see Table XX.

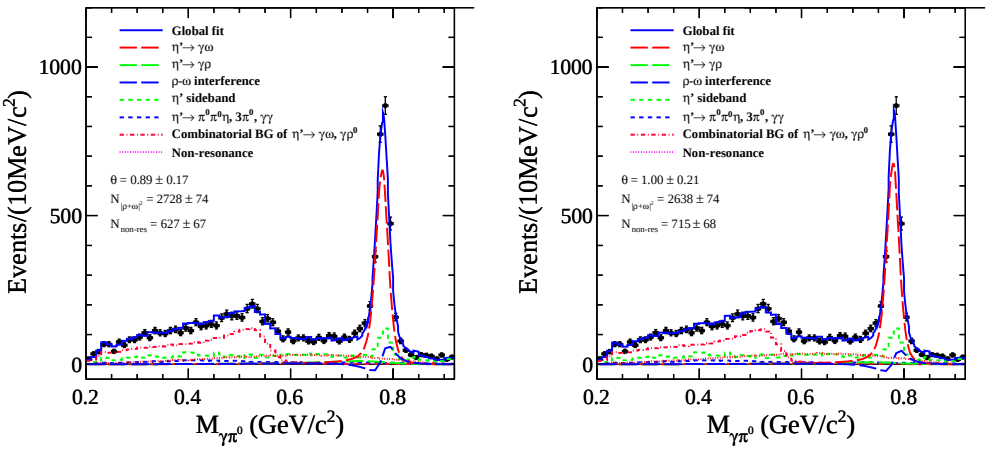

(a)$\alpha = 1.15$. (b)$\alpha = 0.91$.

FIG. 34: Fitting results of $\pi^0\gamma$ invariant mass spectrum with different parameters of α.

TABLE XII: Fitted yields of fit to $M_{\gamma\pi^0}$ with different parameter of α. Here θ is the interference phase; N_ω and $N_{non-res}$ are the fitted yields of ω decay and the non-resonance process.

α	θ	N_ω	$N_{non-res}$
1.15	0.89 ± 0.17	2312 ± 68	627±67
α	θ	N_ω	$N_{non-res}$
0.91	1.00 ± 0.21	2392 ± 73	715±68

H. f

In the fit to $M_{\gamma\pi^0}$, the parameter f related with ratio of yields between the coherent contribution of ρ-ω signals and the combinatorial backgrounds is fixed to be 0.5094 from the MC simulation. We will let it to be free to estimate the systematic error due to the fixed ratio. The fitting results are shown in Fig. 35 and summarized in Table XIII. The maximum difference of yields between the fits and the normal fit will be considered as the systematic error (3.3% for ω and 2.1% for non-resonance) arising from the parameter of fixed ratio, see Table XX.

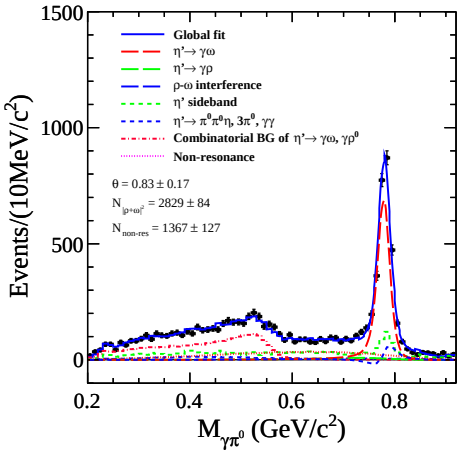

FIG. 35: Fitting results of $\pi^0\gamma$ invariant mass spectrum with free yield of combinatorial backgrounds.

TABLE XIII: Fitted yields of fit to $M_{\gamma\pi^0}$ with free yield of combinatorial backgrounds. Here θ is the interference phase; N_ω and $N_{non-res}$ are the fitted yields of ω decay and the non-resonance process.

θ	N_ω	$N_{non-Res.}$
0.83 ± 0.17	2427 ± 71	684±64

I. π^0 and γ veto

The systematic error due to π^0 and γ veto is estimated from the $J/\psi \to \gamma\eta' \to \gamma\gamma\omega$, $\omega \to \gamma\pi^0$ control sample. The event selection is as follow:

- No good charged track is reconstructed from MDC ($R_{xy} < 1$ cm, $|z| < 10$ cm, $|cos\theta| < 0.93$);
- Good photon selection:

  for barrel, $|cos\theta|$ <0.8, $E > 25.0$ MeV;

  for end cap, $0.86 < |cos\theta|$ <0.92, $E > 50.0$ MeV;

  $N_\gamma = 5$;
- Do five constraints kinematic fit and require $\chi^2_{5C} < 30$. Here the π^0 is reconstructed by one pair of photons excluding the photon with maximum energy;

- In order to suppress the multi-π^0 backgrounds (mainly from $J/\psi \to \gamma\pi^0\pi^0$ backgrounds), we veto π^0 for the three photons except for the two photons used to reconstruct π^0 candidate by $|M_{\gamma\gamma} - M_{\pi^0}| > 18/15/21$ MeV. In order to suppress the multi-π^0 backgrounds and remove the miss-combination of π^0 candidate, the γ veto is performed by requiring $|M_{\gamma\gamma^{\pi^0}} - M_{\pi^0}| > 18/15/21$ MeV/c^2, namely each photon γ^{π^0} used to reconstruct signal π^0 candidate is not allowed to form additional π^0 with any other three photons;

- Select the best ω candidate by $|M_{\gamma\pi^0} - M_{\omega}| < 30$ MeV/c^2;

- In order to remove $J/\psi \to \omega\eta$, $\omega \to \gamma\pi^0$ background, select a best η candidate with the minimum value of $|M_{\gamma\gamma} - M_{\eta}|$ and require the recoiling mass of η doesn't fall in ω mass region ($|Recmass(\eta) - M_{\omega}| > 30$ MeV);

- Select the η' candidate by requiring the minimum value of $|M_{\gamma\omega} - M_{\eta'}|$;

After the above selection, the $\gamma\omega$ invariant mass distributions with different mass windows of π^0 and γ veto for signal MC and Data are shown in Fig. 36 and Fig. 37, respectively. Here the fit PDF is consisted of the signal MC shape convolution a Gaussian function, the MC shape describing the peaking backgrounds of η' decay: $J/\psi \to \gamma\eta' \to \gamma\gamma\rho^0$ ($\rho^0 \to \gamma\pi^0$) and $J/\psi \to \gamma\eta'$, $\eta' \to \pi^0\gamma\gamma$ and a second-order Chebychev Polynomial depicting the other backgrounds. The fitting results are listed in Table XIV. The difference of the ratio of N_{Data}/N_{MC} between 18 MeV mass window of π^0 and γ veto and 15/21 MeV mass window of π^0 and γ veto is estimated as the systematic uncertainty due to the π^0 and γ veto. From Table XIV, we can obtain the systematic error due to the π^0 and γ veto is about 1.0%.

TABLE XIV: Fitted yields of η' signal events for control sample: $J/\psi \to \gamma\eta' \to \gamma\gamma\omega$, $\omega \to \gamma\pi^0$ with different mass windows of π^0 and γ veto.

Mass window of π^0 and γ veto	Signal MC (N_{MC})	Data (N_{Data})
$\|M_{\gamma\gamma^*} - M_{\pi^0}\| > 18$ MeV	19726	2093 ± 52
$\|M_{\gamma\gamma^*} - M_{\pi^0}\| > 15$ MeV	20796	2187 ± 54
$\|M_{\gamma\gamma^*} - M_{\pi^0}\| > 21$ MeV	18757	1991 ± 51

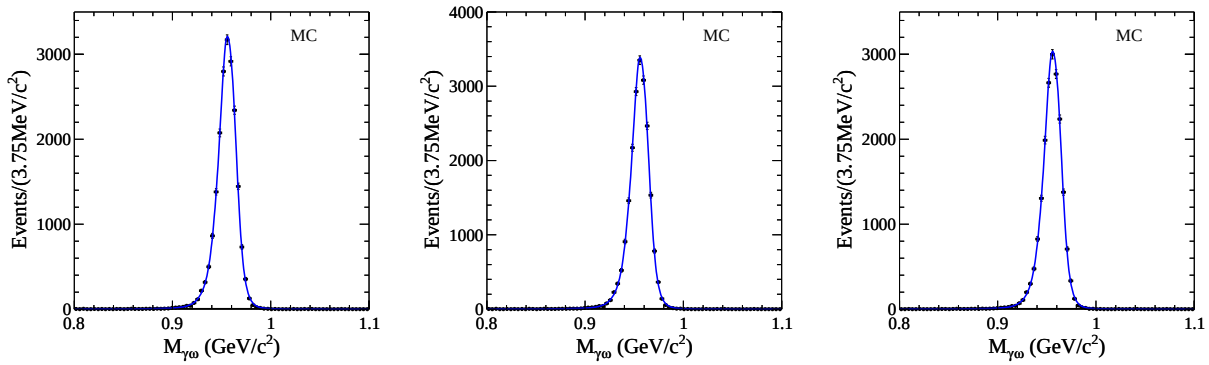

(a)$\pi^0\gamma\gamma$ invariant mass spectrum with veto π^0 and γ by $|M_{\gamma\gamma^*} - M_{\pi^0}| > 18$ MeV.

(b)$\pi^0\gamma\gamma$ invariant mass spectrum with veto π^0 and γ by $|M_{\gamma\gamma^*} - M_{\pi^0}| > 15$ MeV.

(c)$\pi^0\gamma\gamma$ invariant mass spectrum with veto π^0 and γ by $|M_{\gamma\gamma^*} - M_{\pi^0}| > 21$ MeV.

FIG. 36: $\pi^0\gamma\gamma$ invariant mass spectrum of signal MC with different mass windows of π^0 and γ veto.

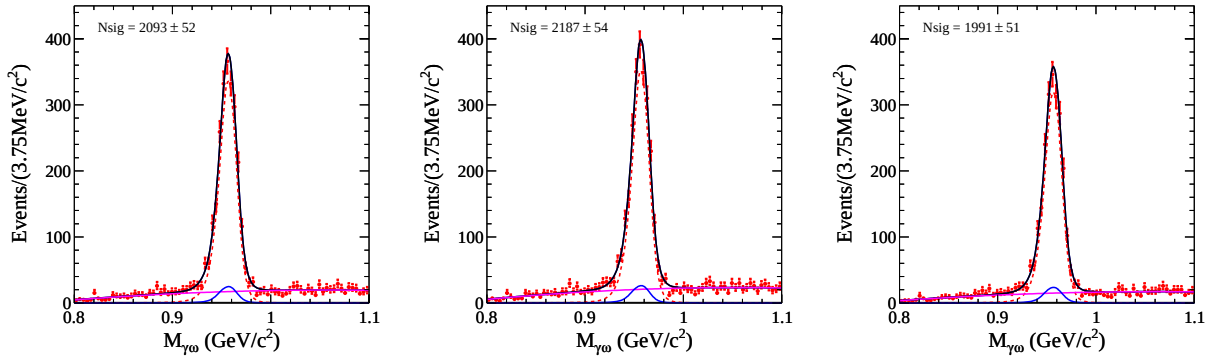

(a)$\pi^0\gamma\gamma$ invariant mass spectrum with veto π^0 and γ by $|M_{\gamma\gamma^*} - M_{\pi^0}| > 18$ MeV.

(b)$\pi^0\gamma\gamma$ invariant mass spectrum with veto π^0 and γ by $|M_{\gamma\gamma^*} - M_{\pi^0}| > 15$ MeV.

(c)$\pi^0\gamma\gamma$ invariant mass spectrum with veto π^0 and γ by $|M_{\gamma\gamma^*} - M_{\pi^0}| > 21$ MeV.

FIG. 37: $\pi^0\gamma\gamma$ invariant mass spectrum of Data with different mass windows of π^0 and γ veto.

J. Peaking Backgrounds

In the fit to η signal, the shape of the peaking background from $\eta \to 3\pi^0$ is fixed to the MC simulation, we consider the possible MC-data discrepancy in the resolution with the smear Gaussian as used in the signal shape, where the σ is taken as the same value of section D. The re-fit results are shown in Fig. 38. Thus the uncertainty is estimated to be 2.6% due to the MC-data difference for the background shape.

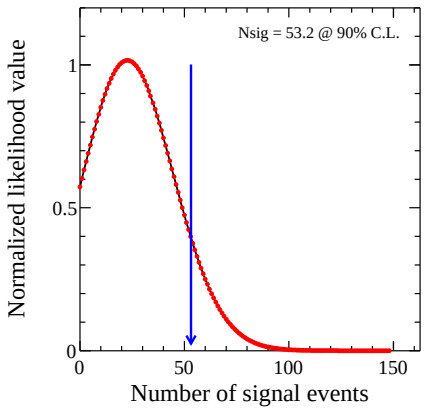

FIG. 38: Likelihood distribution as a function of the signal yield for η refit with the peaking background shape ($\eta \to 3\pi^0$) smearing by Gaussian as used in the signal shape (section D).

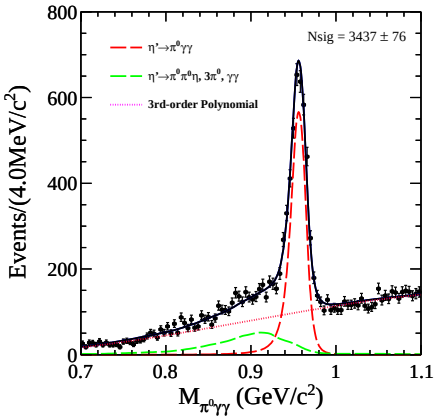

FIG. 39: η' fit situation with one standard deviation of the expected events for $\eta' \to \pi^0\pi^0\eta$, $\eta \to \gamma\gamma$ backgrounds.

K. η' sidebands

In the fit to $M_{\gamma\pi^0}$, the systematic error due to the η' sidebands is estimated from another selection of sideband regions, changing from 1.008 $\sim$ 1.058 GeV/c^2, 0.738 $\sim$ 0.788 GeV/c^2 to 1.018 $\sim$ 1.068 GeV/c^2, 0.728 $\sim$ 0.778 GeV/c^2. The fitting situation and yields of ω signal events and non-resonance process are shown in Fig. 40 and Table XV, respectively. The difference of yields will be considered as the systematic uncertainties (3.0% for ω and 4.0% for non-resonance) arising from the η' sidebands, see Table XX.

TABLE XV: Fitted yields of fit to $M_{\gamma\pi^0}$ with another selection of η' sideband regions. Here θ is the interference phase; N_ω and $N_{non-res}$ are the fitted yields of ω signal events and the non-resonance process.

θ	N_ω	$N_{non-res}$
1.00 ± 0.21	2420 ± 79	643 ± 72

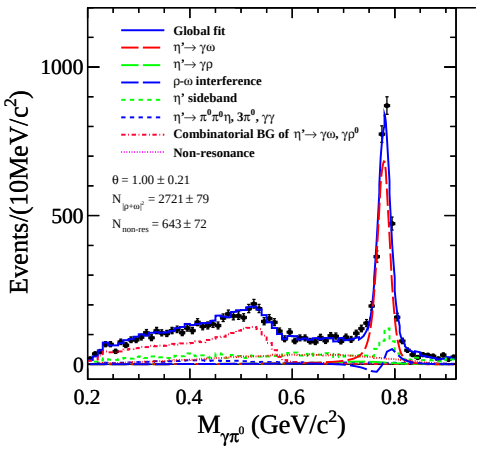

FIG. 40: Fitting results of $\pi^0\gamma$ invariant mass spectrum with another selection of η' sideband regions.

L. Non-Peaking Backgrounds

1. *Fixed backgrounds*

In the fit of η' signal, the expected number of background events from the decay of $J/\psi \to \gamma\eta' \to \gamma\pi^0\pi^0\eta$ ($\eta \to \gamma\gamma$), $\gamma\eta' \to \gamma 3\pi^0$, $\gamma\eta' \to 3\gamma$ are fixed. To estimate the uncertainty, we vary the numbers of expected backgrounds events by one standard deviation from the PDG14 value [22], see Table III. Some fit situations and all the fit yields from changing the expected events for each background mode are shown in Fig. 39 and Table XVI. Therefore the systematic error from fixed backgrounds shape is determined by quadratic of all the systematic errors attribute to the differences of yields when changing the expected events for each background mode. The value of error is summarized as in Table XX.

TABLE XVI: The refit number of signal events (N_S) with one standard deviation of the expected events for backgrounds modes.

Each background mode	$\eta' \to \pi^0\pi^0\eta$	$\eta' \to 3\pi^0$	$\eta' \to \gamma\gamma$
N_S (η' fit)	3437 ± 76	3436 ± 76	3435 ± 76

For the measurement of $\mathrm{d}\Gamma(\eta' \to \pi^0\gamma\gamma)/\mathrm{d}m^2_{\gamma\gamma}$, the re-fitting results with changing the expected events for each background mode ($\eta' \to \pi^0\pi^0\eta$) are shown in APPENDIX C. And

the corresponding systematic errors calculated from the varied fitted yields are tabulated in Table X.

TABLE XVII: The fitted signal yields (N_i^{obs}) and corresponding systematic error (σ_i) are obtained with one standard deviation of the expected events for each fixed background mode. Here $\sigma_{tot.}$ is calculated by quadratic of the three systematic errors (σ_i).

$M^2_{\gamma\gamma}$ $((GeV/c^2)^2)$	$[0., 0.01]$	$[0.01, 0.04]$	$[0.04, 0.0625]$	$[0.0625, 0.09]$	$[0.09, 0.1225]$	$[0.1225, 0.16]$
N_{i1}^{obs}	115±16	375±27	421 ± 25	369±24	394±24	405±24
σ_{i1}	0.9%	0.1%	0.1%	0.3%	0.1%	0.1%
N_{i2}^{obs}	114±16	375±27	421 ± 25	370±24	394±24	405±24
σ_{i2}	0.1%	0.1%	0.1%	0.1%	0.1%	0.1%
N_{i3}^{obs}	115±16	375±27	421 ± 25	370±24	393±24	405±24
σ_{i3}	0.9%	0.1%	0.1%	0.1%	0.3%	0.1%
$\sigma_{tot.}$	1.3%	0.2%	0.2%	0.3%	0.3%	0.2%

$[0.16, 0.2025]$	$[0.2025, 0.25]$	$[0.25, 0.2809]$	$[0.2809, 0.3136]$	$[0.3136, 0.36]$	$[0.36, 0.4225]$	$[0.4225, 0.64]$
464±25	477±25	207±17	101±19	76±12	37±10	67±15
0.1%	0.1%	0.1%	0.1%	0.1%	0.3%	0.2%
464±25	478±25	207±17	101±19	76±12	37±10	67±15
0.1%	0.2%	0.1%	0.1%	0.1%	0.3%	0.2%
465±25	478±25	207±17	101±19	76±12	36±10	68±15
0.2%	0.2%	0.1%	0.1%	0.1%	2.7%	1.5%
0.2%	0.3%	0.2%	0.2%	0.2%	2.7%	1.5%

In the fit to $M_{\gamma\pi^0}$, the expected number of background events from the decay of $\eta' \to \pi^0\pi^0\eta$, $\eta' \to 3\pi^0$, $\eta' \to 2\gamma$ are fixed. To estimate the uncertainty, we vary the numbers of expected backgrounds events by one standard deviation from the PDG14 value [22]. Some fit situations and all the fit yields from changing the expected events for each background mode are shown in Fig. 41. The fit yields of ω signal events and non-resonance process are summarized in Table XVIII. Therefore the systematic error (0.1% for ω and 0.4% for non-resonance) from fixed backgrounds shape is determined by quadratic of all the systematic errors attribute to the differences of yields when changing the expected events for each

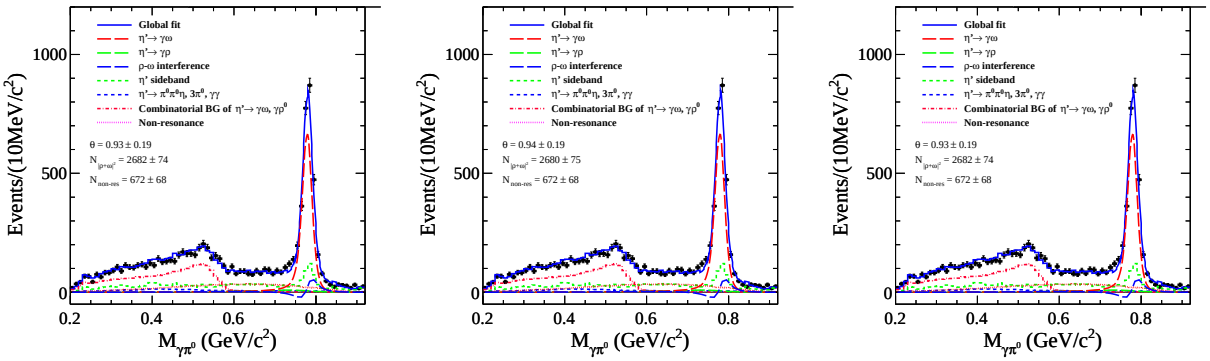

(a)Fitting results of $M_{\pi^0\gamma}$ with changing the expected events of $\eta' \to 2\gamma$ decay by one standard deviation.

(b)Fitting results of $M_{\pi^0\gamma}$ with changing the expected events of $\eta' \to 3\pi^0$ decay by one standard deviation.

(c)Fitting results of $M_{\pi^0\gamma}$ with changing the expected events of $\eta' \to \pi^0\pi^0\eta$ decay by one standard deviation.

FIG. 41: Fitting results of $\pi^0\gamma$ invariant mass spectrum with changing the expected events of fixed backgrounds by one standard deviation.

background mode.

TABLE XVIII: Fitted yields of fit to $M_{\gamma\pi^0}$ with changing the expected events of fixed backgrounds by one standard deviation. Here θ is the interference phase; N_ω and $N_{non-res}$ are the fitted yields of ω signal events and the non-resonance process.

$\eta' \to 2\gamma$	θ	N_ω	$N_{non-res}$
	0.93 ± 0.19	2349 ± 71	672 ± 68
$\eta' \to 3\pi^0$	θ	N_ω	$N_{non-res}$
	0.94 ± 0.19	2353 ± 71	672 ± 68
$\eta' \to \pi^0\pi^0\eta$	θ	N_ω	$N_{non-res}$
	0.94 ± 0.19	2349 ± 70	670 ± 68

2. *Remaining Backgrounds shape*

The uncertainty due to the remaining background shape has been estimated by changing the order of the Chebychev Polynomial from 2 (3) to 3 (4) for η (η') fit . The changes in yields for these variations give systematic uncertainties due to the remaining background

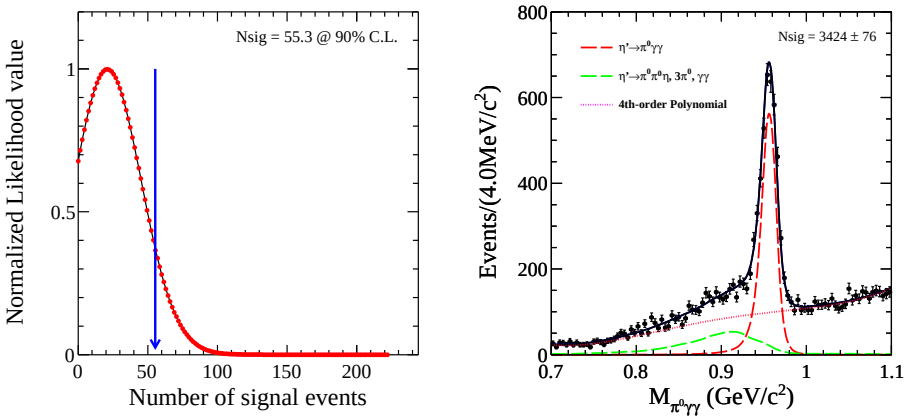

(a)Likelihood distribution as a function of the signal yield for η refit.

(b)η' refit results.

FIG. 42: η (η') refit results with changing the order of the Chebychev Polynomial from 2 (3) to 3 (4) for the other background shape.

shape. The fit results and systematic errors are listed in Fig. 42 and Table XX, respectively.

For the measurement of $\mathrm{d}\Gamma(\eta' \to \pi^0\gamma\gamma)/\mathrm{d}m^2_{\gamma\gamma}$, the re-fitting results width changing the order of the Chebychev Polynomial from 2 to 3 are shown in APPENDIX D. And the corresponding systematic errors calculated from the changed fitted yields are tabulated in Table XIX.

TABLE XIX: Systematic errors due to the order of Polynomial describing the backgrounds for the measurements of $\mathrm{d}\Gamma(\eta' \to \pi^0\gamma\gamma)/\mathrm{d}m^2_{\gamma\gamma}$.

$M^2_{\gamma\gamma}$ $((GeV/c^2)^2)$	$[0., 0.01]$	$[0.01, 0.04]$	$[0.04, 0.0625]$	$[0.0625, 0.09]$	$[0.09, 0.1225]$	$[0.1225, 0.16]$
N_i^{obs}	116±17	379±27	420 ± 25	368±24	397±24	405±24
σ_i	1.8%	1.1%	0.2%	0.5%	0.8%	0.1%
$[0.16, 0.2025]$	$[0.2025, 0.25]$	$[0.25, 0.2809]$	$[0.2809, 0.3136]$	$[0.3136, 0.36]$	$[0.36, 0.4225]$	$[0.4225, 0.64]$
463±25	476±25	203±17	100±19	74±12	36±10	67±15
0.2%	0.2%	1.7%	1.0%	2.6%	2.7%	0.7%

Thus the systematic error due to the non-peaking backgrounds is determined by quadratic of the above two systematic errors, and the final value are summarized in Table XX.

M. Cited Branching Fraction

From the PDG14 value [22], we can know the systematic error due to the used branching fraction of $J\psi \to \gamma\eta'$ decay is 3.1%.

N. Number of J/ψ Events

The systematic error due to the number of J/ψ events is 0.8% [24, 25].

O. Total Systematic Error

The total systematic error for measurement is determined by quadratic of all above systematic errors, and all of them are summarized in Table XX and Table XXI.

TABLE XX: Summary of systematic errors for the branching fraction measurements (%). Here *Inc.* means the inclusive process of $\eta' \to \pi^0\gamma\gamma$ decay, and $non-Res.$ means the contribution of non-resonance process in η' decay.

	$\eta \to \pi^0\gamma\gamma$	$\eta' \to \pi^0\gamma\gamma$ (Inc.)	$\eta' \to \gamma\omega \to \pi^0\gamma\gamma$	$\eta' \to \pi^0\gamma\gamma$ (non-Res.)
Photon detection	5.0	5.0	5.0	5.0
Number of Photons	0.5	0.5	0.5	0.5
5C kinematic fit	3.8	2.7	2.7	2.7
Signal shape	3.1	0.5	1.5	2.1
Signal Model	3.7	1.7	1.2	2.4
π^0 and γ veto	1.0	1.0	1.0	1.0
Fitting range	1.3	0.8	2.6	2.9
α	-	-	1.8	6.7
f	-	-	3.3	2.1
Peaking backgrounds	2.6	–	3.0	4.0
Non-peaking backgrounds	1.3	0.3	0.1	0.4
Cited branching fractions	3.1	3.1	3.1	3.1
Number of J/ψ events	0.8	0.8	0.8	0.8
Total systematic uncertainty	9.2	6.9	8.8	11.3

TABLE XXI: Summary of systematic errors for the measurement of $\mathrm{d}\Gamma(\eta' \to \pi^0\gamma\gamma)/\mathrm{d}m^2_{\gamma\gamma}$ (%).

$M^2_{\gamma\gamma}$ $((GeV/c^2)^2)$	$[0.0, 0.01]$	$[0.01, 0.04]$	$[0.04, 0.0625]$	$[0.0625, 0.09]$	$[0.09, 0.1225]$	$[0.1225, 0.16]$
Photon detection	5.0	5.0	5.0	5.0	5.0	5.0
Number of Photons	0.5	0.5	0.5	0.5	0.5	0.5
5C kinematic fit	2.7	2.7	2.7	2.7	2.7	2.7
Signal shape	1.8	1.6	0.5	0.3	0.3	1.0
Signal Model	1.7	1.7	1.7	1.7	1.7	1.7
π^0 and γ veto	1.0	1.0	1.0	1.0	1.0	1.0
Fitting range	0.9	1.1	0.5	1.6	1.3	1.3
Nonpeaking backgrounds	2.2	1.1	0.3	0.6	0.9	0.2
Cited BR	3.1	3.1	3.1	3.1	3.1	3.1
Number of J/ψ events	0.8	0.8	0.8	0.8	0.8	0.8
Total systematic error	7.5	7.2	6.9	7.0	7.0	7.0

$[0.16, 0.2025]$	$[0.2025, 0.25]$	$[0.25, 0.2809]$	$[0.2809, 0.3136]$	$[0.3136, 0.36]$	$[0.36, 0.4225]$	$[0.4225, 0.64]$
5.0	5.0	5.0	5.0	5.0	5.0	5.0
0.5	0.5	0.5	0.5	0.5	0.5	0.5
2.7	2.7	2.7	2.7	2.7	2.7	2.7
0.2	0.4	1.0	1.0	2.0	1.4	0.8
1.7	1.7	1.7	1.7	1.7	1.7	1.7
1.0	1.0	1.0	1.0	1.0	1.0	1.0
1.5	0.4	1.9	2.5	4.6	4.1	3.7
0.3	0.4	1.7	1.0	2.6	3.8	1.7
3.1	3.1	3.1	3.1	3.1	3.1	3.1
0.8	0.8	0.8	0.8	0.8	0.8	0.8
7.0	6.9	7.4	7.4	8.9	8.9	8.0

X. BRANCHING RATIO

Because of no obvious η signal, we just give out an upper limit of branching fraction of $\mathcal{BR}(\eta \to \pi^0\gamma\gamma)$ on confidence level of 90% as:

$$\begin{aligned}\mathcal{BR}(\eta \to \pi^0\gamma\gamma) &< \frac{N_{up}}{N_{J/\psi} \times \varepsilon \times \mathcal{BR}(J/\psi \to \gamma\eta) \times \mathcal{BR}(\pi^0 \to \gamma\gamma) \times (1 - \sigma_{sys.})} \\ &< 5.2 \times 10^{-4},\end{aligned} \tag{4}$$

where N_{up} (54.6) is the number of η signal events at 90% C.L.; ε (8.05%) is the event selection efficiency from MC simulation; $N_{J/\psi}$ is the J/ψ total number; $\sigma_{sys.}$ is the systematic error (9.2%); $\mathcal{BR}(i)$ is the branching ratio of $J/\psi \to \gamma\eta$ ($\pi^0 \to \gamma\gamma$) decay from PDG14 [22].

For the inclusive process of η' decay, we can obtain:

$$\begin{aligned}\mathcal{BR}(\eta' \to \pi^0\gamma\gamma) &= \frac{N_{obs}}{N_{J/\psi} \times \varepsilon \times \mathcal{BR}(J/\psi \to \gamma\eta') \times \mathcal{BR}(\pi^0 \to \gamma\gamma)} \\ &= (3.20 \pm 0.07(stat.) \pm 0.22(syst.)) \times 10^{-3},\end{aligned} \tag{5}$$

where N_{obs} (3435 ± 76) is the number of η' signal events; ε (16.08%) is the event selection efficiency from MC simulation.

For each $m^2_{\gamma\gamma}$ interval, the fitted signal yield (N_i^{obs}) and event selection efficiency (ϵ_i) are listed in Table XXII. Using the systematic error of Table XXI and the Eq. 7, we can calculate the branching fraction of $\eta' \to \pi^0\gamma\gamma$ decay for each interval, as summarized in Table XXII. Thus the dependence of the decay width on the two-photon invariant mass squared, $\mathrm{d}\Gamma(\eta' \to \pi^0\gamma\gamma)/\mathrm{d}m^2_{\gamma\gamma}$ is depicted in Fig. 44.

TABLE XXII: Branching fractions (BR_i) of $\eta' \to \pi^0\gamma\gamma$ decay for each $m^2_{\gamma\gamma}$ interval. The N_i^{obs} is the fitted yield of η' signal, and ϵ_i is the event selection efficiency determined from the MC simulation.

$M^2_{\gamma\gamma}$ $((GeV/c^2)^2)$	$[0., 0.01]$	$[0.01, 0.04]$	$[0.04, 0.0625]$	$[0.0625, 0.09]$	$[0.09, 0.1225]$	$[0.1225, 0.16]$
N_i^{obs}	114±16	375±27	421 ± 25	370±24	394±24	405±24
ϵ_i	10.7%	14.4%	21.4%	21.3%	20.4%	19.7%
BR_i $(\times 10^{-4})$	$1.60 \pm 0.22 \pm 0.12$	$3.90 \pm 0.28 \pm 0.28$	$2.95 \pm 0.17 \pm 0.20$	$2.60 \pm 0.17 \pm 0.18$	$2.89 \pm 0.18 \pm 0.20$	$3.08 \pm 0.18 \pm 0.22$
$[0.16, 0.2025]$	$[0.2025, 0.25]$	$[0.25, 0.2809]$	$[0.2809, 0.3136]$	$[0.3136, 0.36]$	$[0.36, 0.4225]$	$[0.4225, 0.64]$
464±25	477±25	207±17	101±19	76±12	37±10	67±15
18.4%	15.1%	9.95%	8.55%	14.3%	14.6%	14.8%
$3.78 \pm 0.20 \pm 0.26$	$4.73 \pm 0.25 \pm 0.33$	$3.12 \pm 0.26 \pm 0.23$	$1.77 \pm 0.33 \pm 0.13$	$0.80 \pm 0.13 \pm 0.07$	$0.38 \pm 0.10 \pm 0.03$	$0.68 \pm 0.15 \pm 0.05$

For the η' decay with ω-exchange, we can obtain:

$$\begin{aligned}\mathcal{BR}(\eta' \to \pi^0\gamma\gamma) &= \frac{N_{obs}}{N_{J/\psi} \times \varepsilon \times \mathcal{BR}(J/\psi \to \gamma\eta') \times \mathcal{BR}(\pi^0 \to \gamma\gamma)} \\ &= (2.38 \pm 0.07(stat.) \pm 0.21(syst.)) \times 10^{-3},\end{aligned} \tag{6}$$

where N_{obs} (2350 ± 71) is the fitted events of ω signal; ε (14.77%) is the event selection efficiency from MC simulation. One can see that it is consistent with the PDG14 value [22] $((2.28 \pm 0.21) \times 10^{-3})$.

For the η' decay from the non-resonance contribution, we can obtain:

$$\begin{aligned}\mathcal{BR}(\eta' \to \pi^0\gamma\gamma) &= \frac{N_{obs}}{N_{J/\psi} \times \varepsilon \times \mathcal{BR}(J/\psi \to \gamma\eta') \times \mathcal{BR}(\pi^0 \to \gamma\gamma)} \\ &= (6.30 \pm 0.63(stat.) \pm 0.71(syst.)) \times 10^{-4},\end{aligned} \tag{7}$$

where N_{obs} (670 ± 67) is the fitted yields of η' signal from non-resonance process; ε (15.92%) is the event selection efficiency from MC simulation.

XI. SUMMARY

- The double electromagnetic rare decays of $\eta \to \pi^0\gamma\gamma$ and $\eta' \to \pi^0\gamma\gamma$ have been studied on BESIII through $J\psi \to \gamma\eta$ and $J\psi \to \gamma\eta'$ processes, respectively;

- For η decay, there is no obvious signal and an upper limit of branching fraction at 90% confidence level is obtained: $\mathcal{BR}(\eta \to \pi^0\gamma\gamma) < 5.2 \times 10^{-4}$. The upper limit is consistent with the PDG14 [22] value. In contrast, we list all the measured branching fractions with the blue arrow representing our measurements, see Fig. 43;

- For η' decay, the total branching fraction of inclusive process is measured as: $\mathcal{BR}(\eta' \to \pi^0\gamma\gamma) = (3.20 \pm 0.07(\text{stat.}) \pm 0.22(\text{syst.})) \times 10^{-3}$. The value is much lower than the theoretical predictions [11, 12];

- Assumption the $\eta' \to \pi^0\gamma\gamma$ decay is mainly from the coherent sum of $\rho-$ and $\omega-$exchange, and the other non-resonance contribution, a fit to the $\gamma\pi^0$ invariant mass spectrum is done. The fit gives the branching fractions of $\omega-$exchange and non-resonance process as: $\mathcal{BR}(\eta' \to \gamma\omega \to \pi^0\gamma\gamma) = (2.38 \pm 0.07(\text{stat.}) \pm 0.21(\text{syst.})) \times 10^{-3}$ and $\mathcal{BR}(\eta' \to \pi^0\gamma\gamma)_{non-Res.} = (6.30 \pm 0.63(\text{stat.}) \pm 0.71(\text{syst.})) \times 10^{-4}$, respectively. For the $Br(\eta' \to \gamma\omega \to \pi^0\gamma\gamma)$, our measurement is well consistent with the PDG value; for the non-resonance process, its branching ratio is also consistent with the upper limit of GAMS's measurement which excluded the contribution of ω-exchange;

- Finally it needs to notice that we only obtain an upper limit for the branching fraction of $\eta \to \pi^0\gamma\gamma$ decay which has been measured by other experiments, but we do get a significant measurement for the branching fraction of $\eta' \to \pi^0\gamma\gamma$ decay, for which only an upper limit existed previously and which is of the same order of magnitude of the η decay. Here we give some comments on the different sensitivities of BESIII experiments to the two channels. On the one hand, for η decay in the other experiments, such as $\pi^- p \to \eta n$ (2.8×10^7 η events for Ref. [16, 17]), $\gamma p \to \eta p$ (about 10^7 η events for Ref. [18] and 6×10^7 η events for Ref. [20], respectively) and $\phi \to \gamma\eta$ (1.9×10^7 η

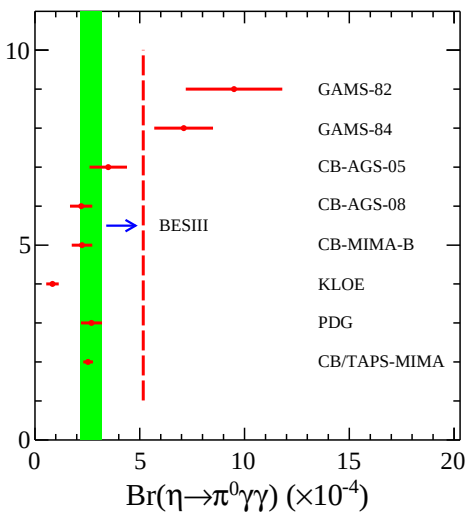

FIG. 43: All measured branching fractions of $\eta \to \pi^0\gamma\gamma$ decay.

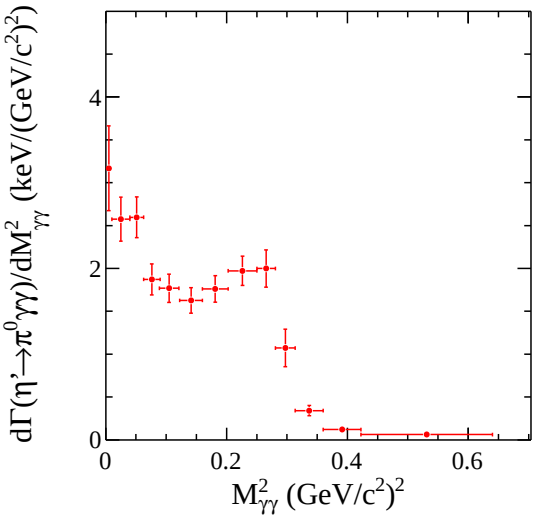

FIG. 44: Measurement for $\mathrm{d}\Gamma(\eta' \to \pi^0\gamma\gamma)/\mathrm{d}m^2_{\gamma\gamma}$.

events for Ref. [19]) reactions, these produced η samples are much larger than the sample of 1.45×10^6 η events obtained from $J/\psi \to \gamma\eta$ radiative decay on BESIII. But for η' decay, because of the more lower cross sections of η' production in $\pi^- p$ and γp reactions, which at least be reduced by one order of magnitude comparison with the corresponding cross sections of η production, see Ref. [20]), the available η' sample of 6.77×10^6 events obtained from $J/\psi \to \gamma\eta'$ radiative decay at BESIII now has the more advantage to study the rare decay of η'. On the other hand, for η decay, in the other experiments, because of close to threshold, the produced η meson moves with a very low momentum. Thus that the energies of the photons from the main background $\eta \to 3\pi^0$ will be higher. Further it's very difficult for this background to loss the two soft photons in event selection. Therefore the background will be suppressed greatly. In particulary, because of the lower momentum of η production, the background shape will be no appearance of a peak under the η mass, see Ref. [16–19];

The results of our measurements for the branching fractions are shown in Table XXIII.

[1] J. Gasser and H. Leutwyler, Nucl. Phys. B 250, 465 (1985).

[2] Ll. Ametller, J. Bijnens, A. Bramon, and F. Cornet, Phys. Lett. B 276, 185 (1992).

TABLE XXIII: Measurement of branching fractions (10^{-4}) for this analysis, where the first errors are statistical and the second ones are systematic, and the comparison with the PDG values [22]. The upper limit is estimated at the 90% C.L..

Decay mode	BESIII (10^{-4})	PDG14 (10^{-4})	Theory (10^{-4})
$\eta \to \pi^0\gamma\gamma$	< 5.2	2.7 ± 0.5	2.54 ± 0.62 (Unitarized χPTh) [9]
$\eta' \to \pi^0\gamma\gamma$ (Inc.)	$32.0 \pm 0.7 \pm 2.2^a$		57 (VMD+LσM) [11]^a 65 (VMD+LσM) [12]^a
$\eta' \to \gamma\omega \to \pi^0\gamma\gamma$	$23.8 \pm 0.7 \pm 2.1$	22.8 ± 2.1	
$\eta' \to \pi^0\gamma\gamma$ (non-Res.)	$6.30 \pm 0.63 \pm 0.71$	< 8.0 @90% C.L.^{b}	

^{a}Containing the contributions of $\rho-$ and $\omega-$exchange
^{b}Deducting the contribution of ω-exchange

[3] W. Alles, A. Baracca, and A. T. Ramos, Phys. Lett. B 349, 555 (1995).

[4] P. Ko, Phys. Lett. B 349, 555 (1995).

[5] S. Bellucci and C. Bruno, Nucl. Phys. B 452, 626 (1995).

[6] J. Bijnens, A. Fayyazuddin, and J. Prades, Phys. Lett. B 379, 209 (1996).

[7] M. Jetter, Nucl. Phys. B 459, 283 (1996).

[8] E. Oset, J. R. Pelaez, and L. Roca, Phys. Rev. D 67, 073013 (2003).

[9] E. Oset, J. R. Pelaez, and L. Roca, Phys. Rev. D 77, 073001 (2008).

[10] J. N. Ng and D. J. Peters, Phys. Rev. D 46, 5034 (1992).

[11] R. Joraa, Nucl. Phys. Proc. Suppl. 207-208, 224 (2010).

[12] R. Escribano, PoS QNP 2012, 079 (2012).

[13] M. M. Achasov et al. (SND Collaboration), Nucl. Phys. B 600, 3 (2001).

[14] F. Binon et al., Yad. Fiz. 33, 1534 (1982); Lett. Nuovo Cimento A 71, 497 (1982).

[15] D. Alde et al. (GAMS-2000 Collaboration), Yad. Fiz. 40, 1447 (1984); Z. Phys. C 25, 225 (1984).

[16] S. Prakhov et al., Phys. Rev. C 72, 025201 (2005).

[17] S. Prakhov, B. M. K. Nefkens, C. E. Allgower, V. Bekrenev,W. J. Briscoe, J. R. Comfort, K. Craig and D. Grosnick et al., Phys. Rev. C 78, 015206 (2008).

[18] S. Prakhov, Proceedings of 11th International Conference on Meson-Nucleon Physics and the

Structure of the Nucleon (MENU 2007) (Julich, Germany, 2007); M. Unverzagt (Crystal Ball at MAMI Collaboration), Nucl. Phys. Proc. Suppl. 198, 174 (2010); A. Starostina, Eur. Phys. J. Special Topics 198, 117 (2011).

[19] P. Gauzzi (KLOE-2 Collaboration), J. Phys. Conf. Ser. 349, 012002 (2012); B. Di Micco et al. (KLOE Collaboration), Acta Phys. Slov. 56, 403 (2006).

[20] M. Unverzagt (Crystal Ball at MAMI Collaboration), η and η' Physics at MAMI, talked in International Symposium Lepton and HadronPhysics at Meson-Factories Messina (Italy) October 13-15, 2013.

[21] B. M. K. Nefkens et al. (A2 Collaboration), arXiv:1405.4904[hep-ex].

[22] K. A. Olive *et al.* (Particle Data Group), Chin. Phys. C 38 090001 (2014).

[23] D. Alde et al. (Serpukhov-Brussels-Los Alamos-Annecy(LAPP) Collaboration), Z. Phys. C 36, 603 (1987).

[24] M. Ablikim *et al.* (BESIII Collaboration), Chinese Phys. C 36, 915 (2012).

[25] With the same approach as for J/ψ events taken in 2009 (see Ref. [24] for more details), the preliminary number of J/ψ events taken in 2009 and 2012 is determined to be 1310.6×10^6 with an uncertainty of 0.8%.

[26] M. Ablikim et al. (BESIII Collaboration), Nucl. Instrum. Methods Phys. Res., Sect. A 614, 345 (2010).

[27] J. Z. Bai et al. (BES Collaboration), Nucl. Instrum. Methods Phys. Res., Sect. A 344, 319 (1994); 458, 627 (2001).

[28] S. Agostinelli et al. (GEANT4 Collaboration), Nucl. Instrum. Meth. A 506, 250 (2003); J. Allison et al., IEEE Trans. Nucl. Sci. 53, 270 (2006).

[29] S. Jadach, B. F. L. Ward and Z. Was, Comput. Phys. Commun. 130, 260 (2000); Phys. Rev. D 63, 113009 (2001).

[30] R. G. Ping et al., HEP&NP. 32, 599 (2008).

[31] A. M. Blik et al., Phys. Atom. Nucl. 72, 231 (2008), Yad. Fiz. 72, 258 (2008).

[32] Guang-Ming Xu et al., BESIII Collaboratin. PWA of $J/\psi \to \gamma\pi^0\pi^0$.

[33] A. M. Blik et al., Phys. Atom. Nucl. 71, 2124 (2008), Yad. Fiz. 71, 2161 (2008).

[34] M. Ablikim et al. (BESIII Collaboration), Phys. Rev. Lett. 108, 182001 (2012).

[35] Shuo-Pin Wen et al., BESIII Collaboratin. Study of J/ψ decays to $\gamma\eta\pi^0$.

[36] M. M. Achasov et al. (SND Collaboration), Phys. Lett. B 559, 171 (2003).

[37] M. Ablikim et al. (BESIII Collobarotion), Phys. Rev. D 81, 052005 (2010).

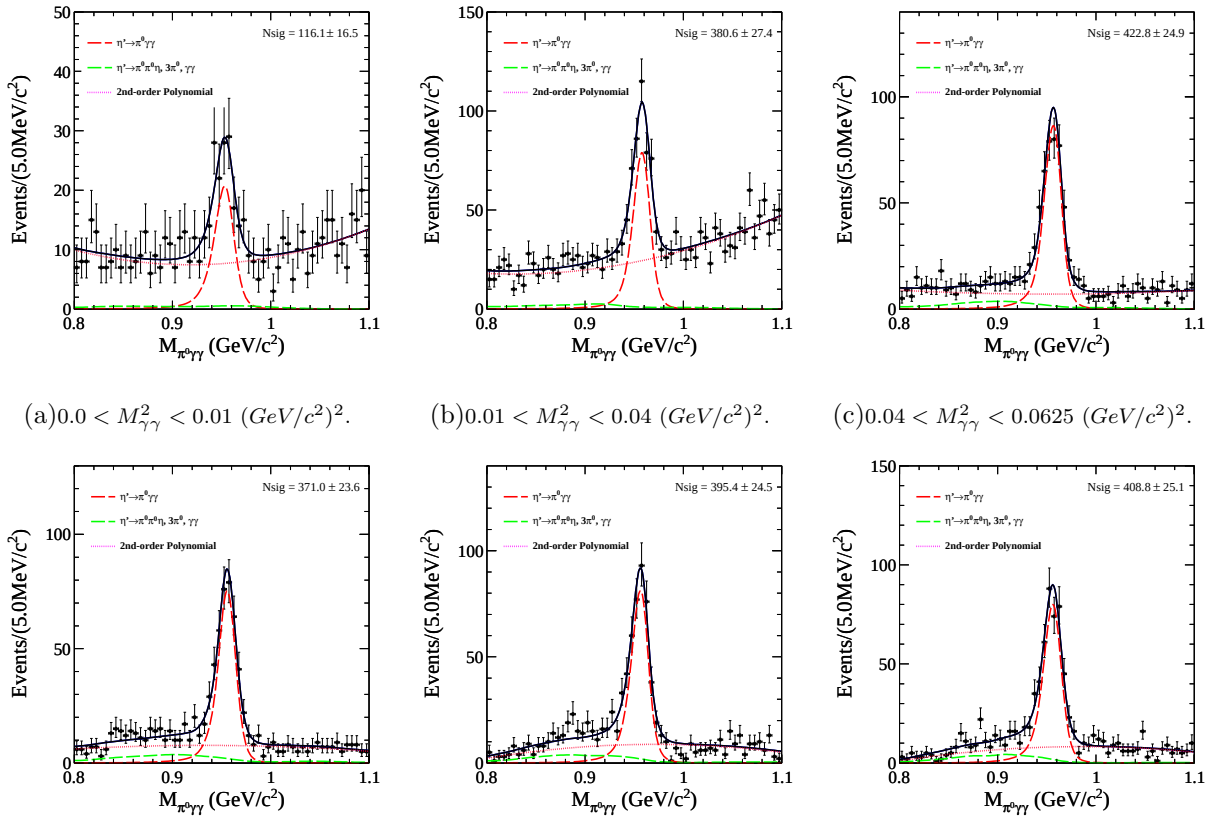

(a)$0.0 < M^2_{\gamma\gamma} < 0.01\ (GeV/c^2)^2$. (b)$0.01 < M^2_{\gamma\gamma} < 0.04\ (GeV/c^2)^2$. (c)$0.04 < M^2_{\gamma\gamma} < 0.0625\ (GeV/c^2)^2$.

(d)$0.0625 < M^2_{\gamma\gamma} < 0.09\ (GeV/c^2)^2$. (e)$0.09 < M^2_{\gamma\gamma} < 0.1225\ (GeV/c^2)^2$. (f)$0.1225 < M^2_{\gamma\gamma} < 0.16\ (GeV/c^2)^2$.

FIG. 45: η' fitting results after considering the MC-data difference in mass resolution for these bins ($(GeV/c^2)^2$) :(a) $M^2_{\gamma\gamma} \subset (0.0, 0.01)$; (b) $M^2_{\gamma\gamma} \subset (0.01, 0.04)$; (c) $M^2_{\gamma\gamma} \subset (0.04, 0.0625)$; (d) $M^2_{\gamma\gamma} \subset (0.0625, 0.09)$; (e) $M^2_{\gamma\gamma} \subset (0.09, 0.1225)$; (f) $M^2_{\gamma\gamma} \subset (0.1225, 0.16)$.

APPENDIX

APPENDIX A: SYSTEMATIC ERROR DUE TO THE SIGNAL SHAPE

For the measurement of $\mathrm{d}\Gamma(\eta' \to \pi^0\gamma\gamma)/\mathrm{d}m^2_{\gamma\gamma}$, for each $m^2_{\gamma\gamma}$ interval, the re-fitting results where the signal PDF is smeared a Gaussian function with the fixed width of 1.5 MeV, namely considering the MC-data difference in mass resolution, are shown in Table 45 and Table 46.

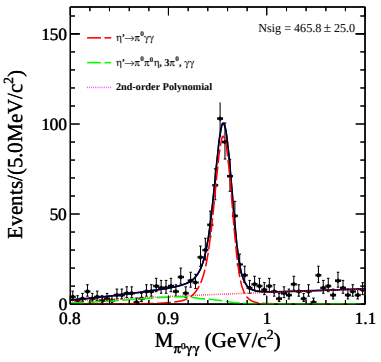

(a)$0.16 < M^2_{\gamma\gamma} < 0.2025\ (GeV/c^2)^2$.

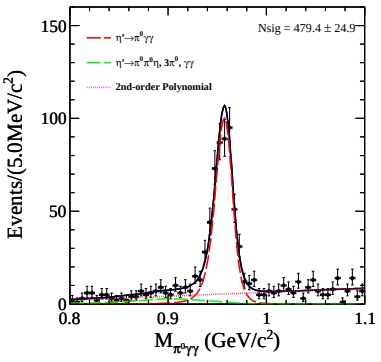

(b)$0.2025 < M^2_{\gamma\gamma} < 0.25\ (GeV/c^2)^2$.

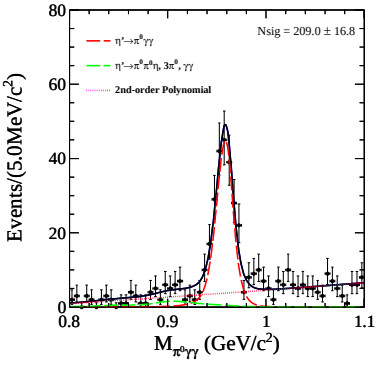

(c)$0.25 < M^2_{\gamma\gamma} < 0.2809\ (GeV/c^2)^2$.

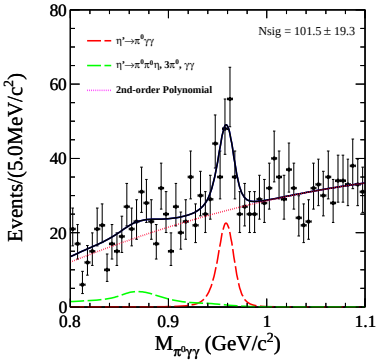

(d)$0.2809 < M^2_{\gamma\gamma} < 0.3136\ (GeV/c^2)^2$.

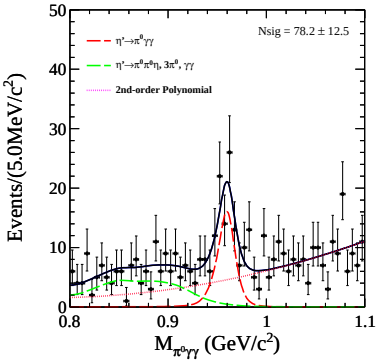

(e)$0.3136 < M^2_{\gamma\gamma} < 0.36\ (GeV/c^2)^2$.

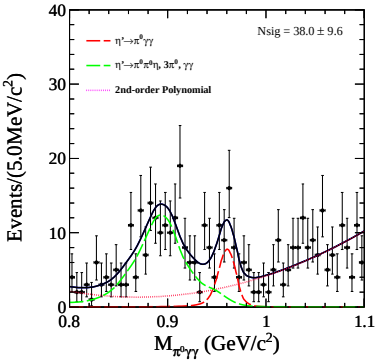

(f)$0.36 < M^2_{\gamma\gamma} < 0.4225\ (GeV/c^2)^2$.

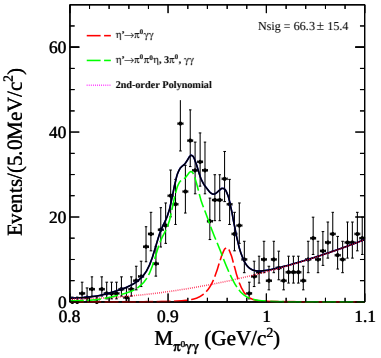

(g)$0.4225 < M^2_{\gamma\gamma} < 0.64\ (GeV/c^2)^2$.

FIG. 46: η' fitting results after considering the MC-data difference in mass resolution for these bins $((GeV/c^2)^2)$: (a) $M^2_{\gamma\gamma} \subset (0.16, 0.2025)$; (b) $M^2_{\gamma\gamma} \subset (0.2025, 0.25)$; (c) $M^2_{\gamma\gamma} \subset (0.25, 0.2809)$; (d) $M^2_{\gamma\gamma} \subset (0.2809, 0.3136)$; (e) $M^2_{\gamma\gamma} \subset (0.3136, 0.36)$; (f) $M^2_{\gamma\gamma} \subset (0.36, 0.4225)$; (g) $M^2_{\gamma\gamma} \subset (0.4225, 0.64)$.

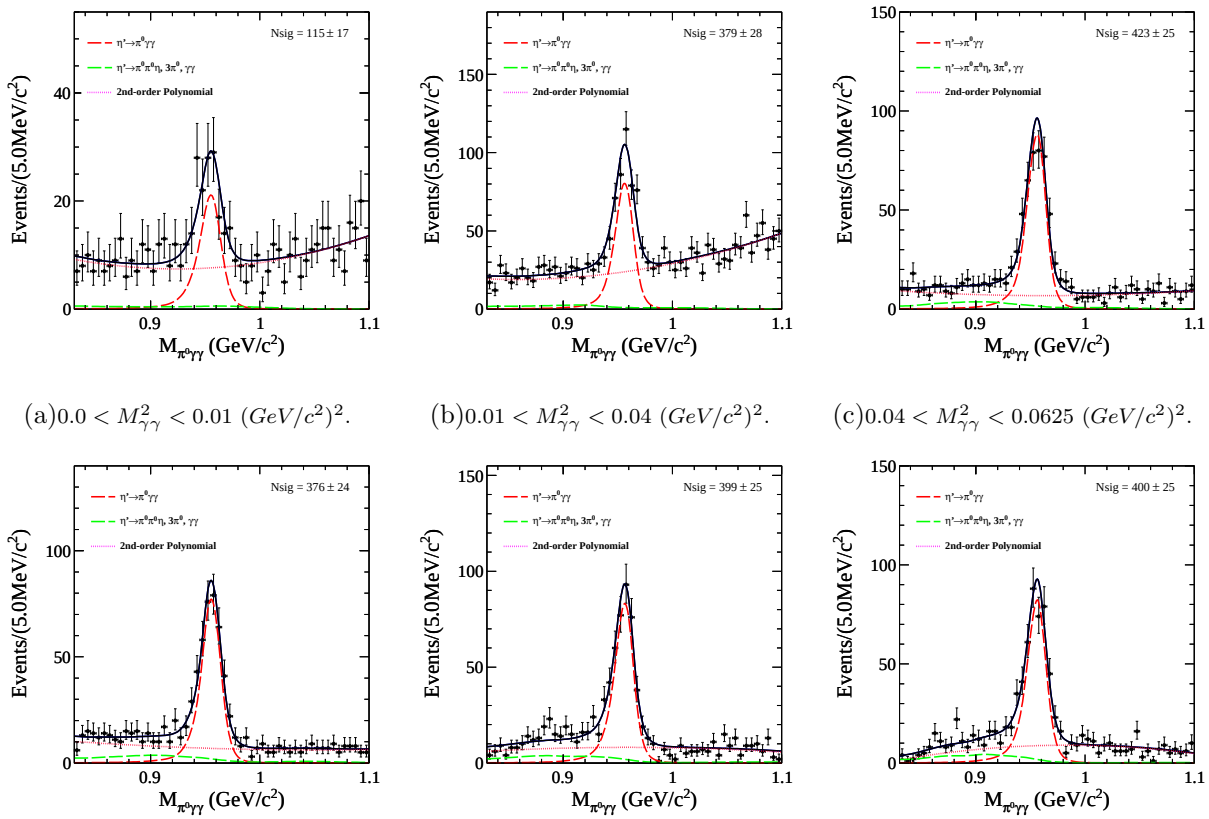

(a)$0.0 < M^2_{\gamma\gamma} < 0.01\ (GeV/c^2)^2$. (b)$0.01 < M^2_{\gamma\gamma} < 0.04\ (GeV/c^2)^2$. (c)$0.04 < M^2_{\gamma\gamma} < 0.0625\ (GeV/c^2)^2$.

(d)$0.0625 < M^2_{\gamma\gamma} < 0.09\ (GeV/c^2)^2$. (e)$0.09 < M^2_{\gamma\gamma} < 0.1225\ (GeV/c^2)^2$. (f)$0.1225 < M^2_{\gamma\gamma} < 0.16\ (GeV/c^2)^2$.

FIG. 47: η' fitting results with an alternative fit range for these bins ($(GeV/c^2)^2$):(a) $M^2_{\gamma\gamma} \subset (0.0, 0.01)$; (b) $M^2_{\gamma\gamma} \subset (0.01, 0.04)$; (c) $M^2_{\gamma\gamma} \subset (0.04, 0.0625)$; (d) $M^2_{\gamma\gamma} \subset (0.0625, 0.09)$; (e) $M^2_{\gamma\gamma} \subset (0.09, 0.1225)$; (f) $M^2_{\gamma\gamma} \subset (0.1225, 0.16)$.

APPENDIX B: SYSTEMATIC ERROR DUE TO THE FIT RANGE

For the measurement of $\mathrm{d}\Gamma(\eta' \to \pi^0\gamma\gamma)/\mathrm{d}m^2_{\gamma\gamma}$, the re-fitting results with an alternative fit range (changing from $0.8 - 1.1$ GeV/c^2 to $0.83 - 1.1$ GeV/c^2) are shown in Table 47 and Table 48.

APPENDIX C: SYSTEMATIC ERROR DUE TO THE FIXED BACKGROUNDS.

For the measurement of $\mathrm{d}\Gamma(\eta' \to \pi^0\gamma\gamma)/\mathrm{d}m^2_{\gamma\gamma}$, the re-fitting results with varying the numbers of expected fixed backgrounds events by one standard deviation from the PDG14 value are shown in Table 49 and Table 50. Here we only show the fitted results coming from the backgrounds of $\eta' \to \pi^0\pi^0\eta$.

APPENDIX D: SYSTEMATIC ERROR DUE TO THE ORDER OF POLYNOMIAL DESCRIBING THE BACKGROUNDS.

For the measurement of $\mathrm{d}\Gamma(\eta' \to \pi^0\gamma\gamma)/\mathrm{d}m^2_{\gamma\gamma}$, the re-fitting results with changing the order of Polynomial from 2 to 3 describing the non-peaking backgrounds are shown in Table 51 and Table 52.

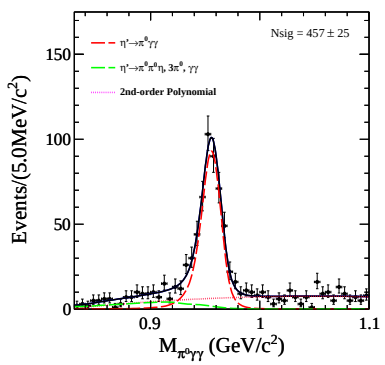

(a)$0.16 < M^2_{\gamma\gamma} < 0.2025\ (GeV/c^2)^2$.

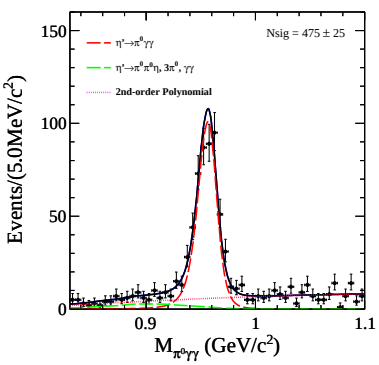

(b)$0.2025 < M^2_{\gamma\gamma} < 0.25\ (GeV/c^2)^2$.

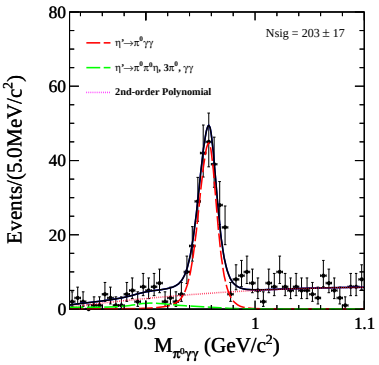

(c)$0.25 < M^2_{\gamma\gamma} < 0.2809\ (GeV/c^2)^2$.

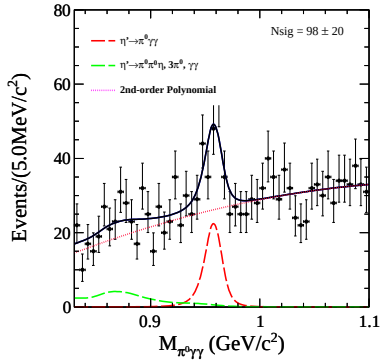

(d)$0.2809 < M^2_{\gamma\gamma} < 0.3136\ (GeV/c^2)^2$.

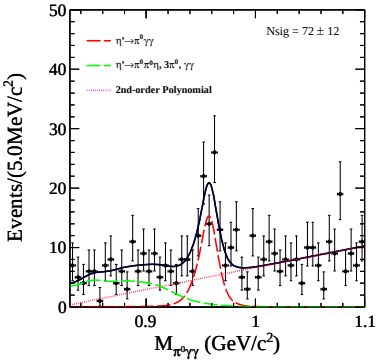

(e)$0.3136 < M^2_{\gamma\gamma} < 0.36\ (GeV/c^2)^2$.

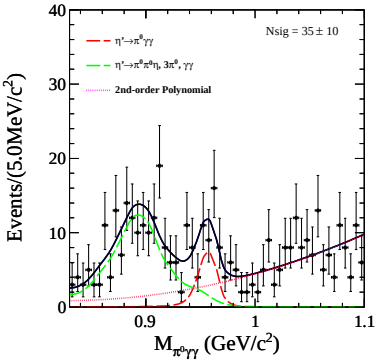

(f)$0.36 < M^2_{\gamma\gamma} < 0.4225\ (GeV/c^2)^2$.

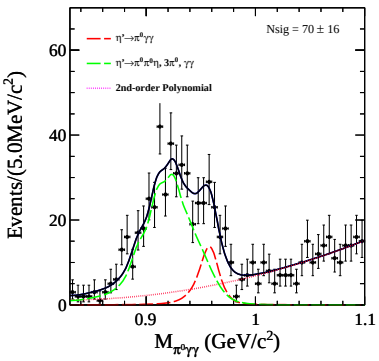

(g)$0.4225 < M^2_{\gamma\gamma} < 0.64\ (GeV/c^2)^2$.

FIG. 48: η' fitting results with an alternative fit ranges for these bins ($(GeV/c^2)^2$): (a) $M^2_{\gamma\gamma} \subset (0.16, 0.2025)$; (b) $M^2_{\gamma\gamma} \subset (0.2025, 0.25)$; (c) $M^2_{\gamma\gamma} \subset (0.25, 0.2809)$; (d) $M^2_{\gamma\gamma} \subset (0.2809, 0.3136)$; (e) $M^2_{\gamma\gamma} \subset (0.3136, 0.36)$; (f) $M^2_{\gamma\gamma} \subset (0.36, 0.4225)$; (g) $M^2_{\gamma\gamma} \subset (0.4225, 0.64)$.

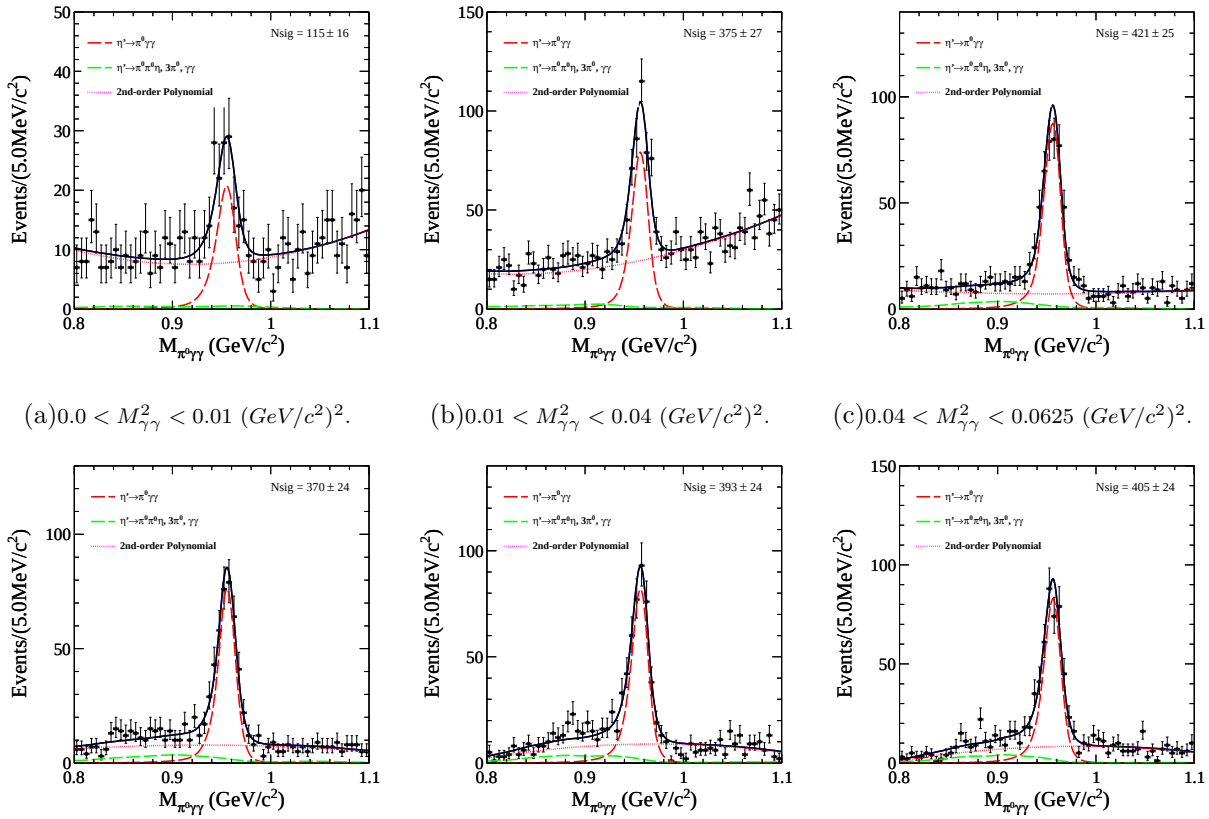

(a)$0.0 < M^2_{\gamma\gamma} < 0.01$ $(GeV/c^2)^2$. (b)$0.01 < M^2_{\gamma\gamma} < 0.04$ $(GeV/c^2)^2$. (c)$0.04 < M^2_{\gamma\gamma} < 0.0625$ $(GeV/c^2)^2$.

(d)$0.0625 < M^2_{\gamma\gamma} < 0.09$ $(GeV/c^2)^2$. (e)$0.09 < M^2_{\gamma\gamma} < 0.1225$ $(GeV/c^2)^2$. (f)$0.1225 < M^2_{\gamma\gamma} < 0.16$ $(GeV/c^2)^2$.

FIG. 49: η' fitting results with varying the numbers of expected fixed backgrounds events by one standard deviation for these bins ($(GeV/c^2)^2$): (a) $M^2_{\gamma\gamma} \subset (0.0, 0.01)$; (b) $M^2_{\gamma\gamma} \subset (0.01, 0.04)$; (c) $M^2_{\gamma\gamma} \subset (0.04, 0.0625)$; (d) $M^2_{\gamma\gamma} \subset (0.0625, 0.09)$; (e) $M^2_{\gamma\gamma} \subset (0.09, 0.1225)$; (f) $M^2_{\gamma\gamma} \subset (0.1225, 0.16)$.

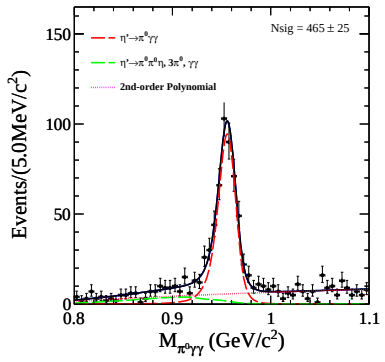

(a)$0.16 < M^2_{\gamma\gamma} < 0.2025$ $(GeV/c^2)^2$.

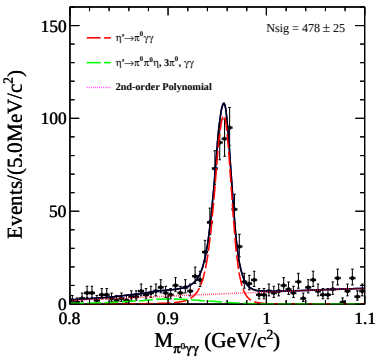

(b)$0.2025 < M^2_{\gamma\gamma} < 0.25$ $(GeV/c^2)^2$.

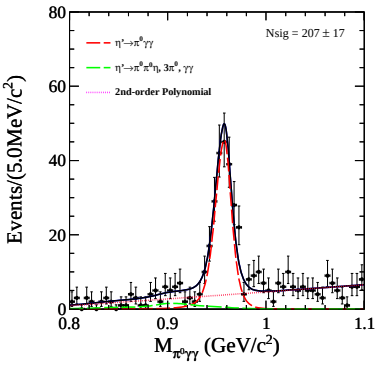

(c)$0.25 < M^2_{\gamma\gamma} < 0.2809$ $(GeV/c^2)^2$.

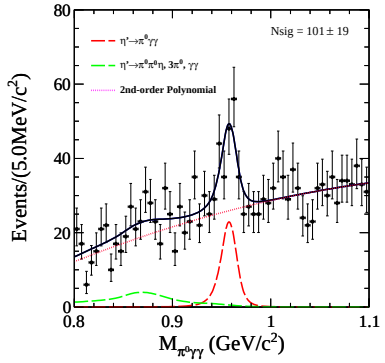

(d)$0.2809 < M^2_{\gamma\gamma} < 0.3136$ $(GeV/c^2)^2$.

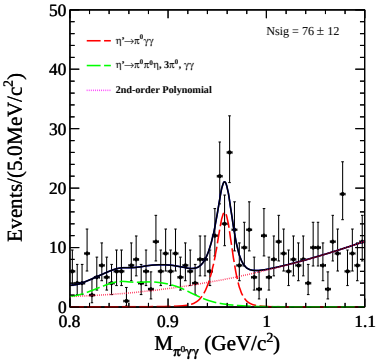

(e)$0.3136 < M^2_{\gamma\gamma} < 0.36$ $(GeV/c^2)^2$.

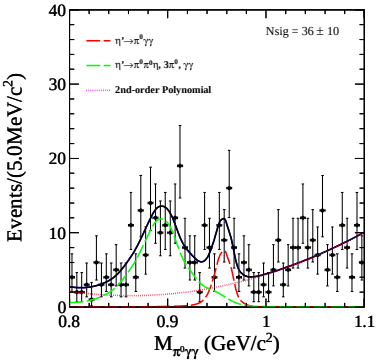

(f)$0.36 < M^2_{\gamma\gamma} < 0.4225$ $(GeV/c^2)^2$.

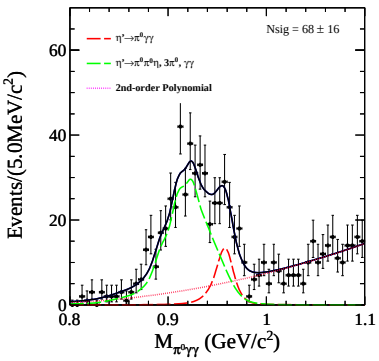

(g)$0.4225 < M^2_{\gamma\gamma} < 0.64$ $(GeV/c^2)^2$.

FIG. 50: η' fitting results with varying the numbers of expected fixed backgrounds events by one standard deviation for these bins ($(GeV/c^2)^2$): (a) $M^2_{\gamma\gamma} \subset (0.16, 0.2025)$; (b) $M^2_{\gamma\gamma} \subset (0.2025, 0.25)$; (c) $M^2_{\gamma\gamma} \subset (0.25, 0.2809)$; (d) $M^2_{\gamma\gamma} \subset (0.2809, 0.3136)$; (e) $M^2_{\gamma\gamma} \subset (0.3136, 0.36)$; (f) $M^2_{\gamma\gamma} \subset (0.36, 0.4225)$; (g) $M^2_{\gamma\gamma} \subset (0.4225, 0.64)$.

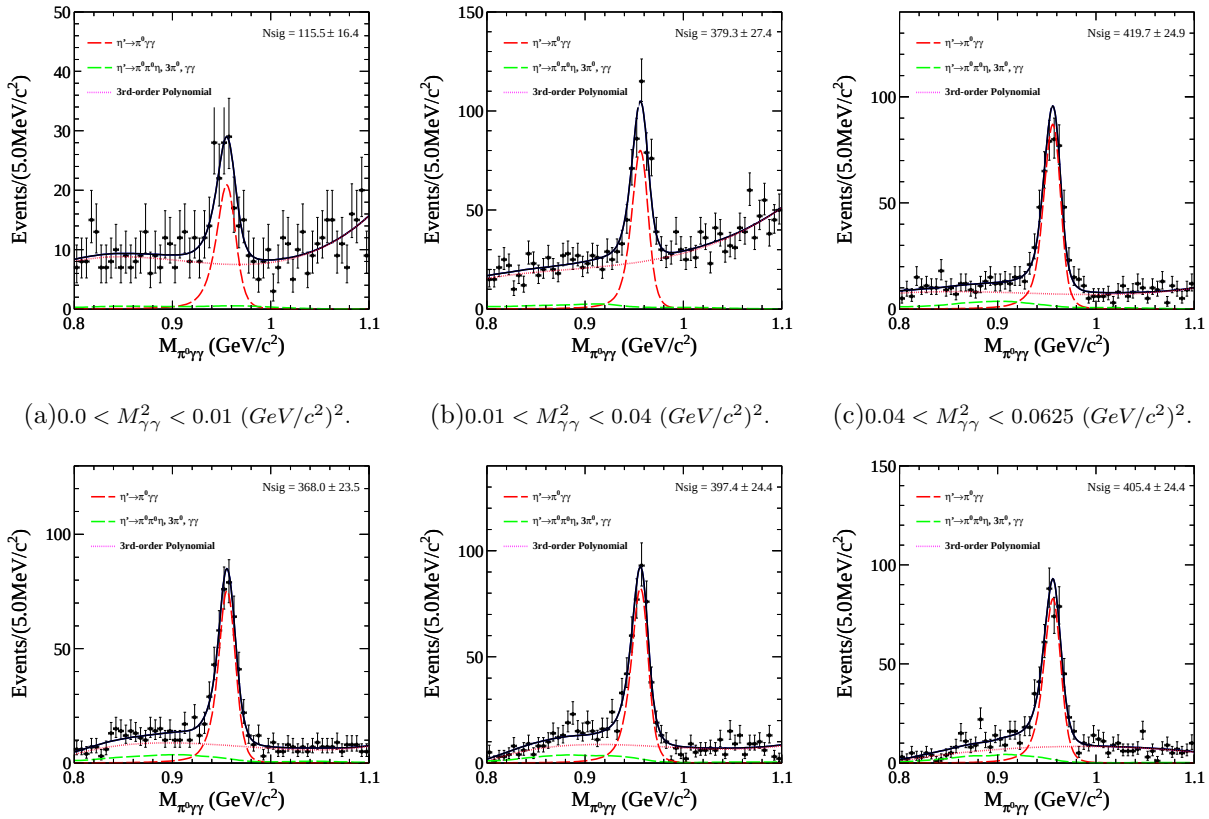

(a)$0.0 < M^2_{\gamma\gamma} < 0.01$ $(GeV/c^2)^2$. (b)$0.01 < M^2_{\gamma\gamma} < 0.04$ $(GeV/c^2)^2$. (c)$0.04 < M^2_{\gamma\gamma} < 0.0625$ $(GeV/c^2)^2$.

(d)$0.0625 < M^2_{\gamma\gamma} < 0.09$ $(GeV/c^2)^2$. (e)$0.09 < M^2_{\gamma\gamma} < 0.1225$ $(GeV/c^2)^2$. (f)$0.1225 < M^2_{\gamma\gamma} < 0.16$ $(GeV/c^2)^2$.

FIG. 51: η' fitting results with changing the order of Polynomial from 2 to 3 describing the non-peaking backgrounds for these bins ($(GeV/c^2)^2$): (a) $M^2_{\gamma\gamma} \subset (0.0, 0.01)$; (b) $M^2_{\gamma\gamma} \subset (0.01, 0.04)$; (c) $M^2_{\gamma\gamma} \subset (0.04, 0.0625)$; (d) $M^2_{\gamma\gamma} \subset (0.0625, 0.09)$; (e) $M^2_{\gamma\gamma} \subset (0.09, 0.1225)$; (f) $M^2_{\gamma\gamma} \subset (0.1225, 0.16)$.

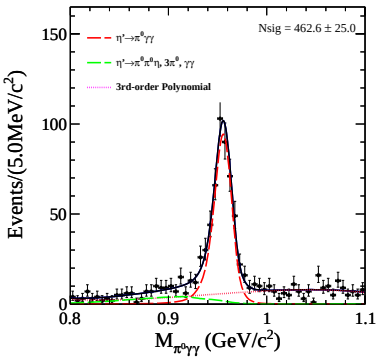

(a)$0.16 < M^2_{\gamma\gamma} < 0.2025\ (GeV/c^2)^2$.

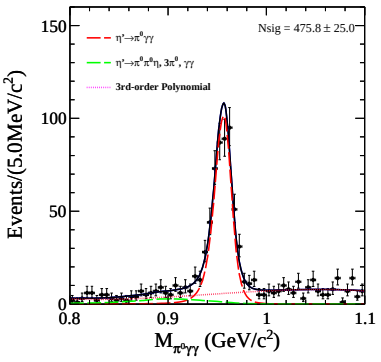

(b)$0.2025 < M^2_{\gamma\gamma} < 0.25\ (GeV/c^2)^2$.

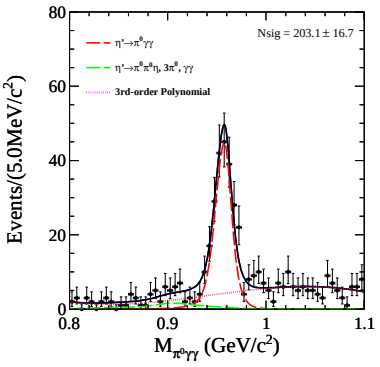

(c)$0.25 < M^2_{\gamma\gamma} < 0.2809\ (GeV/c^2)^2$.

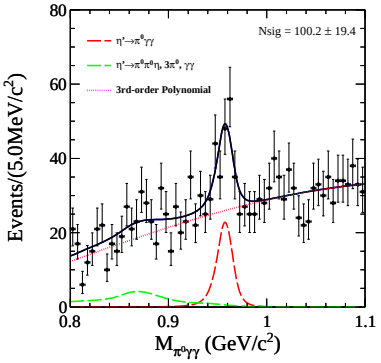

(d)$0.2809 < M^2_{\gamma\gamma} < 0.3136\ (GeV/c^2)^2$.

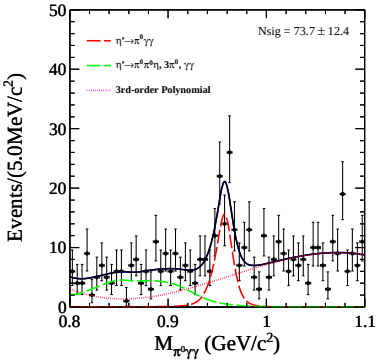

(e)$0.3136 < M^2_{\gamma\gamma} < 0.36\ (GeV/c^2)^2$.

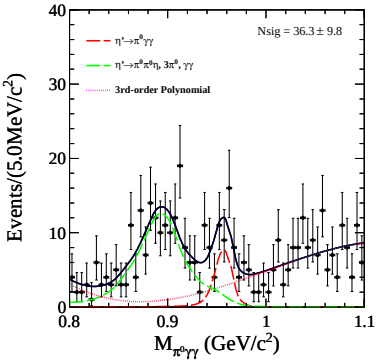

(f)$0.36 < M^2_{\gamma\gamma} < 0.4225\ (GeV/c^2)^2$.

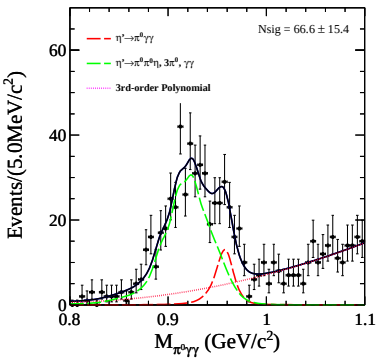

(g)$0.4225 < M^2_{\gamma\gamma} < 0.64\ (GeV/c^2)^2$.

FIG. 52: η' fitting results with changing the order of Polynomial from 2 to 3 describing the non-peaking backgrounds for these bins ($(GeV/c^2)^2$): (a) $M^2_{\gamma\gamma} \subset (0.16, 0.2025)$; (b) $M^2_{\gamma\gamma} \subset (0.2025, 0.25)$; (c) $M^2_{\gamma\gamma} \subset (0.25, 0.2809)$; (d) $M^2_{\gamma\gamma} \subset (0.2809, 0.3136)$; (e) $M^2_{\gamma\gamma} \subset (0.3136, 0.36)$; (f) $M^2_{\gamma\gamma} \subset (0.36, 0.4225)$; (g) $M^2_{\gamma\gamma} \subset (0.4225, 0.64)$.

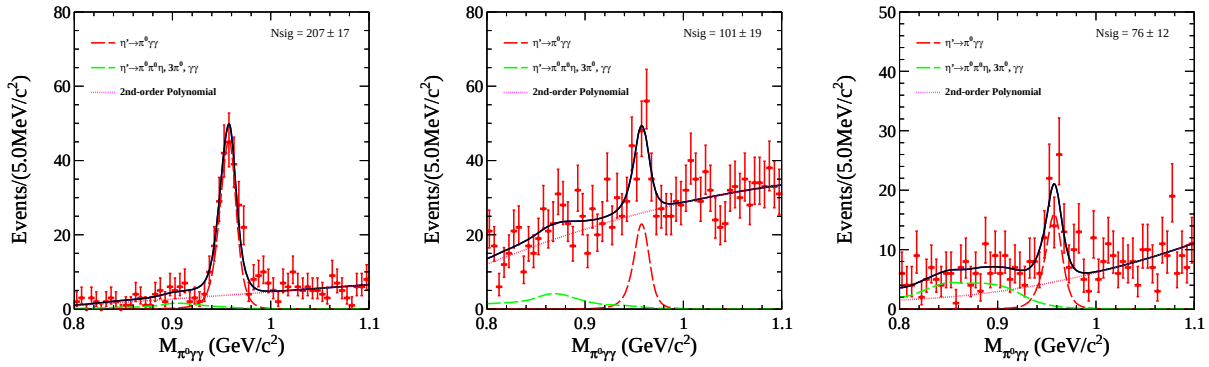

(a)$0.25 < M^2_{\gamma\gamma} < 0.2809\ (GeV/c^2)^2$. (b)$0.2809 < M^2_{\gamma\gamma} < 0.3136\ (GeV/c^2)^2$. (c)$0.3136 < M^2_{\gamma\gamma} < 0.36\ (GeV/c^2)^2$.

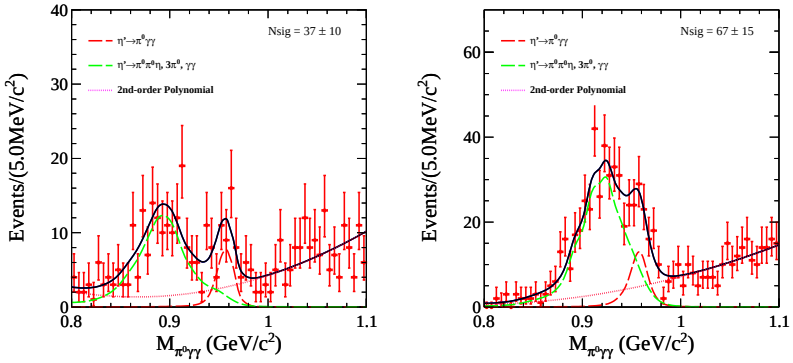

(d)$0.36 < M^2_{\gamma\gamma} < 0.4225\ (GeV/c^2)^2$. (e)$0.4225 < M^2_{\gamma\gamma} < 0.64\ (GeV/c^2)^2$.

FIG. 53: η' fitting results for these bins ($(GeV/c^2)^2$): (a) $M^2_{\gamma\gamma} \subset (0.0, 0.01)$; (b) $M^2_{\gamma\gamma} \subset (0.01, 0.04)$; (c) $M^2_{\gamma\gamma} \subset (0.04, 0.0625)$; (d) $M^2_{\gamma\gamma} \subset (0.0625, 0.09)$; (e) $M^2_{\gamma\gamma} \subset (0.09, 0.1225)$; (f) $M^2_{\gamma\gamma} \subset (0.1225, 0.16)$.